Elucidation of the cellular functions of TrappC11

Daniela Stanga

A Thesis

In the Department

of

Biology

Presented in Partial Fulfillment of the Requirements

For the Degree of

Doctor of Philosophy (Biology) at

Concordia University

Montréal, Quebec, Canada

October 2019

CONCORDIA UNIVERSITY
School of Graduate Studies

This is to certify that the thesis prepared

By: Daniela Stanga
Entitled: Elucidation of the cellular functions of TrappC11

and submitted in partial fulfillment of the requirements for the degree of

Doctor of Philosophy (Biology)

complies with the regulations of the University and meets the accepted standards with respect to originality and quality.

Signed by the final Examining Committee:

_____Chair
Dr. Judith Kornblatt

_____External Examiner
Dr. Shimon Amir

_____External Examiner
Dr. John Presley

_____Examiner
Dr. Alisa Piekny

_____Examiner
Dr. Malcolm Whiteway

_____Supervisor
Dr. Michael Sacher

Approved by

_____
Dr. Robert Weladji, Graduate Program Director

October 14, 2019

_____
Dr. A. Roy, Dean Faculty of Arts and Science

Abstract

Elucidation of the cellular functions of TrappC11

Daniela Stanga, Ph.D.

Concordia University, 2019

Transport protein particle complex component 11 (TRAPPC11) is a subunit of TRAPP III, a protein complex which is involved in membrane traffic, autophagy and maintenance of Golgi structure. The mechanisms by which it functions in these processes are not fully understood. Mutations in human TRAPPC11 have been linked to a wide spectrum of phenotypes including developmental delays, muscular dystrophies, intellectual disabilities, dystroglycanopathies and fatty liver. Here, we show that TRAPPC11 has a role upstream of autophagosome formation in macroautophagy. This contrasts with other TRAPP III proteins that function earlier (TRAPPC8) or later (TRAPPC12) than TRAPPC11 in the pathway. Upon TRAPPC11 depletion, LC3-positive membranes fail to become sealed autophagosomes and are not cleared during starvation conditions. ATG2B and its binding partner WIPI4/WDR45 are thought to be TRAPPC11 interactors, and TRAPPC11 depletion phenocopies the one of either ATG2 or WIPI4, which act in isolation membrane expansion. In the absence of TRAPPC11, recruitment of both these proteins to membranes is defective and fibroblasts from an individual with an altered carboxy-terminus of TRAPPC11 failed to recruit ATG2B-WIPI4, suggesting that this interaction is physiologically relevant. We propose a model whereby the TRAPP III complex coordinates growth and expansion of the isolation membrane through multiple interactions.

TRAPPC11 can also function independent of the complex in the formation of lipid-linked oligosaccharides in *N*-glycosylation, so further research is needed to tease apart the roles of TRAPPC11 independently and within the complex. Collectively, all these dysregulated functions could potentially explain the spectrum of phenotypes seen in individuals having variants of TRAPPC11. The region around the highly-conserved Gly980 appears to be critical for membrane trafficking and *N*-linked glycosylation, causing the muscular weakness phenotype, whereas the extreme carboxy-terminus seems to be involved in

autophagy, being linked to some of the same neurological phenotypes shared with TRAPPC12 variants.

Acknowledgements

To my advisor and mentor Dr. Michael Sacher. Thank you for the invaluable advice, mentorship, teaching and support you provided during all these years. Thank you for your patience and encouragement, and the experience you provided during my training.

I am sincerely grateful for the contributions of my current and former committee members: Dr. Alisa Piekny, Dr. Christopher L Brett, Dr. Malcolm Whiteway and Dr. William Zerges. Their out-of-the-box scientific ideas, constructive criticism, and professional support were greatly treasured and sought-after.

To my present and formal lab mates and colleagues. Thank you for all your support, comments and friendship; you have made these years go by fast and fun, and I couldn't have done it without you.

A special thanks to my colleagues and friends Djenann and Miroslav, aka Dr. Saint-Dic and Dr. Milev, for their invaluable support and friendship along all these years. They also helped me in various instances with different experiments.

I would like also to give a special thank to The Centre for Microscopy and Cellular Imaging (CMCI) at Concordia University and the constant help provided by the centre's operations managers.

Last but not the least I would like to thank to my family, my children, Julia and Edward, and my husband Petru for their unconditional support and love throughout all these years. You mean the world for me!

I dedicate this dissertation to my children,
Julia and Edward.

Contribution of Authors

Figure 2.7A - I did the treatment of the cells and Dr. Milev did stained, analyzed by microscopy and did the statistical analysis.
Figure S2.4A - I did the treatment of the cells and Dr. Milev did stained, analyzed by microscopy and did the statistical analysis.
Figure 3.4B,C - Dr. Milev did stained, analyzed by microscopy and did the statistical analysis.
Figure 3.5 - Dr. Milev did treatment of the cells, analyzed by microscopy and did the statistical analysis.

The cell lines and the BioID experiments used in Chapter 2 were done by Qingchuan Zhao.
RAB1, RAB11 and RAB18 experiments mentioned in the discussion were done by Dr. Milev.
q-PCR analysis used in Chapter 3 was done by Dr. Saint-Dic.
All the clinical analysis from Chapter 2 and Chapter 3 were done by our collaborators.

Table Of Contents

List of Figures

List of Tables

List of Supplemental Figures

List of Abbreviations

aa	amino acid
AMPK	AMP-activated protein kinase
ASH	ASPM, SPD-2, Hydin domain
ATG	Autophagy targeting gene
BafA1	Bafilomycin A_1
COG	Conserved oligomeric Golgi complex
COPI	Coat protein complex I
COPII	Coat protein complex II
CORVET	Class C core vacuole/endosome tethering complex
DFCP1	Zinc finger FYVE domain-containing protein 1
ER	Endoplasmic Reticulum
ERGIC	ER-Golgi intermediate compartment (ERGIC)
ERAD	Endoplasmic-reticulum-associated protein degradation
ESCRT	Endosomal sorting complex required for transport
GAP	GTPase-activating protein
GDP	Guanosine diphosphate
GTP	Guanosine triphosphate
GEF	Guanine nucleotide exchange factor
HOPS	Homotypic fusion and protein sorting complex
LAMP1/2	Lysosome-associated membrane protein 1/2
LC3-PE/LC3-II	Light-chain 3 phosphatidylethanolamine
MAM	Mitochondria-associated ER membrane
MAP1LC3/LC3	Microtubule-associated Protein 1 Light-Chain 3
mTOR	Mammalian target of rapamycin
NF-κB	Nuclear factor kappa B
PAS	Phagophore assembly site
PI3KC3	Phosphatidylinositol 3-kinase class III
PI(3)P	Phosphatidylinositol 3-phosphate
PE	Phosphatidylethanolamine
PROPPINs	β-propellers that bind phosphoinositides

SEDT	Spondyloepiphysealdysplasia Tarda
SNARE	Soluble N-ethylmaleimide-sensitive factor activating protein receptor
SNX18	Sorting nexin18
TBC1D5	Tre-2/Bub2/Cdc16 domain family member 5
Tca	TRAPP complex associated protein
TECPR1	Tectonin beta-propeller repeat containing 1
TGN	Trans-Golgi network
TPR	Tetratricopeptide repeats
TRAPP	Transport protein particle
Trs	Trafficking protein particle complex subunit
ULK1	UNC-51- like kinase 1 complex
VMP1/VAMP	Vesicle associated membrane protein 1
WIPI	WD-repeat protein-interacting phosphoinositide

Chapter 1: Introduction

1.1 Autophagy

Autophagy is a housekeeping process that ensures clearance of damaged cellular components, energy homeostasis by recycling the cytosolic organelles, and protection by removing intracellular pathogens. There are three types of autophagy called macroautophagy, microautophagy and chaperone-mediated autophagy, all leading to proteolytic degradation in the lysosome (Boya et al., 2013). Macroautophagy, henceforth referred to as "autophagy", is conserved across Eukarya and is the most comprehensively studied and the best-characterized of the three types. During this process the cytoplasmic components are delivered for degradation to the lysosomes in double-membrane vesicles called autophagosomes whose biogenesis is tightly regulated by several Autophagy-related proteins (ATG) and membrane trafficking components. Moreover, membrane trafficking machinery is responsible for supplying membranes, lipids and proteins for the formation of autophagosomes and their subsequent fusion with endolysosomal membranes. Although mammalian cells undergo autophagy at a basal level for cellular housekeeping, this process is upregulated under physiological stress conditions such as starvation.

Autophagosomes are formed *de novo* from a double membrane structure called isolation membranes or phagophores, henceforth referred as isolation membranes, which will elongate and entrap the cytoplasmic material. Once formed, the autophagosomes can fuse with multivesicular endosomes forming amphisomes (Eskelinen, 2005) which subsequently fuse with the lysosomes, or alternately autophagosomes can fuse directly with lysosomes forming so-called autolysosomes (Figure 1.1). During fusion with the lysosomes, the inner membrane and the autophagic cargo are degraded by lysosomal hydrolases in the acidic environment (Boya et al., 2013). Formation of an autophagosome includes **(i) nucleation** which refers to all signals that lead to formation of the nascent isolation membrane, **(ii) expansion** which includes membrane modeling and trafficking events that lead to isolation membrane growth and cargo sequestration, and **(iii) closure** which includes the sealing of the isolation membrane and formation of the closed

autophagosome. The transport process of the autophagosomes on the microtubules and their eventual fusion with the endosomes and lysosomes are collectively referred to as **autophagosome maturation** (Figure 1.1).

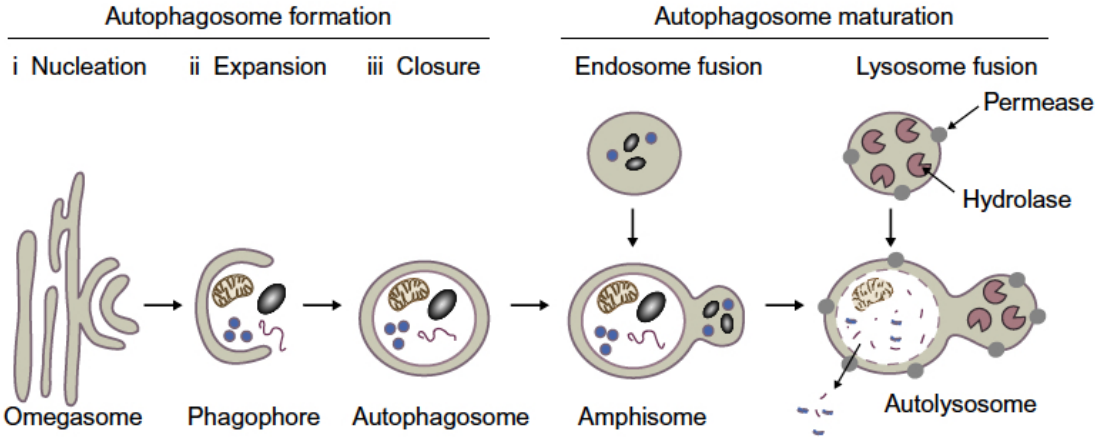

Figure 1.1 Overview of the autophagy pathway

The initial nucleation stage begins with generation of the phagophore/isolation membrane from a specialized cup-shaped ER-associated structure called an omegasome. During the subsequent expansion stage, the isolation membrane elongates and entraps cytoplasmic components into a double membrane structure, which upon closure becomes an autophagosome. Maturation of the autophagosome occurs through multiple fusion events generating either amphisomes or autolysosomes. The sequestered cargo is degraded by lysosomal hydrolases in the acidic environment of the autolysosome, and the degradation products are released back into the cytoplasm through permeases to be reused by the cell as energy sources or building blocks for synthesis of new molecules. Reproduced from (Soreng et al., 2018).

1.2 The Core Autophagy Machinery and its Regulation

The autophagy-related (ATG) proteins involved at different steps in autophagy were identified in yeast genetic screens and are well conserved in mammals (Klionsky et al., 2011; Levine and Klionsky, 2017; Tsukada and Ohsumi, 1993). Much effort was put into the discovery of these proteins and in defining the sequence of the events during autophagy. The core autophagic machinery is crucial for the nucleation of autophagosomes and includes the ATG1/unc-51-like kinase (ULK1) complex, the Vps34/class III phosphatidylinositol 3-kinase (PIK3C3) complex, the ATG12–ATG5–ATG16 complex, and the multi-spanning transmembrane protein ATG9 (Mizushima et

al., 2011; Nakatogawa et al., 2009) (Figure 1.2).

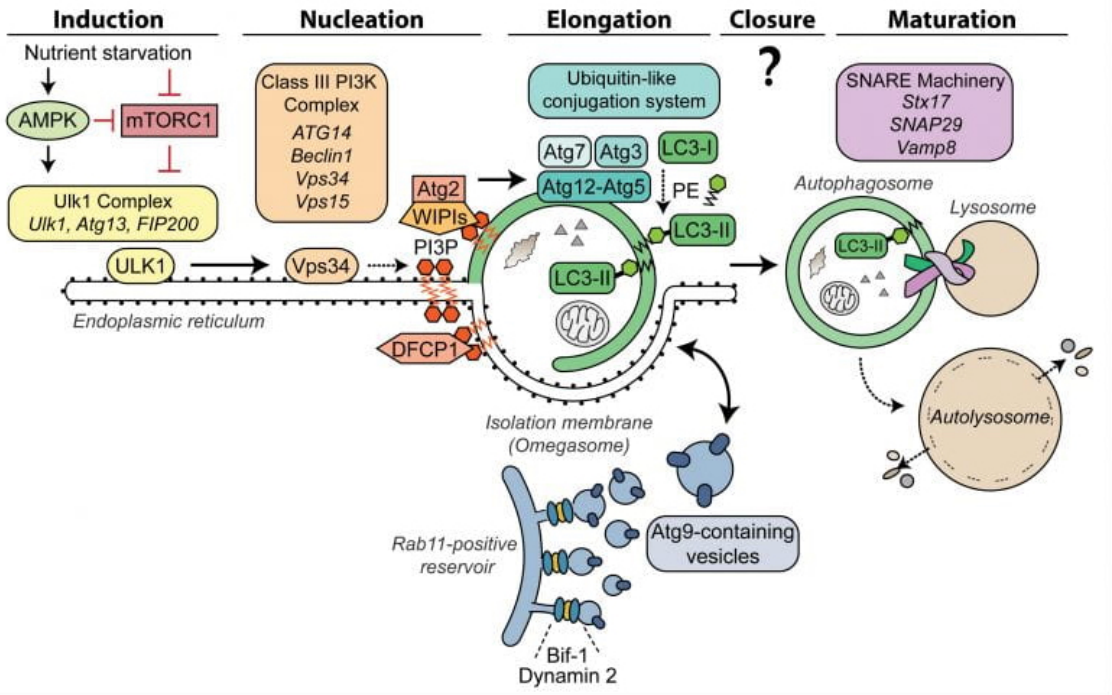

Figure 1.2 Overview of core autophagy machinery

Stress conditions such as nutrient depletion trigger the activation of the ULK1 complex which then promotes nucleation of the isolation membrane by phosphorylating components of the PI3KC3 complex. The latter activates local phosphatidylinositol-3-phosphate (PI(3)P) production at the omegasomes. PI(3)P triggers a chain reaction that leads to recruitment of various molecules important for autophagosome biogenesis. Reproduced from https://sites.psu.edu/hgwanglab/our-research/molecular-regulators-of-autophagy/

In mammals, the ULK1 complex activity (Chan et al., 2009; Hara et al., 2008; Hosokawa et al., 2009; Lee and Tournier, 2011; Mercer et al., 2009) is regulated by energy sensing kinases such as the serine/threonine kinase mechanistic target of rapamycin (mTOR) and AMP-activated protein kinase (AMPK) (Kim et al., 2011; Neufeld, 2010). Thus under glucose starvation, AMPK promotes autophagy by directly activating ULK1 through phosphorylation, while under nutrient-rich conditions, mTOR activity prevents ULK1 activation and disrupts the interaction between ULK1 and AMPK (Kim et al., 2011).

Once activated, ULK1 will trigger the activation of PIK3C3 complex I which specifically phosphorylates phosphatidylinositol to generate PI(3)P. The latter represents a signal for recruitment of the PI(3)P effectors called WD-repeat protein interacting with

phosphoinositides (WIPIs) (discussed below) and zinc-finger FYVE domain-containing protein 1 (DFCP1) to the omegasome (Volinia et al., 1995). WIPI2 recruits the ATG12-ATG5-ATG16L1 (Kuma et al., 2002) complex that triggers the conjugation of LC3 to phosphatidylethanolamine (PE) (Otomo et al., 2013), thus forming the membrane-bound, lipidated form of this protein referred to as LC3-II. The latter is used as a membrane scaffold in autophagosome formation (Johansen and Lamark, 2019).

Another important player in autophagosome biogenesis is the multi-spanning membrane protein ATG9. This is the only membrane protein of the autophagic machinery, and despite the fact that its role is not yet fully understood, it is essential for autophagosome formation in both yeast and mammals. ATG9 localizes to highly mobile cytosolic vesicles called ATG9 vesicles, with each vesicle having around 30 ATG9 molecules (Yamamoto et al., 2012). In nutrient-rich conditions, ATG9 vesicles are trafficked from the trans-Golgi network (TGN) to peripheral ATG9 reservoirs and transiently localize to isolation membranes when autophagy is induced (Imai et al., 2016).

In mammals, ATG9 is internalized from the plasma membrane in AP2-clathrin-coated vesicles and directed to recycling endosomes through interaction with Tre-2/Bub2/Cdc16 domain family member 5 (TBC1D5) (Popovic and Dikic, 2014; Puri et al., 2013). Furthermore, ATG9 and ATG16 vesicles coalesce at recycling endosomes (Popovic and Dikic, 2014), and from there TBC1D14, through interaction with TRAPP III, regulates trafficking of the ATG9 pool from recycling endosomes to the early Golgi, maintaining a cycling pool of ATG9 for initiation of autophagy (Lamb et al., 2016). Whether ATG9 vesicles are incorporated into the isolation membrane remains unclear, although one study using advanced microscopy techniques showed that ATG9 vesicles interact transiently with the isolation membrane (Orsi et al., 2012). Another study reported that ATG9 vesicles are loaded with molecules used for autophagosome biogenesis (Shatz and Elazar, 2019). Delivery of specific proteins through ATG9 vesicles promotes omegasome formation, isolation membrane nucleation and completion of autophagosome formation.

1.3 Autophagosome Biogenesis

Autophagosome biogenesis and maturation relies on membrane input from several endomembrane compartments (Wei et al., 2018) as well as on numerous membrane trafficking components such as coat proteins (Axe et al., 2008), SNAREs (Nair et al., 2011), tethering factors (Davis et al., 2017) and RAB proteins (Szatmari and Sass, 2014).

Autophagy begins with the formation of the isolation membrane and expansion through acquisition of lipids, which will eventually seal and form autophagosomes. The origin and identity of the isolation membrane was the subject of debate for decades, but now it is commonly accepted that isolation membranes are formed *de novo* on pre-existing membranes (Tooze, 2013). Isolation membrane biogenesis in mammalian cells differs from yeast in that there is not a single PAS, but rather several sites mainly formed from PI(3)P-enriched ER structures called omegasomes (Axe et al., 2008) that seem to have multiple curvature sensor molecules (Fan et al., 2011; Takahashi et al., 2007). However, despite this difference, the mechanism of isolation membrane biogenesis is highly conserved between yeast and mammals (Figure 1.2).

Although the nucleation step can occur independently of PI3K activity (Itakura and Mizushima, 2010) the production of PI(3)P is essential for the stability of the membranes and for isolation membrane growth (Karanasios et al., 2013; Koyama-Honda et al., 2013). PI(3)P has the shape of an inverted cone, with the planar surface extruding outwards from the membrane, forming a platform for incoming proteins to bind. Autophagy-specific PI3K complex binds membranes using amphipathic helices and stabilize the isolation membrane upon binding (Fan et al., 2011; Osawa et al., 2019a). PI3KC3 and ULK complexes are recruited to the omegasome and act in a synergistic manner to stimulate PI(3)P production and facilitate the elongation and increased curvature of the isolation membrane. PI(3)P production and WIPI2 recruitment trigger the addition of the ATG12–ATG5–ATG16L1 complex, which facilitates the transfer of LC3 to the isolation membrane.

The supply of biomaterials required for construction of a new isolation membrane comes from different intracellular compartments including ER-exit sites (ERES), Golgi, mitochondria, recycling endosomes and the plasma membrane (Hailey et al., 2010; Hamasaki et al., 2013a; Moreau et al., 2011; Puri et al., 2013; Ravikumar et al., 2010a; Ravikumar et al., 2010b).

1.3.1 Expansion of the Isolation Membrane

Following nucleation, the isolation membrane needs to expand in order to form a closed autophagosome. Yeast has been the prime model system for elongation studies, due to its relative experimental simplicity and its initial exploitation to identify the Atg machinery. In mammals, the process is still not fully understood, but it is known that elongation involves adding membrane lipids from different sources, along with the action of LC3 and ATG12 with their conjugation systems (Hamasaki et al., 2013b; Kabeya et al., 2000; Kabeya et al., 2004; Mizushima et al., 2001). More recent work identified ATG2 as another important player in recruiting and binding lipids (see below).

LC3 family members are involved in isolation membrane growth and autophagosome formation. Conditions that compromise lipidation of LC3 can influence the formation of autophagosomes (Kishi-Itakura et al., 2014; Komatsu et al., 2005; Sou et al., 2008) but do not affect nucleation or formation of the isolation membrane. Moreover, the amount of LC3 correlates with the size of the autophagosomes without affecting their number (Xie et al., 2008). How this peculiar ubiquitin-like protein promotes elongation and closure of the isolation membrane is not clear, however one model argues that LC3 participates in the tethering of small vesicles and promotes hemifusion of liposomes to the growing isolation membrane (Nakatogawa et al., 2007). The balance between conjugation/deconjugation systems (ATG12-ATG5 conjugation system and ATG4 deconjugation) plays an important role in lipidation of LC3 and ultimately in the elongation of the isolation membrane (Welchman et al., 2005).

1.3.2.1 Role of ATG2 in Isolation Membrane Expansion

Recent structural and biochemical analyses of autophagosome biogenesis have identified a new multifunctional protein, ATG2, that is able to tether membranes and incorporate lipids. In mammals ATG2 has two homologs, ATG2A and ATG2B, with redundant function in autophagosome and lipid droplet formation (Velikkakath et al., 2012). Simultaneous depletion of ATG2A and ATG2B produces a block in autophagic flux due to an accumulation of unsealed isolation membranes and clustering of enlarged lipid droplets (Velikkakath et al., 2012). Structural analysis of ATG2 reveals the existence of an amino-terminal membrane binding region with a role in autophagosome formation and in lipid transport (Osawa et al., 2019b; Valverde et al., 2019), an amphipathic helix (residues 1750-1767) with a role in ATG2 localization to lipid droplets and isolation membranes (Tamura et al., 2017), and a carboxy-terminal region (residues 1830–1938) with a role in localizing ATG2 to lipid droplets (Tamura et al., 2017).

The amino-terminal membrane binding region of ATG2A has high similarity with VPS13, a protein known to be involved in lipid transport between organelles at membrane contact sites (Kumar et al., 2018). Moreover, ATG2 and VPS13 both seem to localize to autophagosome-ER contact sites and also share a cup-shaped region containing hydrophobic residues suitable for solubilizing lipids and transporting them between membranes (Kumar et al., 2018; Valverde et al., 2019). The key piece of evidence for their common functions was the ability of the amino-terminal membrane binding domain of ATG2A to rescue the phenotype of a simultaneous depletion of ATG2A and ATG2B (Valverde et al., 2019). This unexpected finding raised the question of how ATG2 is able to tether membranes, since the fragment used for rescue was too small to allow tethering. Although the small fragment is able to transport lipids, the full-length ATG2 likely displays enhanced lipid transport due to existence of two binding domains that cooperatively are used to tether and to transfer phospholipids between different membranes (Chowdhury et al., 2018; Otomo et al., 2018; Valverde et al., 2019). Another suggestion came from the ability of ATG2A to form a complex with the PI(3)P effector WIPI4 (also called WDR45). WIPI4 binds to one of the tips of ATG2A, allowing

the complex to tether a PI(3)P-containing vesicle to another PI(3)P-free vesicle (Chowdhury et al., 2018; Otomo et al., 2018).

The ATG2-WIPI4 interaction is also conserved in yeast, where Atg2 interacts with Atg18, the yeast homologue of WIPI4, and works with Atg9 in the elongation of isolation membranes (Kotani et al., 2018). Although *in vitro* WIPI4 is able to bind PI(3)P in the isolation membrane without assistance (Rieter et al., 2013), *in vivo* it seems that for efficient binding it requires the presence of the amphipathic helix of ATG2 (Kotani et al., 2018). Recent work proposed that ATG2 interacts with GABARAP, an ortholog of LC3, with a role in isolation membrane elongation and localization to lipid droplets (Mihaela Bozic, 2019). However, while the ATG2A-WIPI4 interaction is dispensable for autophagosome biogenesis, the ATG2A-GABARAP interaction is essential. Thus, it was proposed that a combination of the LC3-Interacting Region domain and the amphipathic helix are responsible for proper localization of ATG2 to the isolation membrane and successful lipid transfer.

To create an isolation membrane of 1μm, the average size of an autophagosome, the membrane requires about 25 million lipid molecules. Mammalian cells can form up to hundreds of autophagosomes in a very short amount of time (Maeda et al., 2019). Using comparative studies with a well characterized lipid transport module that accommodates two lipids it was shown that ATG2 is able to transfer about 20 lipid molecules at once (Valverde et al., 2019). However the rate of lipid transfer is too slow to explain the ability of the cell to form so many autophagosomes in such a short period. Since ATG2 is currently the only lipid transfer protein involved in elongation of the isolation membrane, elucidation of its role in autophagosome formation and its ability to tether membranes is essential for understanding the autophagosome biogenesis.

1.3.2.2 Role of WIPI Proteins

Another important component for isolation membrane nucleation and extension is the recruitment of the WIPI proteins (Proikas-Cezanne et al., 2015) that bind the

phosphoinositide lipids (Michell et al., 2006; Proikas-Cezanne et al., 2015) (Figure 1.2). WIPIs are part of a larger family of PI(3)P-interacting proteins called β-propellers that bind phosphoinositides (PROPPINs) (Thumm et al., 2013). In humans there are four members (WIPI1 - WIPI4) each with splicing variants (Proikas-Cezanne et al., 2004). By using homology modeling with WIPI1, it was proposed that WIPI proteins have seven WD repeats folded into a seven-bladed β-propeller (Proikas-Cezanne et al., 2004).

Except for WIPI3 (also known as WDR45L) whose function remains obscure, the functions of the other WIPI proteins in autophagy are clearer. Treatments that induce autophagy cause the relocation of cytoplasmic WIPI1 to ATG12-ATG16L-LC3 positive membranes while treatments that block the formation of PI(3)P prevent the formation of the autophagosomes and relocation of the cytoplasmic WIPI1 (Gaugel et al., 2012; Proikas-Cezanne et al., 2004). The PI(3)P effector function of WIPI1 depends on the ULK1-dependent activation of PI3K3C and production of PI(3)P (Pfisterer et al., 2011).

WIPI2 functions similarly to WIPI1 (Mauthe et al., 2011). It was found that WIPI2 recruits the ATG12–ATG5–ATG16L complex and affects LC3 lipidation. WIPI2 was also linked to retrieval of ATG9 vesicles from the omegasomes, since the depletion of WIPI2 was followed by an accumulation of ATG9 vesicles in these structures (Orsi et al., 2012). In selective autophagy WIPI2 was also found to interact with Tectonin beta-propeller repeat containing 1 (TECPR1), a protein known to be involved in the fusion between autophagosome and lysosome (Chen et al., 2012; Ogawa et al., 2011).

Upon starvation, WIPI4 (also known as WDR45) relocates from the cytosol to LC3-positive structures (Lu et al., 2011). WIPI4 was implicated in omegasome maturation and autophagosome formation due to the observation that WIPI4-depleted cells have an accumulation of unsealed autophagosomes (Lu et al., 2011). WIPI4 homologues in yeast (Zheng et al., 2017) and *C. elegans* (Lu et al., 2011) were found to interact with Atg2 and to act downstream of LC3 in the formation of autophagosomes. Moreover, in humans ATG2 was found to act at the same hierarchical level, with WIPI1 being involved in the completion of autophagosome formation (Itakura and Mizushima, 2010; Velikkakath et

al., 2012).

1.3.2 Autophagosome Completion and Maturation

The mechanism of autophagosome closure is far from being understood, however it is clear that one condition for sealing is achieving the proper length of the isolation membrane (Kishi-Itakura et al., 2014). Even though multiple factors were linked to autophagosome closure, some of them have a role in isolation membrane formation and/or elongation, and therefore the effect on autophagosome closure is not specific to this step and might be indirect (Wen and Klionsky, 2016). Thus, factors that interfere with the lipidation of LC3, such as overexpression of an inactive form of ATG4 (Fujita et al., 2008) or depletion of ATG3 (Sou et al., 2008), or disturbance of ATG9 trafficking (Corcelle-Termeau et al., 2016), act in the elongation of the isolation membrane and have an indirect effect on autophagosome sealing. Recently it was proposed that autophagosome closure occurs through membrane scission, and since the endosomal sorting complex required for transport (ESCRT) is part of membrane-scission machinery (Knorr et al., 2015), it is tempting to speculate that this complex plays a role in autophagosome sealing (Christ et al., 2017). As a result of scission, the elongated isolation membrane will be converted from a cup-shape to a spherical autophagosome. The unsealed autophagosome can still fuse with the lysosomes, however the process is not efficient (Takahashi et al., 2018; Tsuboyama et al., 2016).

After closure, autophagosomes undergo maturation through a series of fusion events with endocytic vesicles and lysosomes, forming autolysosomes where the autophagic cargoes are degraded by proteolytic hydrolases. Although the mechanism involved in lysosome-autophagosome fusion is still unclear, this process must be tightly regulated in order to prevent nonspecific fusion events and ensure the specificity of cargo degradation. In mammalian cells many of the ATG proteins dissociate from the isolation membrane before closure suggesting that their removal is important for autophagosome closure and maturation (Koyama-Honda et al., 2013). Since some of the ATGs bind to isolation membranes through interactions with PI(3)P while others bind through their LC3

interacting domain, the removal of PI(3)P and LC3 following the closure of the isolation membrane destabilizes some ATGs (Kraft and Martens, 2012; Lamb et al., 2013; Mizushima et al., 2011). This destabilization enables ATGs dissociation and recycling.

After closure and maturation, autophagosomes fuse with lysosomes for cargo degradation. Prior to fusion, the autophagosomes and lysosomes must come into proximity, tether, and then fuse in a SNARE-dependent manner. Spatial positioning of the autophagosomes and lysosomes is the first requirement for the fusion. During starvation the lysosomes cluster in the perinuclear region, due to intracellular pH changes (Heuser, 1989), whereas the autophagosomes formed initially in the peripheral region of the cell are transported along the microtubules to the same region in which the lysosomes are located (Fass et al., 2006) (Jahreiss et al., 2008). Similar to membrane fusion, the consumption of autophagosomes through their fusion with lysosomes requires a tethering factor (referred to as HOPS), RAB7, a trans-SNARE complex and different adaptors that link the autophagosomes and lysosomes to the core tethering machinery (Kriegenburg et al., 2018). The autophagosome-lysosome fusion mechanism is still under investigation. Many factors including cholesterol level (Punnonen et al., 1989), glycosylation (Guo et al., 2014), and autophagic lysosome reformation (Yu et al., 2010) seem to influence this mechanism.

Given the requirement for similar non-ATG proteins in autophagosome biosynthesis and fusion and membrane trafficking, it is not unexpected that there is an interplay between these cellular processes regulated by the metabolic conditions of the cells (Staiano and Zappa, 2019). Thus, COPII machinery which is involved in anterograde trafficking, is redirected to autophagosome formation during starvation (Davis et al., 2016). Mammalian TRAPP III, also known to function in membrane trafficking, is involved in maintaining the ATG9 pool required for autophagy upon nutrient deprivation (Lamb et al., 2016; Longatti et al., 2012). The extent of the cross-talk between autophagy and membrane traffic remains to be determined and uncovering the roles of these “multitasking” proteins will give us a better understanding of the mechanisms underlying

autophagosome formation and consumption and perhaps give us tools to treat different diseases (Panda et al., 2019).

1.4 Membrane Trafficking

Intracellular vesicle trafficking is a process required for proper targeting of proteins and lipids within the endomembrane system. It occurs in virtually all cells and is important for maintaining cellular homeostasis, signal transduction, and intracellular compartment identity (Antonescu et al., 2014; Goh and Sorkin, 2013; Irannejad and von Zastrow, 2014; Mellman and Yarden, 2013). Conceptually, vesicular trafficking can be reduced to four common steps: vesicle budding, transport, tethering, and fusion (Bonifacino and Lippincott-Schwartz, 2003). Each of these steps is tightly regulated to ensure that the vesicle formed from the donor membrane will fuse with the appropriate target membrane in a spatiotemporal manner.

Vesicle budding represents selective incorporation of the cargo molecules into emerging vesicles derived from donor membranes with the help of specific coat and adaptor proteins such as clathrin, coat protein complex I (COPI) and coat protein complex II (COPII) (Kirchhausen, 2000). Each of these types of vesicles derives from specific cellular locations (Kreis et al., 1995; Sanderfoot and Raikhel, 1999) with clathrin-coated vesicles derived from the plasma membrane and TGN and fusing with endosomes or lysosomes (Loerke et al., 2009), COPI coated vesicles functioning in Golgi-to-ER and intra-Golgi retrograde traffic (Beck et al., 2009; Reinhard et al., 2003) and COPII coated vesicles functioning in anterograde traffic from the ER to Golgi (Barlowe et al., 1994; Malkus et al., 2002). Despite their different compositions, these coat protein complexes have two common functions: shaping the membranes into spherical vesicles and populating the vesicles with specific cargoes (Gomez-Navarro and Miller, 2016).

Once formed, the vesicles will be transported towards their target or acceptor membrane where the specific cargo will be delivered (Klann et al., 2012). Tethering is crucial for the initial recognition of the vesicle by the target membrane (Li and Yu, 2014; Ohya et al.,

2009; Starai et al., 2008). There are two types of tethering factors: coiled-coil tethers (Brocker et al., 2010; Witkos and Lowe, 2015), and multi-subunit tethering complexes (Brocker et al., 2010). The latter can be further subdivided into those that bind to SNAREs and act as RAB effectors (Meiringer et al., 2011), (Willett et al., 2013), (Dubuke et al., 2015), and those that function as guanine nucleotide exchange factors (GEFs) for RAB proteins including Transport Protein Particle complexes (Jones et al., 2000; Wang et al., 2000) (see below).

After recognition, the membranes fuse and the cargo is delivered into its destination (Bonifacino and Glick, 2004). Important players in this step are the soluble N-ethylmaleimide-sensitive factor activating protein receptor (SNARE) proteins (Chen and Scheller, 2001). They are distributed in distinct subcellular compartments and mediate specific fusion events by specific pairing that drives the formation of a SNARE-pin structure, pulling the two membranes tightly together for fusion (Nichols et al., 1997; Sutton et al., 1998).

RAB guanosine triphosphatases (RAB GTPases) are master regulators of all steps of membrane traffic (Hutagalung and Novick, 2011). They continuously cycle between an active form (GTP-bound) and an inactive form (GDP-bound) (Pereira-Leal and Seabra, 2000). The intrinsic exchange between GDP and GTP is mediated by guanine nucleotide exchange factors (GEFs) while the GTPase activating proteins (GAPs) turn RAB GTPases off by stimulating their ability to hydrolyze GTP into GDP (Ross and Wilkie, 2000). The crosstalk between RABs and their effectors ensures specificity and spatiotemporal regulation of vesicle traffic (Deneka et al., 2003).

1.4.1 TRAPP Complexes

One well-studied multisubunit tethering factor is the TRAPP family of complexes, first identified in yeast as a highly-conserved complex that localizes to the Golgi and functions in ER-to-Golgi transport upstream of SNAREs (Rossi et al., 1995; Sacher et al., 2000; Sacher et al., 1998). It was later revealed that there were at least two TRAPP

complexes: a smaller one known as TRAPP III containing the so-called core of six subunits, along with the additional TRAPP III-specific protein Trs85 (Lynch-Day et al., 2010), and a larger one called TRAPP II that contains the core with Trs65, Trs120, and Trs130 (Sacher et al., 2001). The core of the yeast TRAPP complexes was shown to bind and function as a GEF for the small GTPase Ypt1p in its nucleotide-free state converting it to its active form (Cai et al., 2008; Kim et al., 2006). Subsequent studies suggested that the size of the complex provides specificity such that TRAPP II binds and activates Ypt31/32 (Thomas and Fromme, 2016) and TRAPP III binds and activates Ypt1 (Thomas et al., 2018).

All of the yeast subunits are conserved in higher eukaryotes including humans. Similar to yeast, there are two human TRAPP complexes that contain a core of proteins comprised of TRAPPC1, TRAPPC2, two copies of TRAPPC3, TRAPPC4, TRAPPC5 and TRAPPC6. In addition to this core, TRAPP II also contains TRAPPC9 and TRAPPC10, while TRAPP III contains the core with TRAPPC8, TRAPPC11, TRAPPC12 and TRAPPC13 (Sacher et al., 2000; Sacher et al., 1998; Scrivens et al., 2011) (Figure 1.3). The GEF activity of human TRAPP complexes is incompletely understood. However, it has been suggested that TRAPP II has GEF activity towards the human homologue of Ypt1 called RAB1, and for RAB18 (Li et al., 2017; Yamasaki et al., 2009) while the GEF activity of human TRAPP III has yet to be discovered.

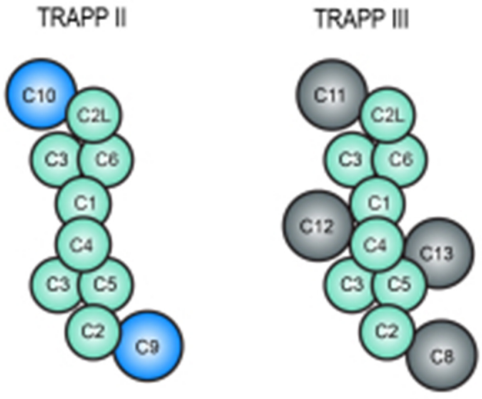

Figure 1.3 Cartoon depicting the stoichiometry and interactions between subunits in mammalian TRAPP complexes.

The core of proteins found in the complexes is colored in green, with the specific subunits colored blue for TRAPP II and grey for TRAPP III. The arrangement of the subunits in the core is based on biochemical and single-particle electron microscopic data. TRAPP II possesses two specific subunits (TRAPPC10 and TRAPPC9) while TRAPP III contains TRAPPC11, TRAPPC12 and TRAPPC13. Reproduced from (Sacher et al., 2019).

1.4.2 TRAPP III

Although TRAPP complexes are evolutionarily conserved, there are some structural differences between the mammalian and yeast TRAPP III complexes. Human TRAPP III has two additional subunits called TRAPPC2L and TRAPPC13 (Bassik et al., 2013; Scrivens et al., 2011) for which the yeast homologues are found in TRAPP II, and two additional subunits called TRAPPC11 and TRAPPC12 are found in the complex for which no yeast homologues have been identified (Scrivens et al., 2011).

The specific subunits of human TRAPP III were linked to various functions in the cell. For example, the essential TRAPPC8 protein functions in autophagy (Behrends et al., 2010), and has been implicated in vesicular transport in the cilia (Schou et al., 2014). The latter role was suggested based on the existence of the ASPM, SPD-2, Hydin (ASH) domains close to the carboxy-terminus known as targeting domains to the centrosome and cilia (Schou et al., 2014). Within the TRAPP III complex three subunits have ASH domains (TRAPPC8, TRAPPC11 and TRAPPC13), however localization to the centrosome has been demonstrated just for TRAPPC8 (Schou et al., 2014)(Figure 1.4). Besides ASH domains, TRAPPC8 has a α-solenoid domain bearing stretches of multiple tetratricopeptide repeats (TPR) close to the amino-terminus known as interaction modules and multiprotein complex mediators (Zeytuni and Zarivach, 2012). Interestingly, these TPR repeats are also found in TRAPPC11 and TRAPPC12 (Schou et al., 2014). Whether either of these two proteins has any role in cilia formation through its ASH domains or whether it is interacting with other proteins through the TPR domains remain to be addressed.

Figure 1.4 Representation of Tetratricopeptide Repeats (TPR) and ASPM, SPD-2, Hydin (ASH) domains

Note the similarity between TRAPPC8 and TRAPPC11 comprising the TPR domains (shown as one region in blue) in the amino-terminus region and two ASH domains (in green) in the carboxy-terminus region. TRAPPC13 has just two ASH domains. Reproduced from (Schou et al., 2014).

TRAPPC11 has a highly conserved 258 residue-long domain called foie gras (residues 263-521) (Scrivens et al., 2011) which seems to have a critical role for the protein functions since deletions in this region lead to unstable protein (Bogershausen et al., 2013). As part of TRAPP III (Scrivens et al., 2011), together with TRAPPC8 and TRAPPC12, TRAPPC11 immunoprecipitated with components of COPII (Bassik et al., 2013; (Zhao et al., 2017), suggesting that TRAPP III is interacting with the COPII vesicle coat. In mammalian cells, depletion of TRAPPC11 led to TRAPP complex disassembly, Golgi fragmentation and early trafficking defects (Scrivens et al., 2011). While TRAPPC11 may also affect autophagy, the mechanism of any such role remains unclear (Behrends et al., 2010). TRAPPC11 can also function independently of the TRAPP complex in the synthesis of dolichol, the molecule required for assembly of the carbohydrate precursor in *N*-linked glycosylation of proteins (DeRossi et al., 2016).

Originally identified in a proteomic study of the human autophagy network (Behrends et al., 2010) and assigned as a TRAPP III subunit (Bassik et al., 2013; Scrivens et al., 2011), TRAPPC12 can also function independently of the complex with a role in mitosis by regulating chromosome congression and kinetochore stability (Milev et al., 2015).

A recent study suggested that TRAPPC13 is important for the retrograde trafficking function of TRAPP III. Thus, depletion of TRAPPC13 led to a sensitization of cells to the Golgi-disrupting agent Brefeldin-A, limiting the ability of cells to respond to Golgi stress (Ramirez-Peinado et al., 2017).

1.4.3 TRAPP III and Diseases

Due to the presence of more than one TRAPP complex, and perhaps due to multifunctional proteins, mutations in human TRAPP complex subunits have been associated with multiple distinct genetic disorders, displaying a wide variation that is often anchored by some overlapping phenotypes.

TRAPPC2 variants cause an X-linked recessive skeletal disorder with a male preponderance called spondyloepiphysealdysplasia tarda (or late onset) (SEDL) (Gedeon et al., 1999). None of the other TRAPP subunits have been linked to this disorder, which has been rationalized by a defect in the secretion of extracellular matrix proteins by chondrocytes (Venditti et al., 2012). However, individuals with variants of either TRAPPC2L (Milev et al., 2018), TRAPPC4 (Van Bergen et al., 2019) TRAPPC6A (Mohamoud et al., 2018) or TRAPPC12 (Milev et al., 2017) instead suffer from global developmental delay, features of neurodevelopmental disorders and intellectual deficit.

Variants in TRAPPC11 are linked to a spectrum of phenotypes. Their common features involve muscular disorders (from limb girdle muscular dystrophy and cardiomyopathy to muscular weakness) and intellectual disabilities (Bogershausen et al., 2013; Fee et al., 2017; Koehler et al., 2017; Larson et al., 2018; Liang et al., 2015; Matalonga et al., 2017). The implication of TRAPPC11 in learning and memory seem to be a conserved function across kingdoms as the *Drosophila* orthologue gryzun has been linked to long-term memory (Dubnau et al., 2003). Other phenotypes linked to variants in TRAPPC11 are fatty liver seen in humans (Bogershausen et al., 2013; Fai Tse et al., 2016; Liang et al., 2015) and zebrafish (Cinaroglu et al., 2011; Sadler et al., 2005), achalasia, alacrima, scoliosis (Koehler et al., 2017) and cataracts (Liang et al., 2015).

Overall, the broad spectrum of cellular phenotypes and clinical features highlights the importance of TRAPP complexes in development and cellular function while also implicating many of the TRAPP subunits in specialized roles. Further studies are needed to tease apart the functions of these proteins within the context of the complex and separately from it.

1.5 Role of TRAPP in Autophagy

TRAPP was first linked to autophagy in yeast when a TRAPP III-specific subunit, Trs85, which is not essential for cell viability, was shown to be essential in selective and non-selective autophagy (Meiling-Wesse et al., 2005). Subsequent work demonstrated that TRAPP III is recruited to the PAS where it activates and recruits Ypt1 (Lynch-Day et al., 2010), triggering the subsequent recruitment of Atg1, the yeast homologue of ULK1 (Wang et al., 2013). Thus, it was proposed that Ypt1 regulates Atg9 vesicle tethering by modulating the delivery of Atg1 to the PAS (Wang et al., 2013). However, other studies support the idea that Atg9 is binding and recruiting TRAPP III to the PAS. Notably, Trs85 co-localizes with Atg9 on the PAS as well as on multiple punctae in the cytosol (Lipatova et al., 2012). Mutations in Atg9 affect the formation of the PAS, and therefore the recruitment of Trs85 to these membranes will not occur (Kakuta et al., 2012). TRAPP III also binds to COPII vesicles at the PAS (Tan et al., 2013), so it is tempting to propose that the role of yeast TRAPP III is to recruit membranes (COPII and Atg9) as materials for the construction of the elongated isolation membrane.

A specific subunit of yeast TRAPP II, Trs130, was proposed to be involved indirectly in autophagy through activation of Ypt31/32 (Zou et al., 2013) which may regulate the trafficking of Atg8 and Atg9 from the trans-Golgi to the PAS (Zou et al., 2013). Mutant strains of Trs130 or Trs65, another specific subunit of yeast TRAPP II, showed an accumulation of Atg8 and Atg9 in the trans-Golgi but not in the PAS, and this phenotype was rescued by GTP-bound Ypt31 or Ypt32 but not by Ypt1 nor the GDP-bound form of

Ypt31 (Zou et al., 2013), suggesting that TRAPP can affect autophagy directly as well as indirectly through its effects on membrane trafficking.

The first evidence of mammalian TRAPP being involved in autophagy was in a proteomic analysis of the autophagy interaction network in human cells under conditions of basal autophagy (Behrends et al., 2010). In this study it was found that depletion of either one of TRAPPC5, TRAPPC8 or TRAPPC11 was followed by a reduction in autophagosome formation, while depletion of TRAPPC12 led to an increase in the number of autophagosomes. Moreover, TRAPP subunits (TRAPPC11, TRAPPC12, TRAPPC8, TRAPPC2L, TRAPPC4 and TRAPPC5) were found in the same sub-network as TECPR1, a protein known to be involved in the fusion of the autophagosome with lysosomes (Behrends et al., 2010). A subsequent study meant to examine genetic modifiers of cellular susceptibility to a toxin called ricin revealed the existence of two mammalian TRAPP complexes, TRAPP II and TRAPP III, and found that TRAPP III interacts with COPII vesicles (Bassik et al., 2013). Knowing that COPII vesicles participate as a source of membrane in the formation of the isolation membrane (Shima et al., 2019), it is tempting to suggest that TRAPP III may participate in autophagosome formation. A recent study proposed an elegant mechanism through which mammalian TRAPP III influences autophagy. The interaction of TBC1D14 from RAB11-positive recycling endosomes with TRAPP III triggers the conversion of RAB11-positive membranes to RAB1-positive membranes, facilitating endosome-to-Golgi traffic of ATG9 vesicles. This mechanism ensures a rapid cycling of ATG9 vesicles under starvation and maintains their supply, which is required for autophagosome formation (Lamb et al., 2016; Longatti et al., 2012). Interestingly, TRAPPC13 depletion promotes cell survival under either induced Golgi stress conditions or mTOR inhibition by reducing the rate of autophagy. The mechanism is still unclear, however it seems that the effect of TRAPPC13 on the activity of RAB1 becomes a rate-limiting factor for autophagy in these stress conditions (Ramirez-Peinado et al., 2017). Similar to yeast, mammalian TRAPP III interacts with ATG9, as evidenced by the ability of TRAPPC13 to immunoprecipitate ATG9 (Ramirez-Peinado et al., 2017). It is not clear how

TRAPPC13 is involved in binding ATG9 without affecting cell survival, when it is known that ATG9 is essential for the initiation of autophagy (Lamb et al., 2016).

1.6 Objectives

Objective 1- Determine the role of TRAPPC11 in autophagy.

Much more is known about the involvement of the yeast TRAPP III complex in secretion and autophagy than its mammalian counterpart. While yeast TRAPP III has just a single non-core subunit, Trs85, mammalian TRAPP III has four additional subunits: TRAPPC8; TRAPPC11; TRAPPC12; and TRAPPC13. There is low sequence similarity between TRAPPC8 and Trs85, and no yeast homologue exists for TRAPPC11 nor for TRAPPC12. There is evidence that TRAPPC12 participates in the retrograde trafficking of ATG9 from peripheral recycling endosomes to the early Golgi (Lamb et al., 2016). The role of mammalian TRAPP III in autophagy, a process affected by membrane trafficking, needs to be deciphered and so I made this my first goal, with a principal focus on TRAPPC11. The findings were published in *Traffic* and are shown here in Chapter 2.

Objective 2- Identification of other roles of TRAPPC11 in the cell.

It has been previously published that depletion of (Scrivens et al., 2011) or mutations in (Bogershausen et al., 2013; Fee et al., 2017; Koehler et al., 2017; Larson et al., 2018; Liang et al., 2015; Matalonga et al., 2017) TRAPPC11 affect membrane traffic. In Chapter 2 I show that TRAPPC11 is important in the recruitment of ATG2 and WIPI4, proteins involved in elongation of the isolation membrane (Stanga et al., 2019). Interestingly, TRAPPC11 can also function independent of the complex in the formation of lipid-linked oligosaccharides in N-glycosylation (DeRossi et al., 2016). Individuals with variants in TRAPPC11 harbour a spectrum of phenotypes including neuromuscular defects and intellectual deficiency, with features including scoliosis, alacrima, steatosis, cerebral atrophy, and fatty liver. My hypothesis was that this spectrum of phenotypes is due to the multiple roles of TRAPPC11 in different cellular functions, including

membrane traffic, autophagy and glycosylation, and thus individuals with mutations in the same region will display similar phenotypes. The results of this study were published in *Scientific Reports* and are shown here in Chapter 3.

Chapter 2: TRAPPC11 Functions in Autophagy by Recruiting ATG2B-WIPI4/WDR45 to Preautophagosomal Membranes.

This Chapter was published as a manuscript in the journal *Traffic* (Stanga et al., 2019). I am responsible for the all figures except Figure 2.7A and Supplemental Figure 2.4A and B in which I prepared the treatment for the cells and Dr. Milev stained them and analyzed them by confocal microscopy.

2.1 Abstract

TRAPPC11 has been implicated in membrane traffic and lipid-linked oligosaccharide synthesis, and mutations in TRAPPC11 result in neuromuscular and developmental phenotypes. Here, we show that TRAPPC11 has a role upstream of autophagosome formation during macroautophagy. Upon TRAPPC11 depletion, LC3-positive membranes accumulate prior to, and fail to be cleared during, starvation. A proximity biotinylation assay identified ATG2B and its binding partner WIPI4/WDR45 as TRAPPC11 interactors. TRAPPC11 depletion phenocopies that of ATG2 and WIPI4 and recruitment of both proteins to membranes is defective upon reduction of TRAPPC11. We find that a portion of TRAPPC11 and other TRAPP III proteins localize to isolation membranes. Fibroblasts from a patient with TRAPPC11 mutations failed to recruit ATG2B-WIPI4, suggesting that this interaction is physiologically relevant. Since ATG2B-WIPI4 is required for isolation membrane expansion, our study suggests that TRAPPC11 plays a role in this process. We propose a model whereby the TRAPP III complex participates in the formation and expansion of the isolation membrane at several steps.

2.2 Introduction

Macroautophagy (autophagy) is a basal process in cells that removes damaged organelles and ensures a ready supply of amino acids for protein synthesis. This process is

upregulated during starvation when nutrients are scarce. Autophagy starts with the nucleation of membranes referred to as the phagophore assembly site in yeast or isolation membranes in higher eukaryotes. The expansion of the isolation membrane is due in part to the input of membranes from sources including mitochondria, the endoplasmic reticulum (ER), mitochondria-ER contact sites, the plasma membrane and endosomes (Axe et al., 2008; Hailey et al., 2010; Hamasaki et al., 2013a; Hayashi-Nishino et al., 2009; Ravikumar et al., 2010a; Young et al., 2006). Upon sealing of the isolation membrane into a fully enclosed, double-membrane-bound autophagosome, its cargo is delivered to the lysosome by autophagosome-lysosome fusion creating autolysosomes where the degradative enzymes of the lysosome hydrolyze the contents of the autophagosome to help re-establish a pool of cellular nutrients.

Proteins acting at various stages of autophagy (ATG) have been identified by genetic screens in yeast and many of these proteins are conserved throughout evolution (Levine and Klionsky, 2017). Much effort has been put into defining the sequence of events in autophagy. Nucleation is initiated by the action of the ULK1 kinase, which activates a phosphatidylinositol-3 kinase-containing complex (Russell et al., 2013). The resulting phosphatidylinositol-3-phosphate (PI(3)P)-rich membranes of the ER subdomain called the omegasome serve as a platform to recruit ATG5-ATG12-ATG16L1, a complex required to lipidate LC3-I, converting it into the autophagy-specific LC3-II (Ichimura et al., 2000). Isolation membrane expansion requires other ATG proteins including ATG2 (Kishi-Itakura et al., 2014), a protein that interacts with a PI(3)P effector called WIPI4/WDR45 (hereafter WIPI4) (Bakula et al., 2017; Baskaran et al., 2012; Behrends et al., 2010; Zheng et al., 2017). Little is known about how the isolation membrane is sealed into a mature autophagosome, although ATG5 and members of the LC3/GABARAP family have been implicated in this process (Kishi-Itakura et al., 2014; Weidberg et al., 2010). Identifying novel regulators of these key autophagy proteins will be of importance for a more complete understanding of this process.

TRAPP is a family of multisubunit complexes implicated in membrane trafficking that were first identified in yeast and are also found in higher eukaryotes (Bassik et al., 2013;

Lynch-Day et al., 2010; Riedel et al., 2018; Sacher et al., 2001; Sacher et al., 1998). Each complex is composed of an identical core of proteins, and additional, complex-specific proteins define their identity, localization and function (Brunet and Sacher, 2014; Kim et al., 2016). Most of the subunits of the complexes are conserved throughout evolution but metazoa have several subunits not found in *Saccharomyces cerevisiae* including TRAPPC11 and TRAPPC12 (Scrivens et al., 2011). These latter two subunits are components of TRAPP III that also contains TRAPPC8 and TRAPPC13 (Bassik et al., 2013). While a role for yeast TRAPP III in autophagy is established (Brunet et al., 2013; Kakuta et al., 2012; Lipatova et al., 2012; Lynch-Day et al., 2010; Shirahama-Noda et al., 2013; Taussig et al., 2014), the role of the human complex in this process is not well understood. A proteomics study initially implicated human TRAPP III in autophagy (Behrends et al., 2010), and several recent studies have further shown a role for TRAPP III in this process (Lamb et al., 2016; Ramirez-Peinado et al., 2017).

To date, two of the human TRAPP III-specific proteins (TRAPPC11 and TRAPPC12) have been implicated in cellular processes distinct from membrane trafficking. These include lipid-linked oligosaccharide synthesis for TRAPPC11 and chromosome congression for TRAPPC12 (DeRossi et al., 2016; Milev et al., 2015). In addition, both proteins have been implicated in human disease that manifests as muscular and neurodevelopmental phenotypes (Bogershausen et al., 2013; Fee et al., 2017; Koehler et al., 2017; Larson et al., 2018; Liang et al., 2015; Matalonga et al., 2017; Milev et al., 2017). Given the overall size of the TRAPP complexes (Kim et al., 2006; Tan et al., 2013; Yip et al., 2010), it is not unreasonable to expect their constituent proteins to have unique interacting partners, thereby allowing the complexes to coordinate distinct events even within a common pathway. Thus, understanding the various roles that the TRAPP proteins play in cell physiology will shed light on the diseases caused by mutations in their genes.

Here, we show that the TRAPP III-specific proteins TRAPPC11, TRAPPC12 and TRAPPC8 affect autophagy. While depletion of TRAPPC8 affected the formation of isolation membranes, TRAPPC11 and TRAPPC12 functioned downstream of this step.

We show that TRAPPC11 interacts with ATG2B, one of the ATG2 homologs, as well as with its binding partner WIPI4. TRAPPC11 depletion phenocopies that of both ATG2 and WIPI4 resulting in unsealed isolation membranes, suggesting that TRAPPC11 functions upstream of isolation membrane closure. In contrast, TRAPPC12 functions after autophagosome formation. We demonstrate that the recruitment of ATG2B and WIPI4 to isolation membranes is dependent upon TRAPPC11 and implicate the carboxy-terminus of TRAPPC11 as important for this recruitment. Fibroblasts from an individual with bi-allelic TRAPPC11 mutations including one at the carboxy-terminus are defective in ATG2B and WIPI4 recruitment. This defect in the fibroblasts was suppressed by wild type TRAPPC11, suggesting that this newly identified interaction is important in human health. We propose a model whereby different TRAPP III proteins participate in various steps in autophagy including isolation membrane formation and expansion, thus implicating TRAPP III in a key role in early autophagy events.

2.3 Materials and Methods

2.3.1 Cell Culture

HeLa cells stably expressing the autophagosomal marker mRFP/GFP-LC3 (Sarkar et al., 2009) and primary fibroblasts were cultured in Dulbecco's modified Eagle medium (DMEM) (Wisent, St. Bruno, Quebec, Canada) supplemented with 10% (vol/vol) fetal bovine serum (FBS; Thermo Fisher Scientific, Waltham, Massachusetts) at 37°C in a humidified incubator with 5% CO2.

2.3.2 Starvation Treatments

The cells were seeded in 6- or 10-cm diameter dishes, washed twice with phosphate-buffered saline (PBS) and incubated with EBSS (Wisent, St. Bruno, Quebec, Canada) for the times indicated in each figure. In some cases, 200 nM Bafilomycin A1 (Sigma-Aldrich, St. Louis, Missouri) was included during a 2-hour starvation to block the fusion of autophagosomes with lysosomes. Proteolytic activity of lysosomes was inhibited by

including both 10 μM E64d (Sigma-Aldrich, St. Louis, Missouri) and 10 μM pepstatin A (Sigma-Aldrich, St. Louis, Missouri) for 3 hours. In some instances, cells starved and treated with Bafilomycin A1 were returned to nutrient-rich medium by washing the cells twice with PBS and incubating in DMEM with 10% FBS for 20 or 40 minutes. The cells were either lysed by harvesting in lysis buffer (150 mM NaCl, 50 mM Tris pH 7.2, 1 mM DTT, 1% Triton X-100, 0.5 mM EDTA, Complete protease inhibitors (Roche, Basel, Switzerland) and analyzed by western blotting, or plated on 18-mm glass coverslips pre-coated with poly-L-lysine (Thermo Fisher Scientific, Waltham, Massachusetts) for immunostaining, or plated on 35-mm glass-bottom four micro-well separation dishes (Greiner, Kremsmunster, Austria) for time-lapse microscopy.

2.3.3 Transfection and RNA Interference

Transfection of siRNAs (Table 2.1) was performed using JetPrime (Polyplus, Illkirch, France) as per the manufacturer's protocol. Sixteen hours prior to transfection, the cells were seeded at 80% confluence. For TRAPPC12 knockdown, cells were incubated with 20nM siRNA for 24 hours. For TRAPPC11, TRAPPC8, TRAPPC2, ATG9A, WIPI4 and ATG2 knockdowns the cells were transfected with 20nM siRNA on day 1, passaged 1:2 on day 2, and re-transfected with siRNA on day 3. The rescue experiments in HeLa cells were performed using siRNA resistant BirA-FLAG-C11 and C11-FLAG-BirA. HeLa cells at 80% confluence were transfected with 20nM TRAPPC11 siRNA, passaged after 24 hours to 50% confluence on a 10-cm dish and transfected with 20nM TRAPPC11 siRNA and 10 μg of DNA. The cells were harvested after 48 hours and processed for membrane recruitment of ATG2B as described below. The constructs used in the rescue experiment in primary fibroblasts were introduced into the cells by electroporation using the Neon Transfection System (Thermo Fisher Scientific, Waltham, Massachusetts). In this case, 1 μg of DNA was used per transfection and the cells were subjected to 1600 V for 20 mseconds, single pulse.

2.3.4 Time-lapse Microscopy

For live-cell imaging, HeLa cells stably expressing mRFP-GFP-LC3 were plated in 35-mm glass-bottom dishes. Time-lapse microscopy was performed after transfection using a 60Å~ (NA 1.4) or 100Å~ (NA 1.46) oil immersion objective, no binning, on an inverted confocal microscope (Live Scan Swept Field; Nikon, Tokyo, Japan), Piezo Z stage (Nano- Z100N; Mad City Labs, Inc., Madison, Wisconsin), and an electron multiplying charge-coupled device camera (512 Å~ 512; iXon X3; Andor Technology, Belfast, United Kingdom). The microscope was equipped with an environmental chamber heated to 37°C with 5% CO2. Images were acquired with NIS-Elements Version 4.0 acquisition software every 10 minutes using a 0.2 second exposure at 0.3 μm increment sizes. Images were deconvolved with AutoQuant X3 software (Media Cybernetics, Rockville, Maryland) and analyzed on Imaris version 7.6 (Bitplane, Belfast, United Kingdom) and ImageJ (National Institutes of Health). For measuring the fusion of autophagosomes a Zeiss LSM 880 Airyscan microscope with a 100Å~ (NA 1.4) oil immersion objective was used. Images were acquired every 20 seconds for 15 minutes at 0.3 μm increment sizes. The vesicles were tracked over time and the intensities of GFP and RFP were measured using Imaris.

2.3.5 Immunofluorescence Microscopy

The cells were gently washed with PBS then fixed with 4% paraformaldehyde (PFA) for 20 minutes at room temperature, quenched with 0.1 M glycine for 10 minutes and permeabilized with 0.1% Triton X-100 for 7 minutes. The cells were then blocked in 5% normal goat serum (Cell Signaling Technology, Danvers, Massachusetts) in PBS for 40 minutes at room temperature. Primary antibodies (Table 2.2) were diluted in 5% normal goat serum and were added to coverslips and incubated for 16 hours at 4°C. Cells were then washed three times with PBS for 10 minutes per wash. DAPI was added during the first wash at a final concentration of 0.1 μg/mL. Cross-adsorbed secondary antibodies (Life Technologies, Carlsbad, California; see Table 3) were diluted in 5% normal goat serum in PBS and applied for 1 hour at room temperature. Coverslips were washed three

times with PBS for 10 minutes per wash, mounted with Prolong Gold AntiFade reagent (Life Technologies, Carlsbad, California), and sealed with nail polish. 12-bit images (1024 Å~ 1024-pixel resolution) were recorded on an Olympus Fluoro View Confocal Laser Scanning microscope. The images were acquired with a 0.3 μm increment size.

2.3.6 Western Blotting

Samples (7 μg total protein for LC3 analysis or 30 μg total protein for all other proteins) were analyzed on either 8% or 15% SDS polyacrylamide gels. The proteins were transferred to nitrocellulose membranes (BioRad, Hercules, California) for ATG2B or polyvinylidene difluoride (PVDF) membrane (Millipore, Burlington, Massachusetts) for all other proteins for 1 hour at 100 V. Membranes were blocked with 5% skimmed milk powder in PBS-T (PBS with 0.1% Tween 20 [vol/vol]) for 1 hour. The primary and secondary antibodies used, and their dilutions, are listed in Table 2.2. Primary antibodies were incubated in PBS-T overnight and secondary antibodies were incubated for 1 hour. Membranes were then incubated with ECL reagent (GE Healthcare, Chicago, Illinois) and detected using an Amersham Imager 600.

2.3.7 Immunoprecipitation

HeLa cells (10^7 cells/10 cm dish) were washed twice with PBS and lysed in 1 mL of ice-cold RIPA buffer (10 mM Tris-Cl pH 8.0, 1 mM EDTA, 1% Triton X-100, 0.1% sodium deoxycholate, 140 mM NaCl, Complete protease inhibitors (Roche, Basel, Switzerland)). The lysate was clarified at 14000Å~g in a precooled microcentrifuge for 15 minutes. A total of 500 μg of lysate was incubated with 30 μL of protein A-agarose beads (50% slurry) (Bioshop Canada) at 4°C for 30 minutes on an orbital shaker. The agarose beads were removed by a brief centrifugation at 5000 rpm in a refrigerated microfuge for 30 seconds. The cleared lysate was incubated overnight at 4°C with 10 μg of TRAPPC11 antiserum. Immune complexes were captured by adding 30μL protein A-agarose bead slurry (blocked with 5% BSA in PBS-T) and gently rocking on an orbital shaker overnight at 4°C. The beads were collected by a brief centrifugation at 5000 rpm in a

refrigerated microfuge for 30 seconds and washed 3 times with 1 mL ice-cold PBS-T. The beads were resuspended in 60 µL 2Å~ Laemmli sample buffer and heated at 95°C for 5 minutes to dissociate the immunocomplexes. The beads were pelleted by centrifugation and SDS-PAGE was performed with the supernatant fraction.

2.3.8 Subcellular Fractionation and Proteinase K Treatment

Subcellular fractionation and treatment of lysates with proteinase K was performed essentially as described in (Velikkakath et al., 2012). Briefly, cells were seeded at full confluence on six-well dishes. HeLa cells were treated with siRNA as indicated in the figure and were cultured in either DMEM with 10% FBS (non-starved) or EBSS containing 200 nM Bafilomycin A1 for 2 hours (starved and autophagosome lysosome fusion-impaired). Cells were then collected and homogenized in 250 µL homogenization buffer (10 mM 4-(2-hydroxyethyl)-1-piperazineethanesulfonic acid [HEPES]-KOH pH 7.4, 0.22 M mannitol, 0.07 M sucrose, and protease inhibitors) by 10 cycles using a syringe with a 27 gauge needle. The post-nuclear supernatant was obtained by centrifugation at 300Å~g for 5 minutes in a refrigerated microfuge. A total of 150 µg of PN was further centrifuged at 7700Å~g for 5 minutes in a refrigerated microfuge to generate the low-speed pellet (LP). The resulting supernatant was centrifuged at 100000Å~g for 30 minutes in a table-top ultracentrifuge in a TLA100 rotor to generate a high-speed pellet (HP) and a high speed supernatant (HS). The LP and HP were resuspended in the same volume of homogenization buffer. To analyze the integrity of the membranes, the LP and HP (250 µL) were either left untreated or incubated with 100 µg/mL proteinase K (Invitrogen, Carlsbad, California) with or without 1% Triton X-100 on ice for 30 minutes. All samples (LP, HP and HS) were precipitated by incubating in 10% trichloroacetic acid (TCA) on ice for 30 minutes, washed with ice-cold homogenization buffer and resuspended in 1X Laemmli sample buffer. The resulting sample was then heated to 95°C for 5 minutes and analyzed by SDS-PAGE followed by western analysis for the indicated proteins. Primary fibroblasts were processed as described for the HeLa cells.

2.3.9 ATG2 Recruitment Assay

Cells were seeded at full confluence on 10 cm dishes and mechanically lysed as described above. A PN was produced as described above and a total of 500 µg of PN was centrifugated at 7700Å~g for 30 minutes to generate the LP. The resulting supernatant fraction was centrifuged at 100000Å~g for 2 hours in a table-top ultracentrifuge in a TLA100 rotor to generate HP and HS fractions. The LP and HP were washed with ice-cold homogenization buffer to remove all traces of non-membrane-bound proteins and resuspended in 1X Laemmli sample buffer. The HS was precipitated with TCA as above, washed with homogenization buffer and resuspended in sample buffer. Samples were heated to 95°C for 5 minutes prior to western analysis.

2.3.10 Proximity Biotinylation (BioID)

The Flp-In/T-REx 293 cell line from Life Technologies was used to generate BioID cell lines with BirA fusion proteins (Roux et al., 2012). Parental cells were seeded in a 10 cm dish with 15ug/mL blasticidin 1 day before transfection to obtain 70% confluency on the day of transfection. Transfections were performed using Jetprime (Polyplus, Illkirch, France) containing 1.5 µg BirA construct (C11-BirA or BirA-C11 in pDEST_pcDNA5_BirA-FLAG_C-term or pDEST_pcDNA5_BirA-FLAG_N-term, respectively, produced by Gateway cloning) and 13.5 µg pOG44. Transfected cells were incubated in a 37°C incubator for 24 hours before changing the medium with fresh antibiotic-free DMEM containing 10% FBS. The following day, cells were passaged at 1:4 dilution (~25% confluence) onto two 10 cm dishes in medium containing 100 µg/mL hygromycin and 15 µg/mL blasticidin. The medium was changed every 2 to 3 days during the 2-week selection until colonies were visible. The colonies were pooled to obtain a polyclonal cell line, which was expanded in medium containing hygromycin and blasticidin. Two control cell lines were generated with pDEST_pcDNA5_BirA-FLAG_N-term or pDEST_pcDNA5_BirA-FLAG_C-term plasmids followed by selection as described above. To obtain purified TRAPPC11-interacting proteins, BirA-C11 and C11-BirA cell lines were grown in 15 cm dishes. At 60% confluency, they were treated

with 50 ng/mL tetracycline for 16 hours at which time the medium was changed and supplemented with 20% FBS, 50 ng/mL tetracycline and 50 μM biotin. After 8 hours, cells were pelleted and lysed in ice-cold RIPA buffer (50 mM Tris pH 7.4, 150 mM NaCl, 1% NP-40, 0.5% sodium deoxycholate, 0.1% SDS, 1 mM EDTA) supplemented with complete-mini protease inhibitor cocktail (Roche, Basel, Switzerland), 1 mM PMSF, 62.5 Units/ml benzonase, and incubated at 4°C for 1 hour. Samples were sonicated in a 4°C ice bath (4 bursts of 10 seconds on low power). After sonication, samples were centrifuged at 4°C for 30 minutes at 13200 rpm in a refrigerated microfuge. Supernatants were incubated with 14 μL streptavidin-Sepharose beads (Sigma) per dish at 4°C for 3 hours to capture the denatured biotinylated proteins. After the incubation, beads were washed five times with RIPA and four times with low detergent buffer (25 mM Tris pH 7.4, 100 mM NaCl, 0.025% SDS). Following the last wash, beads were pelleted and analyzed by mass spectrometry as previously described (Brunet et al., 2016) to identify proteins captured by the BioID purification. Data were analyzed using Scaffold 4 proteomic software.

Table 2.1 List of siRNAs used in this study

Targeted gene	Sense sequence (5′→3′)	Source
TRAPPC2	UCCAUUUUAUGAACCCAAUTT	Life Technologies
TRAPPC8	CAGCUCUCCUAAUACGGUUTT	Life Technologies
TRAPPC11	GGAUUUAUAAACUACAAGGATT	Life Technologies
TRAPPC12	CGGACAAGCUGAACGAACATT	Life Technologies
ATG2A	GCAUUCCCAGUUGUUGGAGUUCCUA	Life Technologies
ATG2B	AGGUCUCUCUUGUCUGGCAUCUUUA	Life Technologies
WDR45/WIPI4	CCAGTGATAAGGGTACTGTCCATAT	Life Technologies
ATG9A	CCAGAACUACAUGGUGGCACUGGUU	Life Technologies

Table 2.2 List of antibodies used in this study

Antigen	Type	Host	IF dil	WB dil	Size (kDa)	Source	Catalog
TRAPPC2	P	r	N/A	1:1000	16	Sacher L	N/A
TRAPPC8	P	r	N/A	1:500	160	Abcam	Ab122692
TRAPPC10	M	m	N/A	1:1000	130	Abnova	H00007109-M01
TRAPPC11	P	r	N/A	1:1000	129	Sacher L	N/A
TRAPPC12	P	r	N/A	1:2500	78	Sacher L	N/A
Tubulin	M	m	N/A	1:5000	50	Sigma-Aldrich	T6199
LC3	P P	r m	1:300 1:100	1:2500 1:1000	15/17 15/17	Abcam Santa Cruz	ab51520 sc-398 822
p62 (SQSTM)	P	r	N/A	1:2500	48	Abcam	ab155686
ATG2B	P	r	1:500	1:1000	240	Abcam	ab116215
ATG12∗	M	m	N/A	1:1000	55	Santa Cruz	sc-271 688
WDR45/WIPI4	M P	M r	1:100 1:100	1:1000 1:1000	40 40	Santa Cruz Aviva	sc-398 272 OAAB09622
ATG9A	M	r	1:300	1:1000	95	Abcam	ab108338
FLAG	M	m	1:300	1:5000	N/A	Sigma-Aldrich	F3165
Cathepsin B	M	m	N/A	1:1000	24-31	Abcam	ab58802
LAMP1	P	r	1:300	N/A	N/A	Abcam	ab24170
GFP	M	m	1:200	N/A	N/A	11 814 460 001	Sigma-Aldrich
Alexa Fluor 488 anti–Rabbit	HCA	g	1:500	N/A	N/A	A-11034	Life Technologies
Alexa Fluor 488 anti–mouse	HCA	g	1:500	N/A	N/A	A-11029	Life Technologies
Alexa Fluor 568 anti–Rabbit	HCA	g	1:500	N/A	N/A	A-11036	Life Technologies
Alexa Fluor 568 anti–mouse	HCA	g	1:500	N/A	N/A	A-11031	Life Technologies
Alexa Fluor 647 anti–mouse	HCA	g	1:500	N/A	N/A	A-21235	Life Technologies

IF, immunofluorescence, g, goat; HCA, highly cross-adsorbed; M, monoclonal; m, mouse; N/A, not applicable; P, polyclonal; r, Rabbit; WB, western blot.
∗molecular size of the ATG12-ATG5 conjugate

2.4 Results

2.4.1 Depletion of TRAPP III Proteins Affects Autophagic Flux

To begin to address the role of TRAPP III proteins in autophagy, we first examined the appearance of the autophagy-specific form of endogenous LC3 (LC3-II) in HeLa cells depleted of TRAPP III proteins by small interfering RNA (siRNA) (Figure 2.1A and Figure S1.1A). While control cells showed an increase in LC3-II levels after 2 hours of starvation that decreased by 4 hours, cells that were depleted of TRAPPC11 showed elevated levels of LC3-II prior to starvation and the increased levels persisted over the 4 hour time course of starvation. Similar results were seen for TRAPPC12-depleted cells. In contrast, and as previously reported (Behrends et al., 2010; Imai et al., 2016), TRAPPC8 depletion blocked the formation of LC3-II, consistent with TRAPPC8 functioning upstream of both TRAPPC11 and TRAPPC12. A similar result was noted for TRAPPC2-depleted cells, the core TRAPP subunit that acts as an adaptor for TRAPPC8 (Brunet et al., 2013; Zong et al., 2011). The cells also contain mRFP-GFP-LC3 and we monitored them for the number of GFP-positive structures during starvation (Figure 2.1B and C). Consistent with the results in Figure 2.1A, both TRAPPC11- and TRAPPC12-depleted cells had a large number of GFP-positive punctae prior to starvation that did not significantly change over the 4 hours of starvation. TRAPPC8- and TRAPPC2-depleted cells did not show any starvation-dependent increase in the number of GFP-positive punctae compared to control cells. We then examined the formation of autolysosomes upon depletion of the TRAPP III proteins in the mRFP-GFP-LC3 cell line. Fusion of autophagosomes with lysosomes ultimately results in quenching of the GFP fluorescence in the more acidic environment, resulting in red punctae. If fusion is blocked, both a red and green (yellow) punctum is seen (Kimura et al., 2007). As shown in Figure 2.1D and quantified in Figure 2.1E, prior to starvation, control cells have few punctae, some of which are red. Upon starvation, there is a large increase in these structures and a large portion of them are red, indicating that autolysosome formation has taken place. Formation of autolysosomes was blocked by the inclusion of Bafilomycin A1, resulting in yellow punctae. In contrast to the control, when either TRAPPC11 or TRAPPC12 was

depleted, we observed a large number of yellow but few red punctae both prior to and following starvation even in the absence of Bafilomycin A1, indicating that these structures have not fused with lysosomes. Depletion of TRAPPC8 resulted in substantially fewer punctae, consistent with a defect in autophagosome formation. Defective autolysosomes formation in TRAPPC11- and TRAPPC12-depleted cells was also seen by examining the lifetime of the GFP-LC3 fluorescence (Figure S1.1B). Individual punctae were monitored over a 120 second time frame and the intensity of the GFP fluorescence, which is a measure of autophagosome-lysosome fusion, was assessed. While the majority of punctae in control cells showed a fluorescence intensity of 20% of the initial (t = 0) intensity or lower, the majority of the punctae in both TRAPPC11- and TRAPPC12-depleted cells were between 30% and 50% of the initial intensity, consistent with a defect in autophagic flux. In addition, the diameter of these structures in TRAPPC11-depleted cells was larger than those seen in control cells (Figure S1.1C). Although the diameter of the structures in TRAPPC12-depleted cells was similar to that of control cells, we noted a population of punctae that were larger in diameter. The reason for these larger structures is unknown. We then assessed the ability of HeLa cells to clear autophagosomes that were formed in the presence of the autophagosome-lysosome fusion inhibitor Bafilomycin A1. Cells were starved for 2 hours in the presence of the inhibitor and then transferred to nutrient-rich medium for up to 40 minutes and the effect on LC3-II was monitored throughout (Figure 2.1F). In control cells, LC3-II was highest following treatment with Bafilomycin A1, and was then rapidly cleared by the 40 minute time point. In contrast, both TRAPPC11- and TRAPPC12-depleted cells did not show any significant clearance of the Bafilomycin A1-induced LC3-II. In TRAPPC8-depleted cells, we were unable to detect significant levels of LC3-II. Collectively, our data suggest that the TRAPP III proteins TRAPPC11, TRAPPC12 and TRAPPC8 are involved in autophagic flux, but the former two may be acting downstream of TRAPPC8.

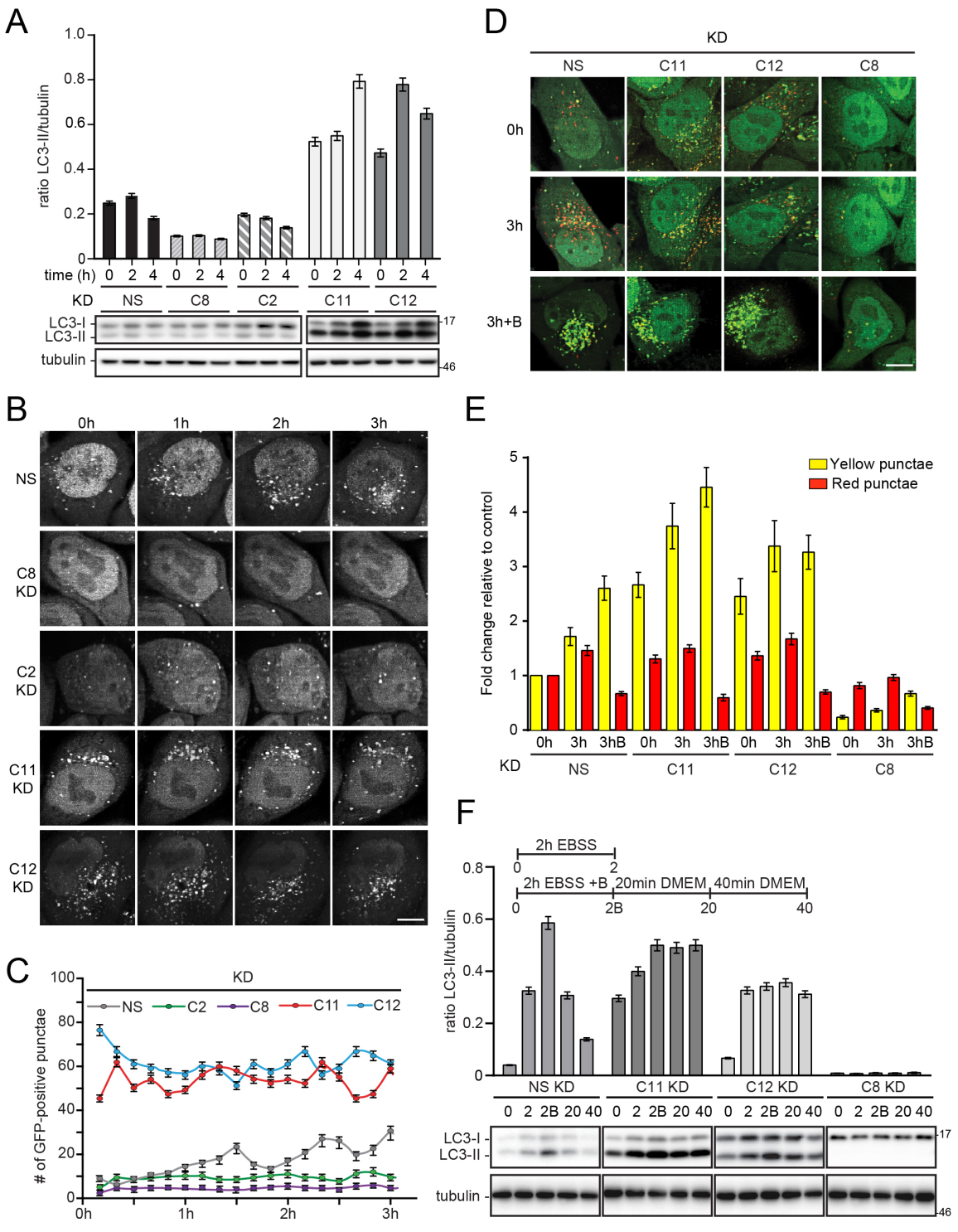

Figure 2.1 Depletion of TRAPPC11 affects autophagic flux

(A) HeLa cells expressing mRFP-GFP-LC3 were subjected to a knockdown with either non-specific (NS) small interfering (siRNA), or siRNA targeting TRAPPC2, TRAPPC8, TRAPPC11 or TRAPPC12. The cells were then placed in starvation (EBSS) medium for the indicated time (in hours). At each time point, lysates were prepared, fractionated on

an SDS-polyacrylamide gel, transferred to PVDF and probed for endogenous LC3 and tubulin. The resulting bands were quantified using Image J and plotted as the ratio of LC3-II to tubulin. Results reflect data from three separate experiments with SEM indicated. Representative immunoblots are shown below the graphs. (B, C) HeLa cells stably expressing mRFP-GFP-LC3 were treated as in panel (A), transferred into starvation (EBSS) medium and imaged every 10 minutes for three hours. GFP-LC3-positive structures were counted using Imaris software and plotted in Graphpad Prism. A total of 10 cells were quantified at each time point in (C). The times above the panels in (B) indicate the time in starvation (EBSS) medium. (D) HeLa cells stably expressing mRFP-GFP-LC3 were left untreated or treated with siRNA as in (A). The cells were then either left in nutrient-rich (DMEM) medium or transferred to starvation (EBSS) medium for 3 hours either with or without 200 nM Bafilomycin A1. Panels from the merged GFP and RFP channels are shown. (E) Quantification of the red (autolysosome) and yellow (isolation membrane or autophagosome) punctae from panel (D) was performed on a minimum of 10 cells. The error bars indicate SEM. (F) HeLa cells were treated as in (A). One sample also received 200 nM Bafilomycin A1 for 2 hours (2B). The Bafilomycin A1-treated cells were then transferred into fresh nutrient-rich (DMEM) medium for up to 40 minutes. Lysates were prepared and processed for western analysis and representative immunoblots are shown below each graph. The scale bars in panels (B) and (D) are 20 μm. Numbers to the right of immunoblots denote the migration of molecular size standards in kD. The extent of each of the knockdowns is shown in Figure S1.1.

2.4.2 TRAPPC11 Interacts with ATG2B-WIPI4

Given the involvement of TRAPPC11 in disease, we decided to focus on this protein to better understand its role in human health. We employed a biotin proximity ligation screen (BioID) to identify interacting partners that might help to elucidate the role of TRAPPC11 in autophagy (Roux et al., 2012). The screen was performed with both an amino- and carboxy-terminal fusion protein of TRAPPC11 with the BirA biotin ligase (BirA-C11 and C11-BirA, respectively), and it was done two times to verify the accuracy of the partners identified. As expected, a number of TRAPP III subunits were identified including TRAPPC8, TRAPPC12 and TRAPPC13 (Table 2.3). Interestingly, peptides for both TRAPPC8 and TRAPPC13 were identified more robustly with the C11-BirA construct compared with BirA-C11, suggesting that these proteins may interact with the amino-terminus of TRAPPC11. Strikingly, besides TRAPPC11 itself, peptides derived from the autophagy protein ATG2B were the most abundant identified. These peptides were nearly all detected using the BirA-C11 construct, suggesting that ATG2B interacts with the carboxy-terminus of TRAPPC11. We also identified peptides from WIPI4, a

protein that forms a complex with ATG2B. Like ATG2B, these peptides were preferentially identified by the BirA-C11 construct (Table 2.3).

Table 2.3 Proteins identified and corresponding peptide count in a proximity biotinylation screen with TRAPPC11

* also known as WIPI4

Protein	Total peptides				Unique peptides			
	BirA-C11		C11-BirA		BirA-C11		C11-BirA	
	Trial#1	Trial#2	Trial#1	Trial#2	Trial#1	Trial#2	Trial#1	Trial#2
TRAPPC2L	19	17	3	8	5	5	2	4
TRAPPC8	4	6	15	23	4	6	12	19
TRAPPC11	**384**	**432**	**68**	**164**	**58**	**58**	**33**	**45**
TRAPPC12	12	12	14	19	9	8	11	12
TRAPPC13	1	0	11	17	1	0	7	11
ATG2B	**110**	**128**	**1**	**2**	**59**	**58**	**1**	**2**
WDR45*	**21**	**23**	**0**	**1**	**11**	**10**	**0**	**1**

Cell lines stably expressing BirA-TRAPPC11 (BirA-C11) or TRAPPC11-BirA (C11-BirA) were generated in Flp-In T-Rex 293 cells. The cell lines and controls (just expressing BirA) were treated with tetracycline to induce expression of the BirA constructs and supplemented with biotin. Lysates were prepared, the biotinylated proteins were captured on streptavidin-agarose beads and processed for mass spectrometric analysis. The experiment was performed on two separate occasions and the number of total peptides and unique peptides was quantified. Note that in all cases except for ATG2B in C11-BirA the background was 0 peptides. In the stated exception, the background exceeded the experimental case.

We next examined whether TRAPPC11 depletion in HeLa cells results in a similar phenotype to ATG2 and WIPI4 depletion. Note that both ATG2 paralogues, ATG2A and ATG2B, were depleted because a previous study showed that these proteins may have a redundant function (Velikkakath et al., 2012). When compared with control, the TRAPPC11, ATG2 and WIPI4 depletions showed elevated levels of LC3-II prior to starvation (Figure 2.2A and quantified in Figure S2.2). These levels increased slightly during starvation. The phenotype was not further exaggerated by a double TRAPPC11/ATG2 or TRAPPC11/WIPI4 depletion, or by a triple TRAPPC11/ATG2/WIPI4 depletion. A similar result was seen for depletion of

TRAPPC12, but depletion of TRAPPC8 did not result in detectable levels of LC3-II consistent with our earlier result (Figure 2.2F). The latter phenotype was similar to that of depletion of ATG9A, a protein that acts early in autophagy and blocks formation of isolation membranes (Orsi et al., 2012). Using HeLa cells expressing mRFP-GFPLC3, we found that, as previously reported (Velikkakath et al., 2012), ATG2 depletion resulted in an increased number of GFP-LC3 punctae that were generally larger in size compared to those in control cells and were seen even prior to starvation (Figure 2.2B and C). These structures persisted over a 5-hour starvation period. A similar phenotype was noted upon depletion of either of TRAPPC11, TRAPPC12 or WIPI4. In contrast, the phenotype resulting from depletion of TRAPPC8 was similar to that of ATG9A depletion where few if any GFP-positive punctae were seen. It was previously shown that many of the LC3-positive punctae that result from ATG2 depletion are also positive for autophagy proteins that are components of functional complexes including ULK1, WIPI1, ATG5, ATG14 and ATG9 (Velikkakath et al., 2012). Similarly, we found that depletion of TRAPPC11 and WIPI4 also result in LC3-positive structures that co-localize with these early-acting autophagy proteins (Figure 2.2D). Therefore, by several different criteria we find that depletion of TRAPPC11 phenocopies that of either ATG2 or WIPI4.

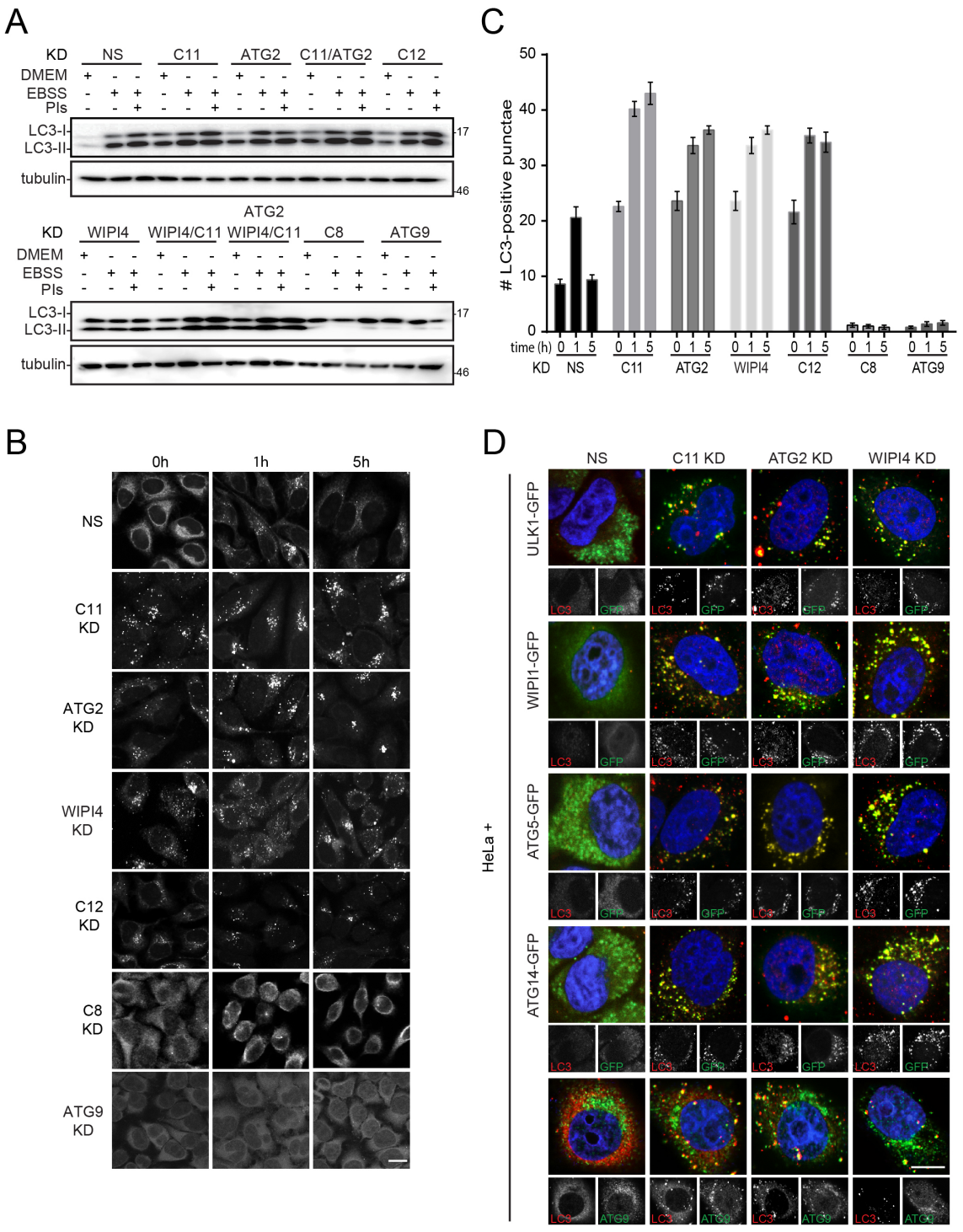

Figure 2.2 TRAPPC11 depletion phenocopies an ATG2B or WIPI4 depletion.

(A) HeLa cells were treated with non-specific (NS) siRNA or siRNA targeting either TRAPPC11, TRAPPC12, TRAPPC8, ATG2A and ATG2B (ATG2), WIPI4, ATG9A, both TRAPPC11 and ATG2 or WIPI4, or siRNA targeting the three transcripts

TRAPPC11, ATG2 and WIPI4. The cells were left in nutrient-rich (DMEM) medium or transferred into starvation (EBSS) medium for 2 hours with or without the protease inhibitors E64d and pepstatin A. Lysates were prepared and the levels of LC3 and tubulin were detected by western analysis. (B) HeLa cells were treated with non-specific (NS) siRNA or siRNA targeting the indicated transcripts. The cells were then transferred to starvation (EBSS) medium for the times indicated. The cells were then fixed and stained with anti-LC3 antibody. (C) The number of LC3-positive punctae in panel (B) were quantified using Imaris from deconvoluted images and plotted. A total of 25 cells at each time point were used in the quantification. Error bars indicate SEM. (D) HeLa cells or HeLa cells expressing GFP-tagged ULK1, WIPI1, ATG5 or ATG14 as indicated in the figure were treated with non-specific (NS) siRNA or siRNA targeting either TRAPPC11, ATG2 or WIPI4. The cells were then stained for LC3 or, in the case of HeLa cells, LC3 and ATG9A. Endogenous GFP fluorescence or ATG9A fluorescence was imaged and overlayed onto the LC3 fluorescent signal. The scale bars in (B) and (D) represent 20 μm. Numbers to the right of the immunoblots denote the migration of molecular size standards in kD.

2.4.3 Depletion of TRAPPC11 Results in Unsealed Isolation Membranes

Because ATG2 proteins function prior to the sealing of isolation membranes into enclosed autophagosomes (Kishi-Itakura et al., 2014; Velikkakath et al., 2012), we employed a protease protection assay to determine whether TRAPPC11 depletion also affected this step of autophagy. This assay faithfully reports the state of the isolation membranes in both mammalian and lower eukaryotic systems (Klionsky et al., 2016; Velikkakath et al., 2012; Zhou et al., 2017). Following depletion, HeLa cells were either left in nutrient-rich medium or subjected to starvation for 2 hours in the presence of Bafilomycin A1, after which various membrane fractions were collected. The membranes were either untreated, treated with proteinase K, or solubilized in Triton X-100 before proteinase K treatment (Figure 2.3A). In control cells under nutrient-rich conditions, LC3 (in the form of LC3-I) was mostly in the supernatant fraction (HS). Upon starvation, LC3-II was formed and largely found in the low-speed membrane fraction (LP). The protein in both the LP and the high-speed membrane fractions (HP) were resistant to proteinase K treatment but could be digested if the membranes were first solubilized with detergent, suggesting that autophagosomes were formed. In contrast, TRAPPC11-depleted cells under nutrient-rich conditions showed LC3-II in both the LP and HP membrane fractions, consistent with the presence of abundant LC3-positive structures prior to starvation. These pools of LC3-II were sensitive to proteinase K in the absence of

detergent, suggesting that the LC3-II on the membranes is completely exposed to the surroundings. The same result was observed upon starvation of the TRAPPC11-depleted cells. The results in the TRAPPC11-depleted cells were similar to those seen for either ATG2- or WIPI4-depleted cells. In contrast, while LC3-II was detected both prior to and following starvation in TRAPPC12-depleted cells, this form of LC3 was resistant to proteinase K treatment in the absence of detergent, suggesting that autophagosome formation has occurred in the absence of TRAPPC12. In order to confirm that TRAPPC12 functions downstream of both ATG2 and TRAPPC11, the assay was performed following TRAPPC11/TRAPPC12 and ATG2/TRAPPC12 double depletions. In both cases, LC3-II was sensitive to proteinase K treatment in the absence of detergent (Figure 2.3B), supporting the notion that both ATG2 and TRAPPC11 function upstream of TRAPPC12. Consistent with the near complete absence of presumably LC3-II positive structures following TRAPPC8 depletion, only LC3-I was detected in this assay and this form of the protein did not fractionate in either of the membrane fractions (Figure 2.3A). This was phenotypically similar to what was seen for depletion of ATG9A (Figure 2.3A). Thus, although depletion of either TRAPPC11 or TRAPPC12 results in an increase in the number of LC3-positive cellular structures, only those formed in response to TRAPPC11 depletion are unsealed membranes, similar to those seen upon ATG2 or WIPI4 depletion.

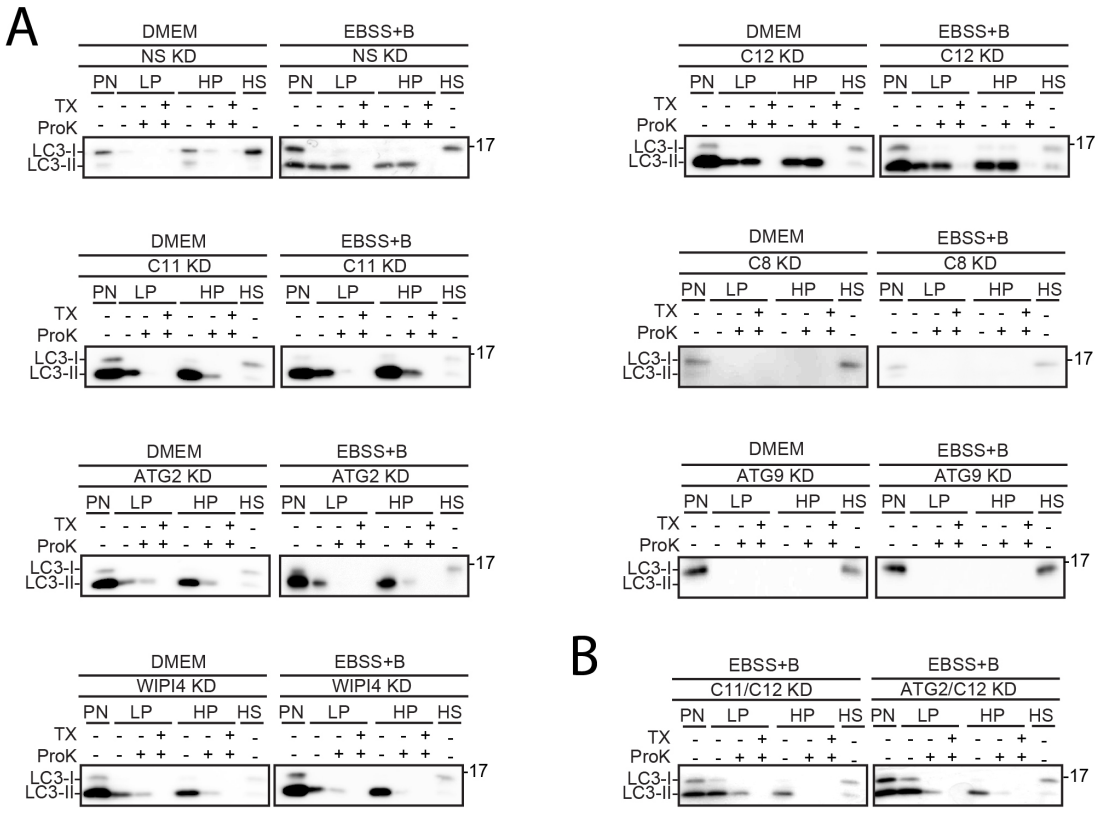

Figure 2.3 Depletion of TRAPPC11 results in unsealed isolation membranes.

HeLa cells were treated with non-specific (NS) siRNA or siRNA targeting either of TRAPPC11, TRAPPC12, TRAPPC8, ATG2, WIPI4 or ATG9A. The cells were left in nutrient-rich medium (DMEM) or transferred to starvation medium (EBSS) for 2 hours in the presence of Bafilomycin A1. Lysates were prepared and processed for the membrane sealing assay as described in Materials and Methods. Prior to fractionation, some samples were treated with proteinase K (ProK) or with ProK in the presence of 1% Triton X-100. The fractions, composed of a postnuclear supernatant, low-speed pellet (LP), high-speed pellet (HP) and high-speed supernatant (HS), were probed for LC3. Note that isolation membranes and autophagosomes appear in the LP and/or HP fractions. Numbers to the right of the immunoblots denote the migration of molecular size standards in kD. (B) HeLa cells were depleted of both TRAPPC11 and TRAPPC12 or of ATG2 and TRAPPC12. The cells were starved for 2 hours in the presence of Bafilomycin A1. Lysates were prepared and processed as described in (A).

2.4.4 Recruitment of ATG2B and WIPI4 to Isolation Membranes is Dependent Upon TRAPPC11

We next investigated whether TRAPPC11 was required to recruit ATG2B and WIPI4 to membranes during starvation. The recruitment was first examined biochemically using

the cell fractionation assay performed in Figure 2.3. In this case, we probed for the presence of ATG2B, WIPI4, TRAPPC11, TRAPPC12 and TRAPPC8. We also included ATG9A and ATG12 as two autophagy proteins that function at different steps compared with TRAPPC11. ATG9A also served as a membrane protein control and in all cases where ATG9A was not the subject of the knockdown, the protein appeared exclusively in the membrane fractions as expected. The recruitment assay was performed in HeLa cells that were unstarved or starved for 2 hours in the presence of Bafilomycin A1. The cells were either untreated or depleted of either one of the TRAPP III proteins, ATG2, WIPI4 or ATG9A (Figure 2.4). Upon depletion of TRAPPC11, less ATG2B and WIPI4 were found in the membrane fractions following starvation when compared with control. In contrast, TRAPPC12 depletion did not affect the membrane association of either ATG2B or WIPI4 following starvation compared with control. Neither TRAPPC11 nor TRAPPC12 depletion affected the recruitment of ATG12 to membranes. In contrast, while TRAPPC8 depletion also affected the recruitment of ATG2B and WIPI4 to membranes, this depletion prevented recruitment of ATG12 to membranes (Figure 2.4), likely due to the absence of isolation membranes. Although depletion of ATG2 prevented recruitment of WIPI4 to membranes, and WIPI4 depletion prevented recruitment of ATG2B to membranes, neither of depletion affected recruitment of any TRAPP III proteins or of ATG12 to membranes (Figure 2.4). As expected, and similar to the TRAPPC8-depleted cells, depletion of ATG9A prevented the recruitment of all proteins examined to membranes, consistent with its role in isolation membrane formation.

We then assessed recruitment of ATG2B and WIPI4 to endogenous LC3 structures in HeLa cells depleted of either TRAPPC11, TRAPPC12 or TRAPPC8 (Figure 2.5A and B). Neither of ATG2B, WIPI4 nor LC3 localize to a substantial amount of punctae in control cells under nutrient-rich conditions. Upon starvation, these cells showed an increased number of LC3, ATG2B and WIPI4 structures, many of which overlap. As shown earlier in HeLa cells (Figure 2.1B and 2.2B), TRAPPC11 depletion resulted in a substantial number of LC3 punctae under nutrient-rich conditions and their numbers increased upon starvation. Importantly, we did not detect a concomitant increase in either of ATG2B or WIPI4 punctae in either nutrient-rich or starved conditions following

depletion of TRAPPC11 (Figure 2.5A and B). This was in contrast to the TRAPPC12-depleted cells where, although there were numerous LC3 structures both prior to and during starvation, there were also numerous ATG2B and WIPI4 punctae co-localizing with LC3. Depletion of TRAPPC8 did not result in LC3-positive structures, nor in ATG2B or WIPI4 punctae, similar to what was seen upon ATG9A depletion (Figure 2.5A and B). We conclude that the presence of ATG2B and WIPI4 on LC3-positive punctae in starved cells is dependent upon TRAPPC11 but not upon TRAPPC12.

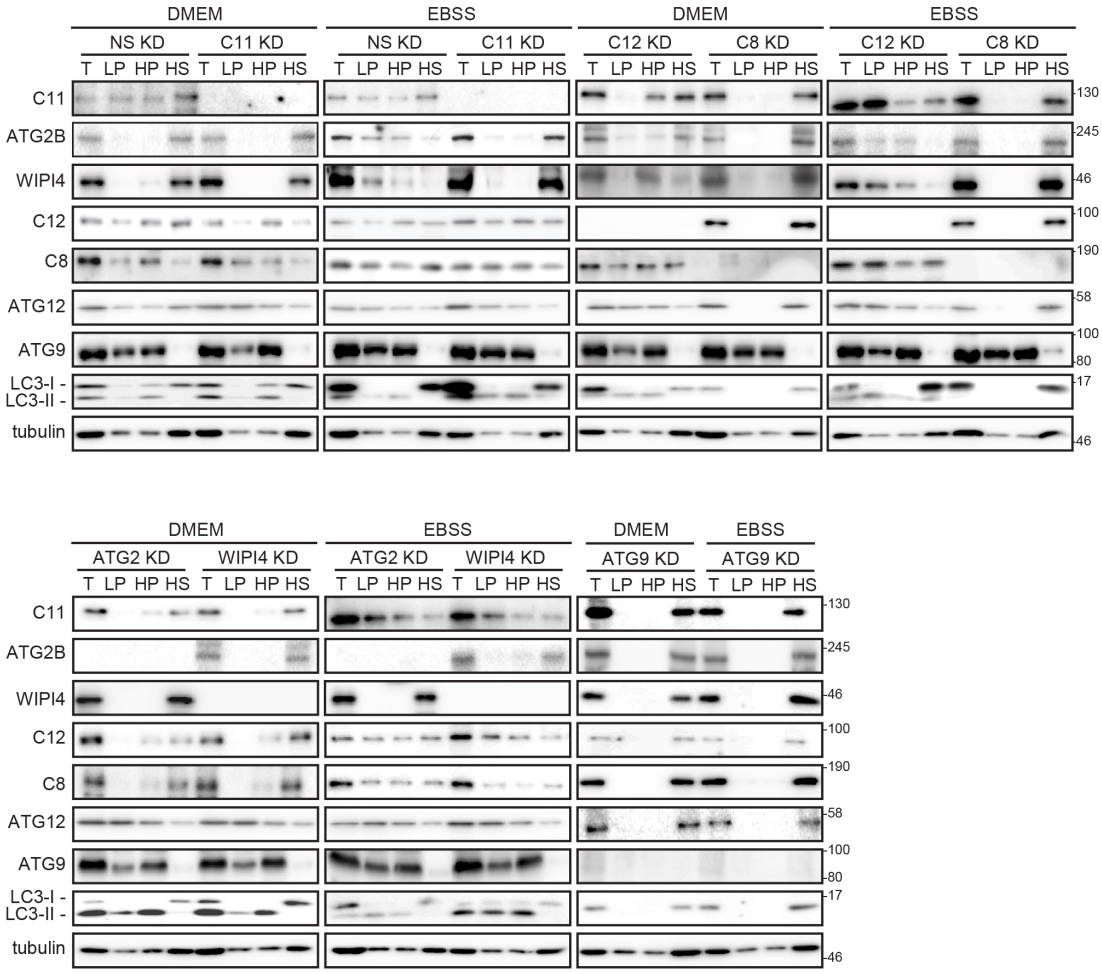

Figure 2.4 ATG2B-WIPI4 recruitment to membranes is impaired by TRAPPC11 depletion.

HeLa cells were treated with non-specific (NS) siRNA or siRNA targeting either TRAPPC11, TRAPPC12, TRAPPC8, ATG2, WIPI4 or ATG9A. Cells were grown in either nutrient-rich (DMEM) or starvation (EBSS) medium for 2 hours. Lysates were prepared and processed for membrane recruitment as described in the Materials and

Methods section. The fractions, composed of a postnuclear supernatant, low-speed pellet (LP), high-speed pellet (HP) and high-speed supernatant (HS), were probed for the indicated proteins. Note that half the amount of tubulin was loaded in the PN fraction in order to obtain an exposure that shows tubulin in the other fractions without grossly overexposing the PN signal. Numbers to the right of the immunoblots denote the migration of molecular size standards in kD.

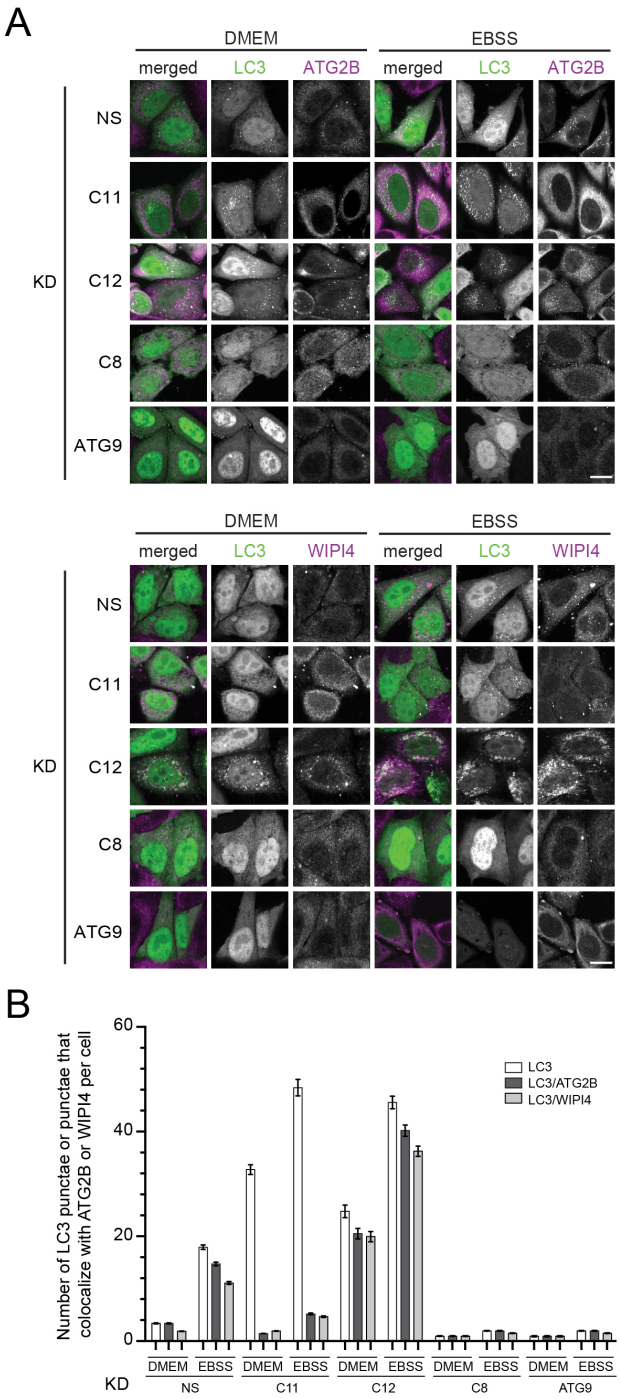

Figure 2.5 Recruitment of ATG2B-WIPI4 to LC3-positive membranes is impaired by TRAPPC11 depletion

(A) HeLa cells were treated with non-specific (NS) siRNA or siRNA targeting either TRAPPC11, TRAPPC12, TRAPPC8 or ATG9A. The cells were grown in nutrient rich (DMEM) or starvation (EBSS) medium for 2 hours at which time the cells were fixed and stained with anti-ATG2B or anti-WIPI4 IgG. (B) The LC3-positive and the ATG2B- or WIPI4-positive punctae in (A) were quantified using Imaris. A total of 25 cells were used

for quantification in each sample. Error bars represent SEM. The scale bar in (A) represents 20 μm.

2.4.5 The TRAPPC11 Interaction with ATG2B-WIPI4 is Dependent Upon ATG9 Function

Our results thus far suggest that TRAPPC11 interacts with ATG2B-WIPI4, a complex that functions upstream of the sealing of isolation membranes into autophagosomes. Consistent with this notion is the fact that the consequences of TRAPPC11 depletion are phenotypically identical to that of either ATG2 or WIPI4 depletion. Suspecting that we might see an enhanced interaction between TRAPPC11 and ATG2B during starvation, we immunoprecipitated TRAPPC11 at various time points following starvation and probed for TRAPP proteins and ATG2B. As expected and reported previously (Bassik et al., 2013; Scrivens et al., 2011), TRAPPC11 co-immunoprecipitated with TRAPPC12, TRAPPC2 and TRAPPC8, but not with the TRAPP II subunit TRAPPC10 (Figure S2.3). Although an interaction with ATG2B was detected, we did not see a starvation-dependent increase in this interaction over time. Rather, there seemed to be a spike in the interaction at the 2-hour time point. The reason for this transient increase is not clear. In yeast, the TRAPP III complex was shown to interact with ATG9 (Kakuta et al., 2012). Another study demonstrated an interaction between yeast ATG2-ATG18 (the ATG2 and WIPI4 homologs, respectively) with ATG9 (Gomez-Sanchez et al., 2018). These studies prompted us to examine whether the interaction between ATG2B-WIPI4 and mammalian TRAPP III also included ATG9A. As shown in Figure 2.6, immunoprecipitation of TRAPPC11 co-precipitated ATG2B and WIPI4, but not ATG9A. However, depletion of ATG9A abrogated the interaction between TRAPPC11 and both ATG2B and WIPI4. Furthermore, depletion of ATG2B prevented WIPI4 from co-immunoprecipitating with TRAPPC11. These results suggest that the TRAPPC11 interaction with ATG2B-WIPI4 is dependent upon ATG9A function and further show that TRAPPC11 does not interact with WIPI4 in the absence of ATG2B.

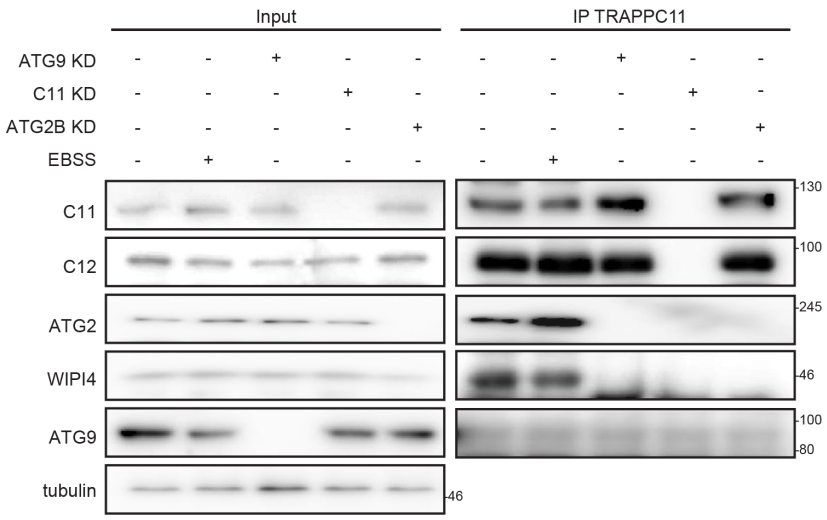

Figure 2.6 The interaction between TRAPPC11 and ATG2B-WIPI4 is regulated by ATG9A.

HeLa cells were treated with non-specific (NS) siRNA or siRNA targeting either TRAPPC11, ATG9A or ATG2. The NS-treated samples were subjected to starvation to induce the formation of isolation membranes. Lysates were prepared and incubated with anti-TRAPPC11 IgG. The total lysates and the immunoprecipitates were probed by western analysis for the presence of TRAPPC11, ATG2B, WIPI4 and ATG9A. Numbers to the right of the immunoblots denote the migration of molecular size standards in kD.

2.4.6 A Portion of TRAPP III Localizes to Isolation Membranes

Our results thus far suggest that a portion of TRAPPC11, and perhaps TRAPP III, localizes to isolation membranes where it interacts with ATG2B-WIPI4. Autophagosome formation follows a maturation process where proteins function sequentially to produce these organelles. Two such proteins that are thought to associate with isolation membranes are ATG5 and WIPI1 (Grimmel et al., 2015). Thus, we used HeLa cells that express GFP-tagged versions of these proteins to assess their colocalization with TRAPP III proteins. Cells were either starved for 0.5 hours in the presence of Bafilomycin A1 to prevent autolysosome formation, or depleted of either ATG2 or WIPI4, conditions that lead to a buildup of isolation membranes (Figure 2.2B). The cells were then immunostained for either TRAPPC8, TRAPPC11 or TRAPPC12 and GFP. As shown in Figure 2.7A, ~10% to 15% of the ATG5 or WIPI1 punctae formed during brief starvation were also positive for the TRAPP III proteins. This percentage increased to ~20% to 25%

following depletion of either ATG2 or WIPI4. A similar increase in TRAPP protein co-localization was seen using an LC3-GFP cell line (Figure S2.4). The co-localization is not likely incidental because (a) overlap was assessed using thin (0.4-1 μm) three-dimensional sections and not flattened images, and (b) TRAPP protein-positive structures decreased in the ATG2 and WIPI4 knockdowns compared with starvation conditions (not shown) yet the co-localization increased during the knockdowns. These co-localization results suggest that a portion of TRAPP III proteins, including TRAPPC11, transiently localize to early autophagic membranes. Knowing that TRAPPC11 localizes to isolation membranes and is thus in proximity to ATG2B-WIPI4, we decided to more formally test the notion that the carboxy-terminus of TRAPPC11 is important for this interaction (see Table 2.3). To this end, we depleted HeLa cells of TRAPPC11 and assessed whether the defective recruitment of ATG2B and WIPI4 could be suppressed by expression of BirA-C11 (a free carboxy-terminus) or C11-BirA (a blocked carboxy-terminus) using the same biochemical membrane recruitment assay as above (Figure 2.4). As shown in Figure 2.7B, depletion of TRAPPC11 prevented the starvation-induced increase in membrane-associated ATG2B and WIPI4 but not that of ATG12, an ATG protein acting at a step upstream of TRAPPC11. Overexpression of BirA-C11 resulted in an increase in membrane associated ATG2B and WIPI4 following starvation, while overexpression of C11-BirA resulted in a much smaller increase. The differences were not due to expression-level differences (Figure 2.7C). These results are consistent with the notion that the carboxy-terminus of TRAPPC11 is important for the recruitment of ATG2B-WIPI4 to isolation membranes.

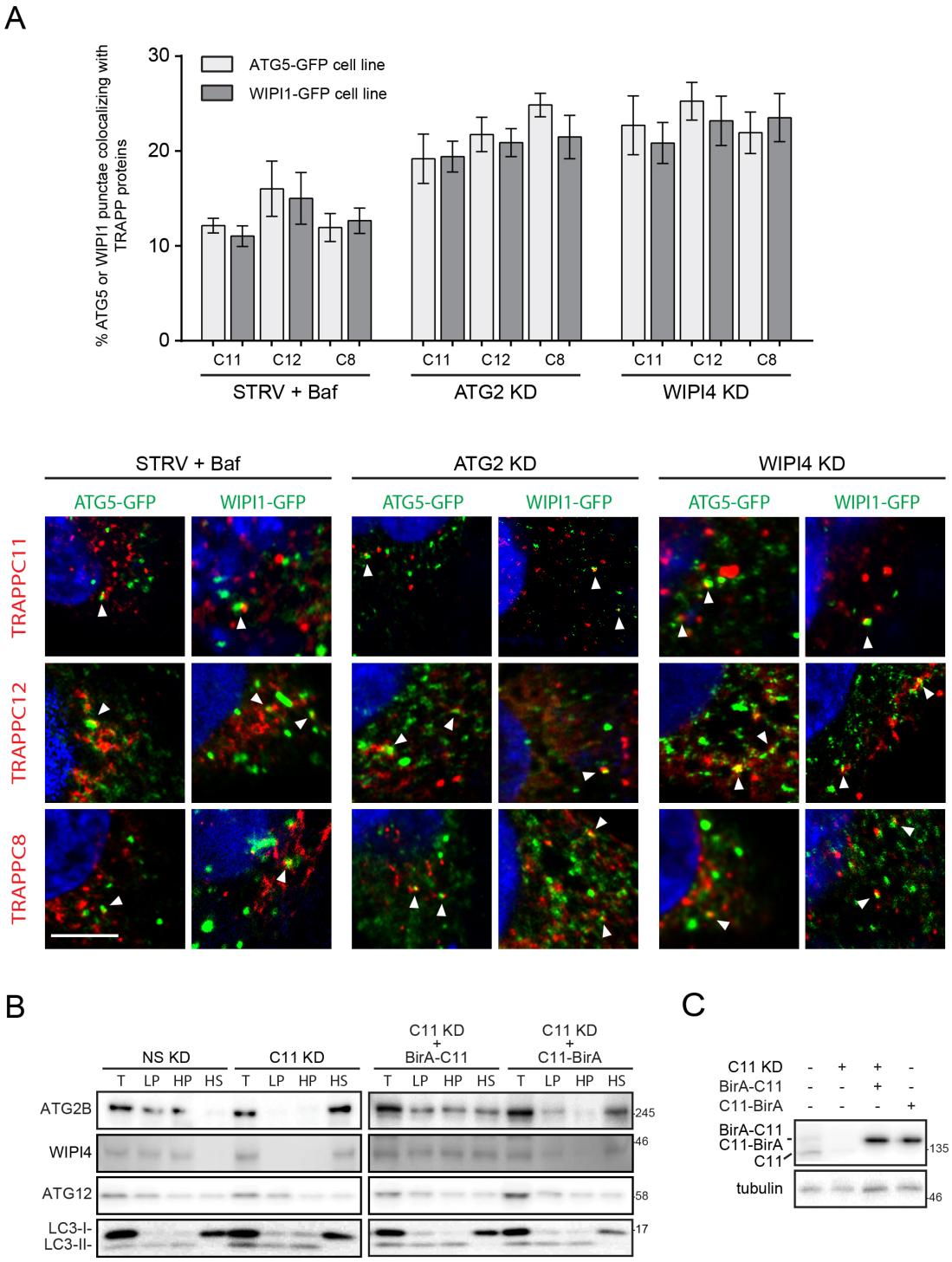

Figure 2.7 A portion of TRAPP III localizes to isolation membranes.

(A) HeLa cells stably expressing either ATG5-GFP or WIPI1-GFP were either starved for 30 minutes in EBSS containing Bafilomycin A1 or treated with siRNA targeting either ATG2 or WIPI4. The cells were then immunostained for one of the TRAPP III proteins (TRAPPC8, TRAPPC11 or TRAPPC12) and GFP. Representative images are

shown below the graph, with examples of co-localizing punctae indicated by a white arrowhead. The co-localization between TRAPP protein- and ATG5- or WIPI1-positive structures was quantified using Imaris and is plotted as the percentage of GFP-positive punctae that were positive for the indicated TRAPP III protein. A minimum of 10 cells were counted and the SEM is indicated. The scale bar represents 5 μm. In non-starved cells there were no visible ATG5-GFP or WIPI1-GFP punctae. (B) HeLa cells were depleted of TRAPPC11 using siRNA. The cells were then left untransfected or transfected with either BirA-C11 or C11-BirA. The cells were subsequently starved for 2 hours in EBSS and the recruitment of ATG2B, WIPI4 or ATG12 to membranes was monitored as described in the Materials and Methods section. (C) Lysate from the non-specific knockdown (lane 1), TRAPPC11 knockdown (lanes 2-4) either untransfected (lane 2) or transfected with either BirA-C11 (lane 3) or C11-BirA (lane 4) were probed with anti-TRAPPC11 antibody to assess expression levels of the BirA-tagged TRAPPC11 constructs. Numbers to the right of the immunoblots denote the migration of molecular size standards in kD.

2.4.7 Fibroblasts from an Individual with TRAPPC11 Mutations Fail to Recruit ATG2B-WIPI4 to Membranes

A number of individuals with TRAPPC11 mutations have now been reported (Bogershausen et al., 2013; Fee et al., 2017; Koehler et al., 2017; Larson et al., 2018; Liang et al., 2015; Matalonga et al., 2017). Because the carboxy-terminus of TRAPPC11 appears to be important for ATG2B-WIPI4 recruitment to membranes (Figures 2.7C and Table 2.3), we examined the fibroblasts from one individual harboring the compound heterozygous mutations p.Ala372_Ser429del and p.Asp1127Valfs*47 in TRAPPC11 (note that a more detailed characterization of this individual will be reported elsewhere) to determine if this newly-identified interaction was physiologically relevant. This individual was chosen because the latter allele results in a frame shift at amino acid 1127, only 6 residues from the carboxy-terminus. We first examined whether these cells displayed a defect in autophagic flux compared with control fibroblasts. Included in this analysis were fibroblasts from a patient with the homozygous p.Glu49Argfs*14 mutation in TRAPPC12 (Milev et al., 2017). Fibroblasts were untreated or starved for 2 hours in the presence of Bafilomycin A1, at which point they were returned to nutrient-rich medium and the appearance/disappearance of LC3-II was monitored. In control fibroblasts, the Bafilomycin A1-dependent increase in LC3-II levels was reverted to near unstarved levels following 40 minutes in nutrient-rich medium (Figure 2.8A). In contrast,

fibroblasts from the TRAPPC11 patient (PatC11) showed elevated levels of LC3-II prior to starvation that did not substantially increase after Bafilomycin A1 treatment. These elevated levels of LC3-II did not diminish upon transfer into nutrient-rich medium. The fibroblasts from the patient with the TRAPPC12 mutation (PatC12) showed a starvation-induced increase in LC3-II levels that were slightly reduced upon transfer to nutrient-rich medium. These results suggest that both PatC11 and PatC12 have a defect in autophagic flux. We then examined the recruitment of ATG2B-WIPI4 by the biochemical fractionation procedure described above (Figure 2.3). While control fibroblasts showed a starvation-induced appearance of ATG2B and WIPI4 in the membrane fractions, PatC11 cells did not (Figure 2.8B). In contrast, PatC12 cells showed ATG2B and WIPI4 in the membrane fraction even prior to starvation. Because reduced recruitment of ATG2B and WIPI4 to membranes could result in unsealed autophagosomes, we employed the protease protection assay to examine this scenario. While the LC3-II-positive membranes in control and PatC12 fibroblasts were largely resistant to proteinase K treatment, those in PatC11 were sensitive (Figure 2.8C).

Finally, we examined the fibroblasts for recruitment of ATG2B and WIPI4 to punctae during starvation. Control fibroblasts showed a starvation-dependent increase in ATG2B and WIPI4 punctae (Figure 2.8D and Figure S2.5A). In contrast, PatC11 fibroblasts did not show such an increase, consistent with a role for TRAPPC11 in ATG2B-WIPI4 recruitment. In PatC12, a large number of ATG2B- and WIPI4-positive punctae were present prior to starvation, suggesting that recruitment of ATG2B-WIPI4 was already taking place in these cells. The defect in starvation dependent ATG2B and WIPI4 punctae formation in PatC11 was due to the TRAPPC11 mutations since this defect was suppressed by wild type TRAPPC11 fused at its amino-terminus, but not fused at its carboxy-terminus, to BirA (Figure 2.8E and Figure S 2.5B). This latter result is consistent with the earlier notion that the carboxy-terminus of TRAPPC11 is important for the recruitment of ATG2BWIPI4. Collectively, our studies on these fibroblasts from an individual with TRAPPC11 mutations suggest that some TRAPPC11 mutations may result in defective recruitment of ATG2B-WIPI4 and dysregulated autophagy.

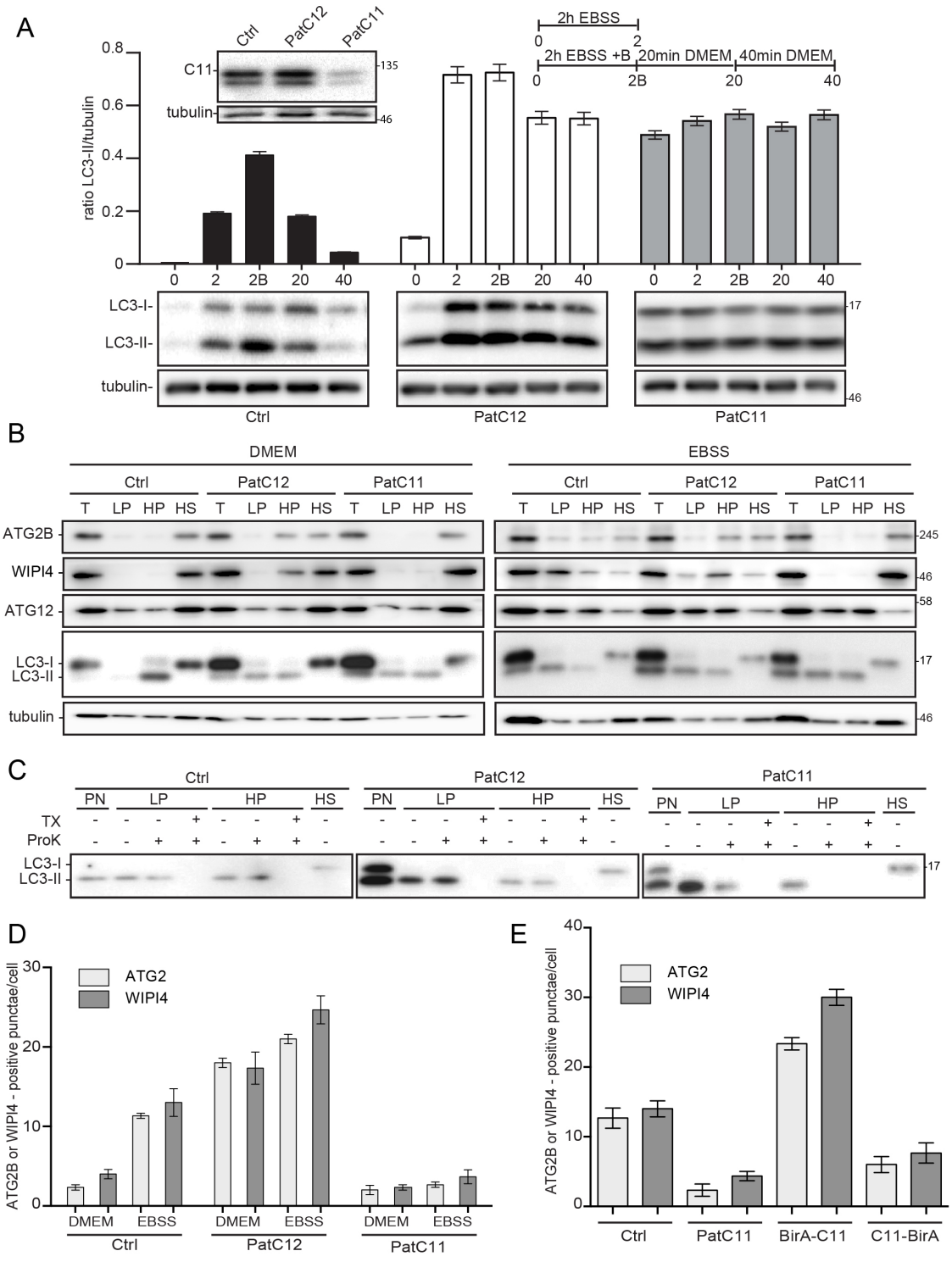

Figure 2.8 Fibroblasts from an individual with TRAPPC11 mutations are defective in ATG2B-WIPI4 recruitment.

(A) Control fibroblasts and fibroblasts derived from patients with bi-allelic TRAPPC12 (PatC12) or TRAPPC11 (PatC11) mutations were transferred into starvation medium with or without Bafilomycin A1 for 2 hours. The Bafilomycin A1-treated cells were then

transferred into fresh nutrient-rich (DMEM) medium for up to 40 minutes. Lysates were prepared and LC3 and tubulin were detected by western analysis. A schematic of the treatment is shown above the graph. The inset shows a western analysis for TRAPPC11 in all three cell lines. (B) The same fibroblasts as in (A) were grown in either nutrient rich (DMEM) or starvation (EBSS) medium for 2 hours. Lysates were prepared and processed for membrane recruitment detection by floatation as described in the Materials and Methods section. The indicated proteins were detected by western analysis. Note that half the amount of tubulin was loaded in the PN fraction in order to obtain an exposure that shows tubulin in the other fractions without grossly overexposing the PN signal. (C) The same fibroblasts as in (A) were grown in starvation (EBSS) medium for 2 hours in the presence of Bafilomycin A1. Lysates were prepared and processed for the membrane sealing assay as described in the Materials and Methods section. Prior to fractionation, some samples were treated with proteinase K (ProK) or with ProK in the presence of 1% Triton X-100. The fractions, composed of a postnuclear supernatant, low-speed pellet (LP), high-speed pellet (HP) and high-speed supernatant (HS), were probed for LC3. Note that the exposure for the PatC12 immunoblot is longer than for the others in order to reveal the LC3-II bands. (D) The same fibroblasts as in (A) were grown in nutrient-rich (DMEM) or starvation (EBSS) medium for 2 hours. The cells were then fixed and stained with anti-ATG2B or anti-WIPI4 antibody. The ATG2B (light gray bars) and WIPI4 (dark gray bars) punctae were quantified from a total of 25 cells for each condition. Representative images are shown in Figure S 2.5A. (E) Control (Ctrl) and PatC11 fibroblasts were grown in nutrient-rich (DMEM) medium and left untransfected (Ctrl and PatC11) or PatC11 cells were transfected by electroporation with a construct expressing either BirA-C11 or C11-BirA as indicated. The cells were then fixed and stained with anti-ATG2B or anti-WIPI4 antibody. The ATG2B (light gray bars) and WIPI4 (dark gray bars) punctae were quantified from a total of 25 cells for each condition. Representative images are shown in Figure S2.5B. Numbers to the right of the immunoblots denote the migration of molecular size standards in kD.

2.4.8 Depletion of TRAPPC11 and TRAPPC12 Also Affect Lysosomal Activity

Both TRAPPC11 and TRAPPC12 function in membrane traffic (Scrivens et al., 2011) and one study implicated TRAPPC11 in lysosomal function (Bogershausen et al., 2013). While the autophagic flux defect resulting from TRAPPC11 depletion is due to unsealed autophagosomes, altered lysosomal proteolytic activity might explain the autophagic flux defect associated with TRAPPC12 depletion given that, in this case, sealed autophagosomes are forming (Figure 2.3A). We first assessed lysosomal proteolytic activity by examining the ability of HeLa cells depleted of either TRAPPC12, TRAPPC11 or ATG2 to process the lysosomal protease cathepsin B. Processing of this enzyme relies upon a proteolytically-active lysosome resulting in a cleaved, active, mature form (Hanewinkel et al., 1987). Depletion of either TRAPPC12 or TRAPPC11

resulted in greatly reduced levels of mature cathepsin B (Figure 2.9A). This may be due to a defect in trafficking of certain proteases, including cathepsin B, to the lysosome along the biosynthetic pathway (Scrivens et al., 2011; Wendler et al., 2010). In contrast, depletion of ATG2 did not result in a cathepsin B processing defect. We then more directly examined lysosomal proteolytic activity using the fluorogenic substrate DQ-BSA. Upon delivery of DQ-BSA to the lysosomes, fluorescence is dequenched as a result of proteolytic activity (Mora et al., 2010). As shown in Figure 2.9B, depletion of either TRAPPC12 or TRAPPC11 resulted in much less fluorescence of DQ-BSA in the lysosome compared with control. This was again in contrast to ATG2 depletion, which showed strong DQ-BSA-dependent fluorescence. The DQ-BSA defect in TRAPPC11- or TRAPPC12-depleted cells was not because of an endocytic defect since uptake of a fluid-phase marker in the absence of either protein was not affected (Figure S 2.6). This result supports the notion that both TRAPPC11 and TRAPPC12 affect lysosomal activity, likely due to a membrane trafficking defect in the biosynthetic pathway. If reduced proteolytic activity in lysosomes following TRAPPC12 depletion accounts for the autophagic flux defect (Figures 2.1 and 2.2), we would expect to observe an overlap between LC3 and the lysosomal marker LAMP1 following TRAPPC12 depletion, an indication that autolysosomes are indeed formed. As expected for unsealed membranes that form in response to depletion of either ATG2 or TRAPPC11, there was little overlap between the LC3-positive structures and LAMP1 (Figure 2.9C and D). Similarly, depletion of TRAPPC12 also resulted in low overlap between the LC3-positive structures and LAMP1, suggesting that the autophagic flux defect following TRAPPC12 depletion is upstream of autolysosome formation. Thus, although TRAPPC12 depletion results in lysosomes with reduced proteolytic activity, this does not account for the autophagic flux defect in these cells. Overall, our results indicate that during autophagy, ATG2 and TRAPPC11 function upstream of TRAPPC12. They further illustrate that TRAPPC11 and TRAPPC12 also affect lysosome activity most likely through a defect in biosynthetic trafficking to the lysosome, although this second function does not account for the autophagic flux defect seen upon TRAPPC11 or TRAPPC12 depletion.

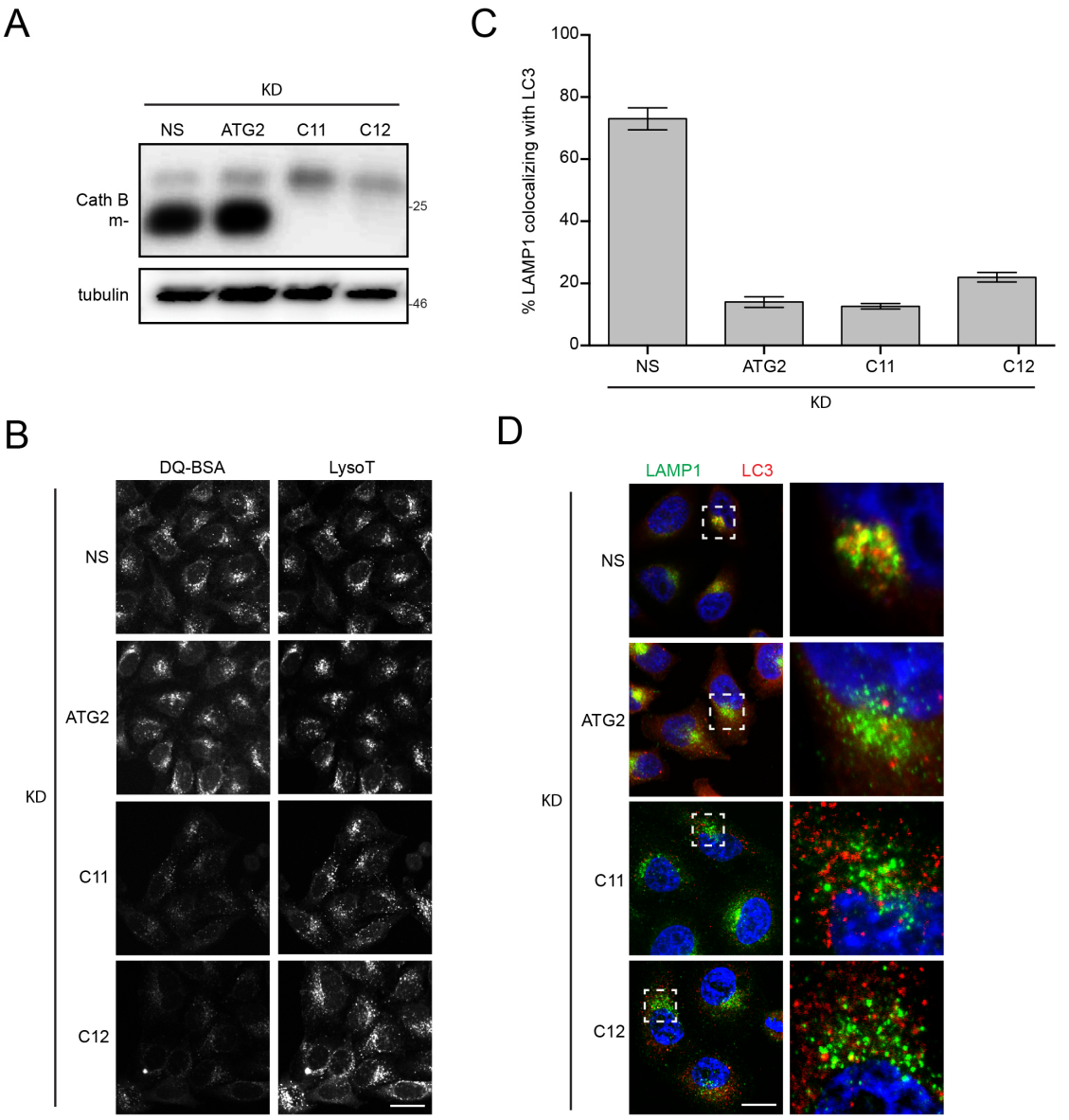

Figure 2.9 Lysosomal proteolytic activity is reduced upon depletion of either TRAPPC11 or TRAPPC12.

(A) HeLa cells were treated with nonspecific (NS) siRNA, or siRNA targeting either TRAPPC11, TRAPPC12 or ATG2. Lysates were prepared and fractionated by SDS-PAGE and then probed for cathepsin B. The mature (m) form of the enzyme is indicated. (B) The same cells in (A) were treated with DQ-BSA and lysotracker (LysoT), and processed for fluorescence microscopy as described in the Materials and Methods section. All images were obtained using the same exposure conditions. (C) The same cells as in (A) were fixed and stained for the lysosomal marker protein LAMP1 and for LC3. Co-localization between the two signals was determined using Imaris. Representative cells are displayed in (D). A minimum of 25 cells was used for the

quantification and the percentage of LAMP1 punctae that were also positive for LC3 is displayed. Numbers to the right of the immunoblots denote the migration of molecular size standards in kD. The scale bars in (B) and (D) represent 20 μm.

2.5 Discussion

Here, we have shown that depletion of three different TRAPP III associated proteins results in an autophagic flux defect suggesting a function in autophagy, but the specific steps in which these proteins function differ. Whereas TRAPPC8 affects formation of isolation membranes, TRAPPC11 is required upstream of the isolation membrane enclosure that leads to the formation of autophagosomes. TRAPPC12 acts downstream of TRAPPC11 after autophagosome formation. We also demonstrate that a fraction of each protein is associated with LC3-positive membranes suggesting that a portion of TRAPP III localizes to isolation membranes/autophagosomes. We examined the function of TRAPPC11 in more detail and found that it is required for recruitment of ATG2B-WIPI4.

Combined with previous studies, we propose a model for the role of the TRAPPC11-containing TRAPP III complex in isolation membrane formation and expansion (Figure 2.10). Work in S. cerevisiae has shown that yeast TRAPP III interacts with ATG9-containing vesicles (Kakuta et al., 2012). This interaction was mediated by Trs85, the yeast homologue of TRAPPC8. In the yeast system, initial recruitment of TRAPP III was ATG9-dependent. A functional link between mammalian ATG9A and TRAPPC8 was also demonstrated (Imai et al., 2016; Lamb et al., 2016). Thus, it is not unexpected that TRAPPC8 depletion would function upstream of isolation membrane formation and resemble an ATG9A depletion as we report here. Our model also suggests that recruitment of ATG2B-WIPI4 by TRAPPC11 serves several purposes. Previous work demonstrated that depletion of ATG2 resulted in unsealed membranes that did not fuse with lysosomes and it was suggested that ATG2 is required for isolation membrane elongation (Kishi-Itakura et al., 2014; Velikkakath et al., 2012). More recently, it has been suggested by both in vitro and in vivo studies that ATG2 can function as a tether during this process (Chowdhury et al., 2018; Gomez-Sanchez et al., 2018; Kotani et al., 2018), prior to an ATG5-dependent sealing of the membranes into autophagosomes

(Kishi-Itakura et al., 2014). It has also been implied that WIPI4 regulates the association of ATG9A with LC3-containing membranes (Saitsu et al., 2013). Because ATG9A only associates transiently with LC3-membranes (Orsi et al., 2012), it is tempting to speculate that another consequence of the TRAPPC11-dependent recruitment of ATG2B-WIPI4 is the facilitation of the release of ATG9A from nascent isolation membranes/omegasomes.

It is unclear at which step TRAPPC12 functions. Here, we have shown that autophagosomes are sealed following depletion of TRAPPC12 (Figure 2.3) and thus the protein functions downstream of TRAPPC11. The poor co-localization between LC3 and the lysosomal marker LAMP1 following TRAPPC12 depletion suggests that the role of TRAPPC12 in autophagy is prior to autolysosome formation. We can envision three possible functions for TRAPPC12 in this scenario. First, TRAPPC12 could recruit a late-acting factor necessary for the fusion event, such as the putative interacting partner TECPR1 (Behrends et al., 2010), a protein previously implicated in autophagosome-lysosome fusion (Chen et al., 2012). Second, it could be required to facilitate the activity of an as yet unidentified autophagosomal membrane protein necessary for formation of autolysosomes. Finally, it may be required as a second or supplemental tethering factor between autophagosomes and lysosomes. Although TRAPP complexes were first thought to act as tethers, a direct role in this process has yet to be shown. In addition, the HOPS complex has been suggested to mediate the tethering between autophagosomes and lysosomes (Jiang et al., 2014), so it is unclear if another tethering factor would be required. Further studies on TRAPPC12 will be required to determine its role in this late step of autophagy.

Mutations in TRAPPC11 have been linked to disease (Sacher et al., 2019). The phenotypes are broad and include liver and eye involvement, achalasia, alacrima and intellectual deficit. However, virtually all individuals with TRAPPC11 mutations display some form of muscular pathology or an elevated creatine kinase level. Using fibroblasts derived from an individual with a compound heterozygous TRAPPC11 mutation, we have shown that they display a defect in autophagic flux likely due to impairment in ATG2B-WIPI4 recruitment to isolation membranes. With TRAPPC11 now linked to a

role in autophagy, there are three distinct cellular roles for this protein including lipid-linked oligosaccharide synthesis and membrane traffic in the endomembrane system (DeRossi et al., 2016; Scrivens et al., 2011). It is unclear which dysregulated cellular process contributes to the clinical phenotype or whether it is a combination of all three.

Indeed, both defective autophagy and glycosylation have been implicated in muscular dystrophies, particularly those caused by improper glycosylation of the protein dystroglycan (Michele et al., 2002; Sandri et al., 2013). Interestingly, one individual with a TRAPPC11 mutation was recently shown to have a dystroglycanopathy (Larson et al., 2018). Furthermore, the glycosyltransferases essential for some of the modifications on dystroglycan are Golgi-resident enzymes that utilize the biosynthetic pathway to reach their destination (Grewal et al., 2005; Keramaris-Vrantsis et al., 2007; Matsumoto et al., 2004; Yoshida et al., 2001). Further studies are required to tease apart the various functions of TRAPPC11 and their effects on muscle physiology.

We also considered the possibility that the cellular phenotypes seen upon depletion of the TRAPP III proteins might be due to impaired guanine nucleotide exchange factor (GEF) activity for RAB1 because this GTPase has been implicated in autophagosome biogenesis (Zoppino et al., 2010). In yeast, it is known that TRAPP III acts as a GEF for the RAB1 homologue Ypt1 (Thomas et al., 2018), and that Ypt1 is important for recruitment of both ATG1, the functional homologue of mammalian ULK1, and ATG11 (Lipatova et al., 2012; Wang et al., 2013). In higher eukaryotes, only TRAPP II, and not TRAPP III, was reported to act as a GEF for RAB1 (Li et al., 2017; Yamasaki et al., 2009). Thus, it seemed unlikely that depletion of TRAPP III proteins would affect GEF activity for RAB1. Nevertheless, we examined whether a dominant-negative form of RAB1 could phenocopy a TRAPPC11 depletion, and whether a constitutively-active form of RAB1 could suppress the phenotype resulting from TRAPPC11 depletion. Neither was observed (not shown) suggesting that the phenotypes seen upon depletion of TRAPP III proteins are not because of an effect on the activity of RAB1.

Several pieces of evidence implicate the carboxy-terminus of TRAPPC11 in the

recruitment of the ATG2B-WIPI4 complex. First, of the TRAPPC11 mutations in the compound heterozygous individual examined in this study, one allele (p.Asp1127Valfs*47) has a frame shift mutation starting six amino acids from the carboxy-terminus of this 1133 amino acid-long protein. The second allele (p.Ala372_Ser429del) results in an unstable protein (Bogershausen et al., 2013). Because a reduced level of TRAPPC11 is detected in the cell lysate from these fibroblasts, it is likely to be due to the p.Asp1127Valfs*47 variant. Given that ATG2B-WIPI4 is not recruited to membranes in these cells, a role for the carboxy-terminus in ATG2B-WIPI4 recruitment could be inferred. The BioID results are also consistent with this notion. In this case, biotinylation of both ATG2B and WIPI4 was more efficient using BirA-C11 (free-carboxy-terminus) compared to C11-BirA. This was not due to an expression-level difference because expression levels of the BirA constructs were essentially the same (not shown). The specific affinity is in addition supported by the fact that C11-BirA showed preference for some other proteins compared to BirA-C11 (eg, TRAPPC8 and TRAPPC13).

Finally, we demonstrate better recruitment of ATG2B and WIPI4 to membranes with BirA-C11 compared to C11-BirA in both HeLa and fibroblast cells. Our study not only implicates TRAPP III proteins in autophagy, but it provides evidence that TRAPPC11 and TRAPPC12 are also required for proper proteolytic function of the lysosome. This is likely due to their role in biosynthetic membrane trafficking (Scrivens et al., 2011; Wendler et al., 2010). While it is possible that altered lysosomal activity could affect formation of autolysosomes (Seranova et al., 2017), we do not favor this possibility for several reasons. In the case of TRAPPC11 depletion, the autophagic flux defect is caused by the resulting unsealed isolation membranes because sealed membranes are required for autolysosome formation (Kishi-Itakura et al., 2014). This notion is further supported by the ATG2 knockdown that showed normal lysosomal activity with respect to cathepsin B and DQ-BSA (Figures 2.9 A and B), yet these unsealed structures did not fuse with the lysosomes (Figure 2.9 C and D). Thus, there appears to be no correlation between lysosomal proteolytic activity and isolation membrane sealing. In the case of TRAPPC12 depletion, there was poor co-localization between the lysosomal marker

LAMP1 and LC3, suggesting that its functions in biosynthetic membrane traffic and autophagy are probably unrelated, although this will require more experimentation to better clarify.

The precise function of ATG2 in autophagosome formation and its recruitment to membranes is unclear, but recent studies suggest it may function in isolation membrane expansion. An ultrastructural study on mouse and human cells indicated that upon depletion of ATG2, isolation membranes failed to expand (Kishi-Itakura et al., 2014). Some of the structures in the ATG2-depleted cells appeared circular in shape. However, because circular structures were not seen in ATG2A/ATG2B double knockout cells (Tamura et al., 2017), such structures in the depleted cells probably resulted from an incomplete inactivation of the protein. Indeed, only small membranes were seen in the absence of both ATG2 proteins, supporting the notion that ATG2 is required for isolation membrane elongation. Recent studies demonstrated an in vitro tethering ability for ATG2A (Chowdhury et al., 2018) (Kotani et al., 2018), consistent with its role in membrane elongation. While the extreme amino-terminus of ATG2 is required for isolation membrane binding in vivo (Tamura et al., 2017), the interactions that regulate its membrane association are unclear. Because WIPI proteins are recruited to PI(3)P-containing membranes (Grimmel et al., 2015), and WIPI4 interacts with ATG2, WIPI4 is thought to recruit ATG2 to such membranes that form after starvation. However, this complex still interacts in vitro with artificial liposomes devoid of PI(3)P (Zheng et al., 2017) (Chowdhury et al., 2018; Kotani et al., 2018). Thus, the recruitment of ATG2 in vivo may in fact be regulated by a number of different factors, and we propose that TRAPPC11 is one such factor.

Our present study places TRAPPC11 upstream of ATG2B, prior to the ATG5-dependent sealing of isolation membranes. Furthermore, our study implicates ATG2B-WIPI4 recruitment to isolation membranes as critical for human health. Indeed, the function of WIPI4 has also been implicated in human health (Saitsu et al., 2013) (Haack et al., 2012). Future studies will be aimed at characterizing the membranes that form in the absence of TRAPPC11 in both HeLa cells and primary fibroblasts derived from individuals with

TRAPPC11 mutations at the ultrastructural level, as well as detailing the distinct roles of each TRAPP III subunit in the formation of isolation membranes.

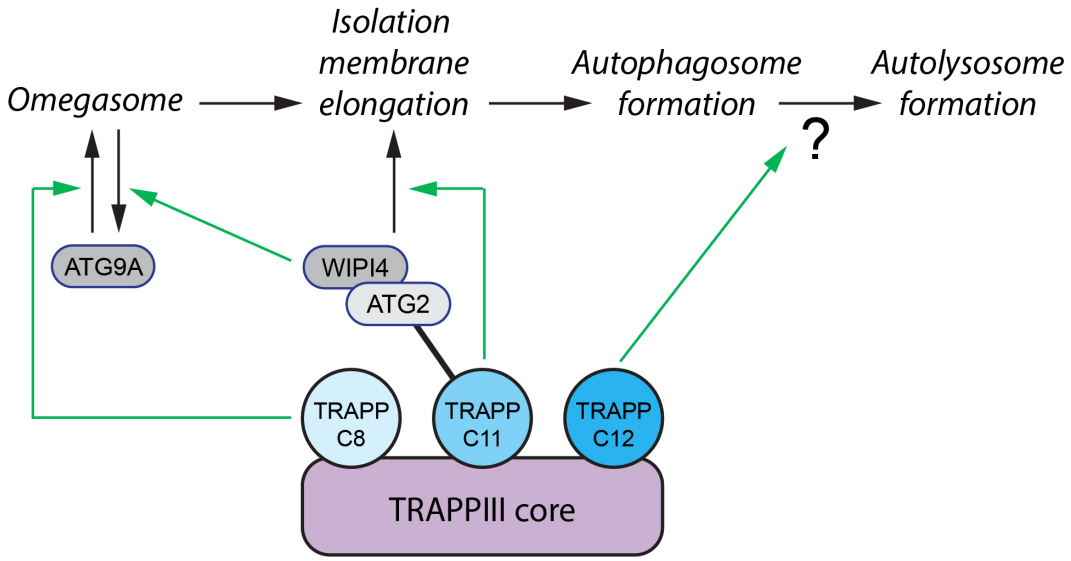

Figure 2.10 A model for the role of TRAPP proteins in autophagy.

The model depicts the various stages of autophagy and which stage is affected by the TRAPP III proteins. The green arrows indicate that the TRAPP protein influences that particular step. The dark line connecting TRAPPC11 to ATG2B is based on the BioID result (Table 2.3). See text for details.

2.6 Supporting information

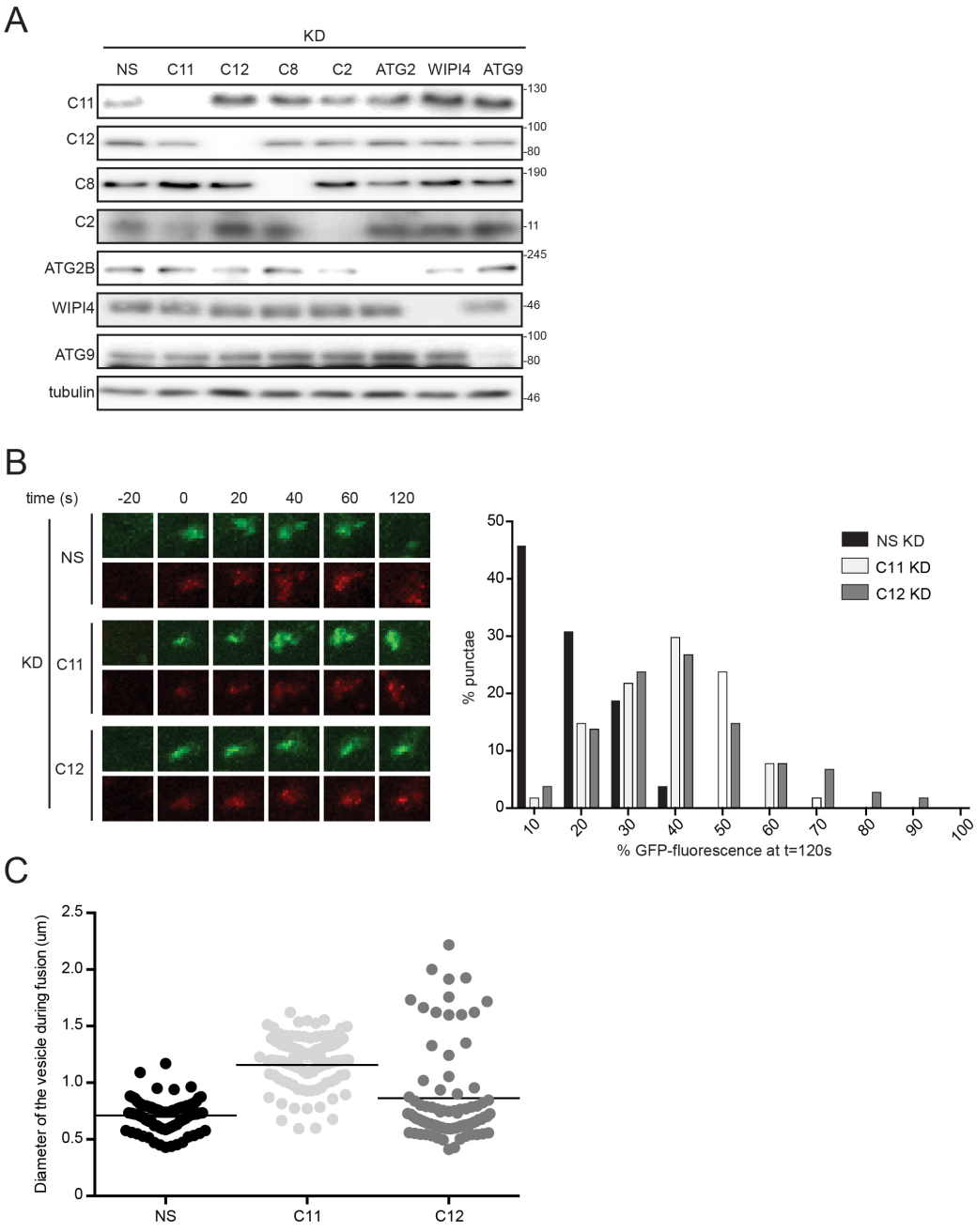

Figure S2.1 (Related to Figure 2.1)

(A) HeLa cells stably expressing mRFP-GFP-LC3 were transfected with siRNAs targeting the indicated genes. Lysates were fractionated by SDS-PAGE and probed for the indicated proteins by western blotting. (B) HeLa cells stably expressing mRFP-GFP-LC3 were left untreated or treated with siRNA targeting TRAPPC11 or TRAPPC12. The cells were then transferred to starvation (Earle's Balanced Salt Solution [EBSS]) medium for 1 hour. At that time, the live cells were imaged every 20 seconds for 10 minutes.

Individual GFP-positive punctae (N = 25-40 in different cells) were followed and the fluorescence intensity was measured at time $t = 0$ and again at time $t = 120$ seconds. The percent GFP intensity ($100 \times [\text{intensity}_{t = 120\ \text{seconds}}/\text{intensity}_{t = 0\ \text{secods}}]$) was plotted vs the percentage of punctae displaying that intensity. Representative individual GFP-LC3 punctae in live cells over the course of the 120-second time-frame are shown. Note the decrease in GFP fluorescence, but not RFP fluorescence, for untreated HeLa cells indicating fusion between autophagosomes and lysosomes. A similar decrease in GFP fluorescence is not seen for TRAPPC11- and TRAPPC12-depleted cells. (C) HeLa cells stably expressing mRFP-GFP-LC3 were transfected with siRNAs targeting either TRAPPC11 or TRAPPC12. GFP-positive punctae were measured in Imaris following deconvolution of the images in AutoQuant. N values are 77 (NS KD), 80 (C12 KD) and 127 (C11 KD). The mean diameter is shown as a black horizontal line. Numbers to the right of the immunoblots denote the migration of molecular size standards in kD.

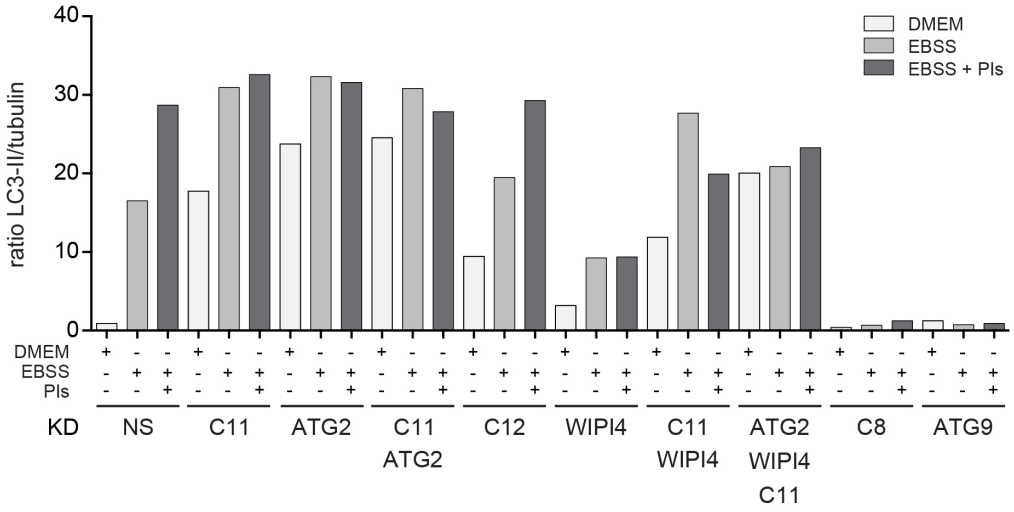

Figure S2.2 (Related to Figure 2.2)

Quantification of the western blot in Figure 2A was performed This blot and the bar graph are representative of two independent experiments.

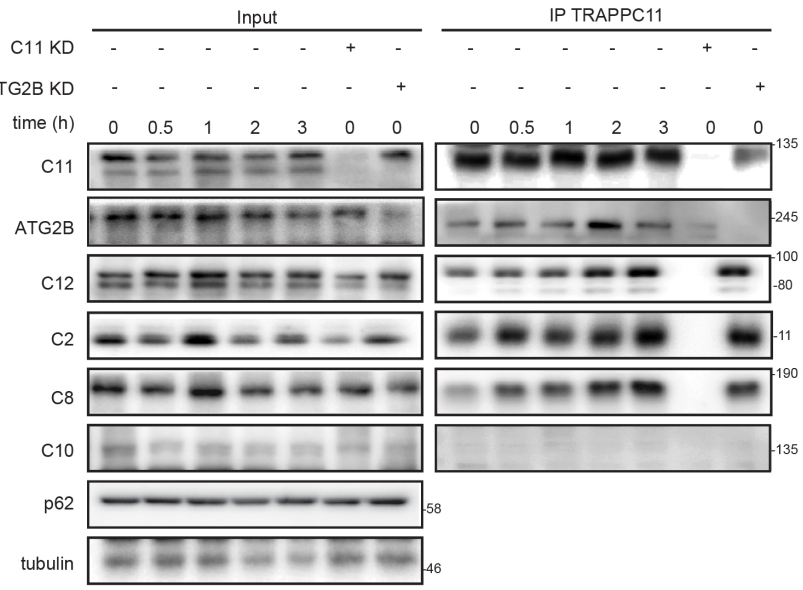

Figure S2.3 (Related to Figure 2.6)

HeLa cells were treated with siRNA targeting either TRAPPC11 or ATG2. The cells were then transferred into starvation medium and lysates were prepared at the times indicated in hours. A portion of the samples was treated with anti-TRAPPC11 antibody. The indicated proteins were detected by western analysis. Numbers to the right of the immunoblots denote the migration of molecular size standards in kD.

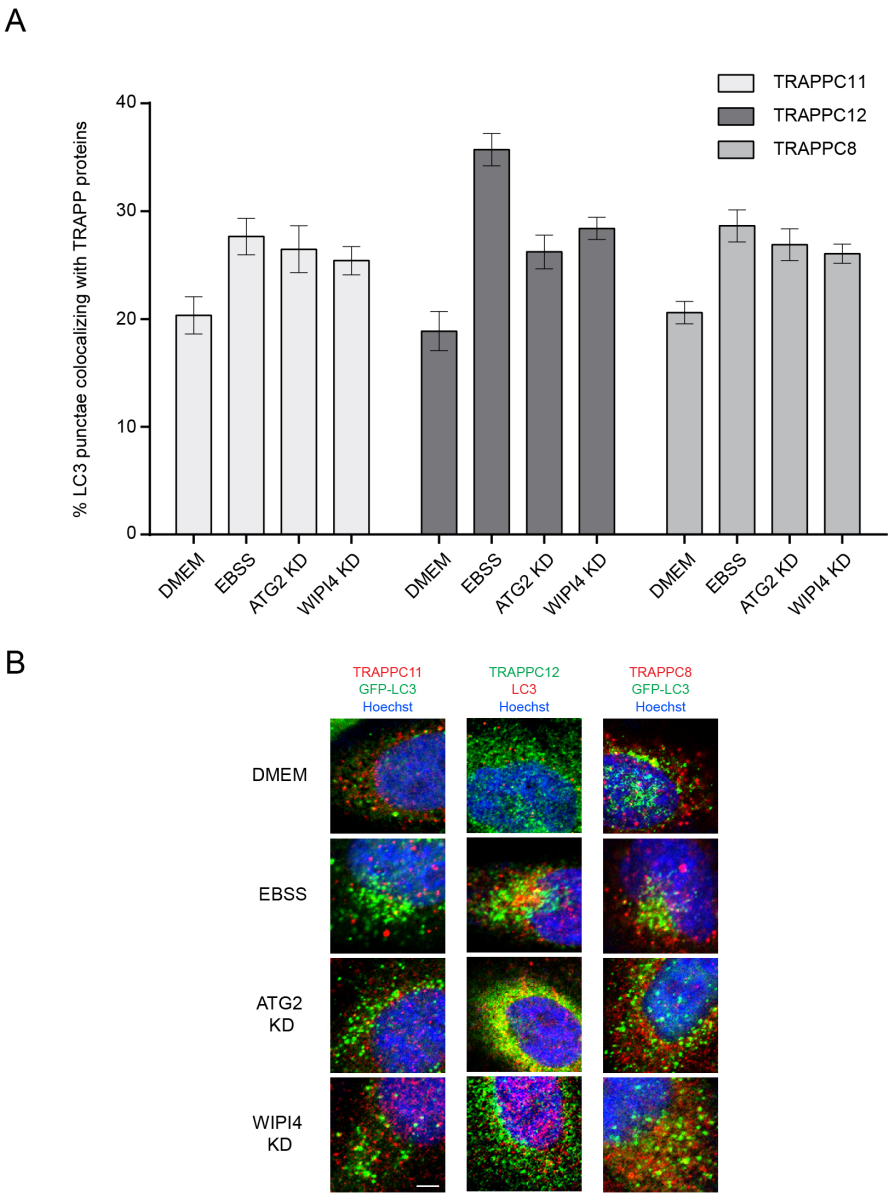

Figure S2.4 (Related to Figure 2.7)

(A) HeLa cells were untreated or treated with siRNA targeting either ATG2 or WIPI4. The untreated cells were either left in nutrient-rich medium (DMEM) or starved for 2 hours (EBSS) in the presence of 200 nM Bafilomycin A1. The cells were then stained for one of the TRAPP III proteins (TRAPPC8, TRAPPC11 or TRAPPC12) and LC3. Representative images are shown in (B). The co-localization between TRAPP protein- and LC3-positive structures was quantified using Imaris and is plotted as the percentage of LC3-positive punctae that were positive for the indicated TRAPP III protein. A total of

15 cells were counted and the SEM is indicated. The scale bar represents 20 µm. Significance was assessed using a one way ANOVA with a post hoc Fisher's protected least squares difference using SPSS version 24. Asterisks indicate increases whose p values are less than 0.05 relative to the corresponding non-starved controls.

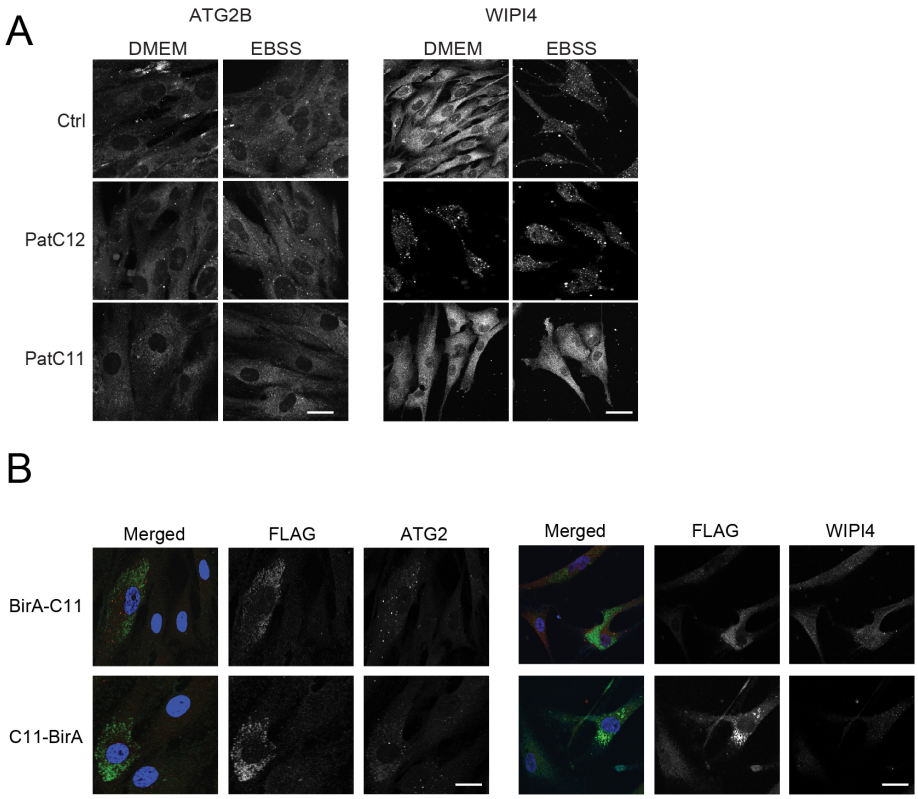

Figure S2.5 (Related to Figure 2.7)

(A) Fibroblasts from control, PatC11 and PatC12 were unstarved (DMEM) or starved for 2 hours (EBSS). The cells were then fixed and stained for ATG2B or WIPI4. The images are representative images used for the quantification in Figure 8D. (B) The same cells as in (A) were electroporated with a construct expressing either BirA-C11 or C11-BirA as indicated. Transfected cells were identified by anti-FLAG antibody. The cells were stained for either ATG2B or WIPI4. Quantification in Figure 2.8E was performed on both the transfected and non-transfected cells. The scale bars represent 20 µm.

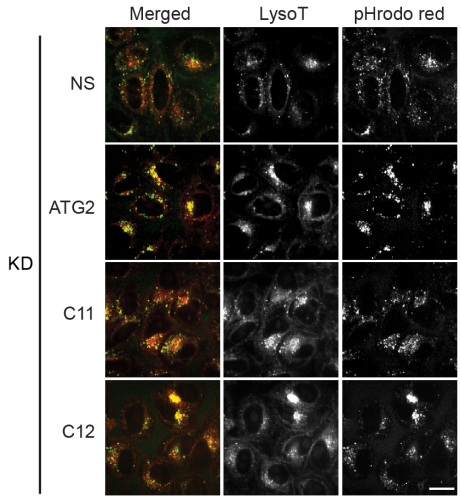

Figure S2.6 (Related to Figure 2.9)

HeLa cells were untreated or depleted of either TRAPPC11, TRAPPC12 or ATG2. The cells were then incubated with the fluid-phase marker pHrodo Red and Lysotracker Green to assess endocytosis. Images were obtained 20 minutes after addition of the fluorescent dyes. The scale bar represents 20 μm.

Chapter 3: Characterization of Three TRAPPC11 Variants Suggests a Critical Role for the Extreme Carboxy-terminus of the Protein

This Chapter was published as a manuscript in the journal (Milev et al., 2019) I shared first authorship of this paper with Miroslav Milev and I am responsible for the following figures: Figure 3.4a and Figure 3.6 (a, b, c, d, e), while Dr. Milev is responsible for the figures: Figure 3.4b and c and Figure 3.5. The q-PCR analysis was done by Dr. Saint-Dic and the clinical analysis was done by our collaborators.

3.1 Abstract

TRAPPC11 was identified as a component of the TRAPP III complex that functions in membrane trafficking and autophagy. Variants in TRAPPC11 have been reported to be associated with a broad spectrum of phenotypes but all affected individuals display muscular pathology. Identifying additional variants will further our understanding of the clinical spectrum of phenotypes and will reveal regions of the protein critical for its functions. Here we report three individuals from unrelated families that have bi-allellic TRAPPC11 variants. Subject 1 harbors a compound heterozygous variant (c.1287+5G>A and c.3379_3380insT). The former variant results in a partial deletion of the foie gras domain (p.Ala372_Ser429del), while the latter variant results in a frame-shift and extension at the carboxy terminus (p.Asp1127Valfs*47). Subjects 2 and 3 both harbour a homozygous missense variant (c.2938G>A; p.Gly980Arg). Fibroblasts from all three subjects displayed membrane trafficking defects manifested as delayed endoplasmic reticulum (ER)-to-Golgi transport and/or a delay in protein exit from the Golgi. All three individuals also show a defect in glycosylation of an ER-resident glycoprotein. However, only the compound heterozygous subject displayed an autophagic flux defect. Collectively, our characterization of these individuals with bi-allelic TRAPPC11 variants highlights the functional importance of the carboxy-terminal portion of the protein.

3.2 Introduction

The transport protein particle complexes are a family of related multisubunit protein complexes that share a core of subunits and contain complex-specific proteins that impart their differing functions. The TRAPPC11 protein was initially identified as a component that associates with the TRAPP III complex (Scrivens et al., 2011; Wendler et al., 2010). This complex was originally reported to play an as yet undefined role in membrane trafficking in the biosynthetic pathway. More recently, a role for the TRAPP III-specific subunits in autophagy was proposed (Behrends et al., 2010; Lamb et al., 2016; Ramirez-Peinado et al., 2017; Stanga et al., 2019). Specifically, the TRAPPC11 protein of this complex was shown to function upstream of autophagosome sealing, while TRAPPC12 functions prior to autophagosome-lysosome fusion (Stanga et al., 2019). Although the yeast TRAPP III complex has been implicated as a guanine nucleotide exchange factor (GEF) for Ypt1 (Jones et al., 2000; Thomas et al., 2018; Wang et al., 2018), the RAB target of the human TRAPP III complex is still unclear. Interestingly, *Drosophila* TRAPP III was shown to be capable of nucleotide exchange on RAB1 (Riedel et al., 2018). Whether all of the proteins of the TRAPP III complex function independently in other cellular processes is still unclear but two subunits, TRAPPC11 and TRAPPC12, appear to function in *N*-linked glycosylation (TRAPPC11), and mitosis and recruitment of the COP II coat (TRAPPC12) to the exclusion of other TRAPP III proteins (DeRossi et al., 2016; Milev et al., 2015; Zhao et al., 2017). Thus, elucidating the roles of TRAPP III proteins both within and outside of the complex is important to better understand their cellular functions. In the case of TRAPPC11 and other TRAPP proteins, it is possible that regions or domains of the protein may play a role in different cellular pathways.

To date, a number of variants in the genes encoding TRAPP proteins have been described (Sacher et al., 2019). While variants in a core subunit called TRAPPC2 exclusively result in a skeletal defect, those in TRAPPC11 result in neuromuscular defects as well as a broad spectrum of other clinical features including scoliosis, alacrima, steatosis, intellectual deficit and cerebral atrophy (Bogershausen et al., 2013; Fee et al., 2017; Koehler et al., 2017; Larson et al., 2018; Liang et al., 2015; Matalonga et al., 2017; Wang

et al., 2018). This may be due to the various processes that are impacted by TRAPPC11 within the cell.

The domain structure of TRAPPC11 indicates several regions that may be involved in either protein-protein interactions or may be important for its function. For example, a region spanning amino acids 263-561, referred to as the foie gras domain, is well-conserved through evolution, suggesting a critical function for this domain. Variants within this domain have been reported including an in-frame deletion (Bogershausen et al., 2013; Larson et al., 2018; Matalonga et al., 2017; Wang et al., 2018), further highlighting the importance of this region. In addition, a well-conserved 60-amino acid stretch near the carboxy terminus referred to as the gryzun domain has also been noted, although its functional significance remains unknown. Most studies on TRAPPC11 variants have assessed membrane trafficking defects and Golgi morphology and found either one or both to be defective (reviewed in (Sacher et al., 2019)).

The mapping of natural variants in a protein is useful in elucidating its function and allowing clinicians and researchers to better predict the cellular consequences of new variants. In the case of TRAPP proteins, a missense variant in TRAPPC2 that changes aspartate 47 to tyrosine was shown to affect the interaction between TRAPPC2 and both TRAPPC8 and TRAPPC9 (Brunet et al., 2013; Zong et al., 2011). A similar missense variant in TRAPPC2L results in elevated levels of the active form of the GTPase RAB11 (Milev et al., 2018). In other instances, such as for described variants in TRAPPC9 (Sacher et al., 2019), it remains unclear how they affect the function of the protein. Thus, identifying new variants and individuals with previously-described variants will further our understanding of the importance of specific regions of TRAPP proteins.

Here, we describe three individuals with either compound heterozygous or homozygous variants in *TRAPPC11*. All three individuals have variants at or near the carboxy-terminus of the protein. The compound heterozygous individual also has an in-frame deletion in a highly-conserved central region of the protein that was previously reported (Bogershausen et al., 2013). The purpose of this study was to analyze in detail the effects

of these genetic defects on protein function. The clinical and cell biological features for each individual support the notion that the carboxy-terminus of the protein is critical for biological function.

3.3 Materials and Methods

This study was carried out in accordance with the Declaration of Helsinki. Written informed consent was obtained from patients and/or their parents or guardians. All experimental protocols were approved by the ethical committee of the Medical Faculty of the University of Giessen, Germany, and by the Comitè d'Ètica d'Investigació Clínica (CEIC) de la Fundació Sant Joan de Déu (Fundacion Sant Joan de Déu Ethics Committee on Clinical Research (CEIC)). Methods were carried out in accordance with the relevant guidelines and regulations.

3.3.1 Molecular Genetics

Whole exome sequencing, data processing and analysis were performed as previously described (Johnson et al., 2017) and confirmed by Sanger sequencing.

3.3.2 Histology

Open muscle biopsies were taken from the lateral vastus muscles (S1, S2 and S3) or the deltoid muscle (S1), oriented and frozen according to standard procedures. Frozen sections (10 μm for S1 and 6 μm for S2 and S3 for histology and histochemistry, and 7 μm for immunohistochemistry) were examined using routine histological and histochemical stains including haematoxylin and eosin (HE) and modified Gomori trichrome and cytochrome oxidase (COX/SDH) (Dubowitz et al., 2014). Immunohistochemical analysis was performed using a Bench Mark XT automatic staining platform (Ventana, Heidelberg, Germany; Ultraview Universal DAB Detection kit) with the following primary antibodies: anti-MHC neonatal, anti-MHC slow, anti-Myotilin and anti-α-dystroglycan. The sections were examined on a Nikon Eclipse 80i

microscope equipped with a CCD camera. For transmission electron microscopy (TEM) in S2 and S3, small biopsies were fixed in 6% glutaraldehyde/0.4 M phosphate buffered saline (PBS) and were processed with a Leica EM TP tissue processor. Ultrathin sections were contrasted with 3% lead citrate-$3H_20$ with a Leica EM AC20 (ultrastain kit II) and examined on a Zeiss EM109 TEM equipped with a sharp eye digital camera.

3.3.3 Membrane Trafficking Assays

Fibroblasts were maintained in DMEM supplemented with 10% fetal bovine serum. In order to examine ER-to-Golgi trafficking, the RUSH assay was performed (Boncompain et al., 2012) and quantified as previously described (Milev et al., 2017). Trafficking of VSVG-GFP ts045 was performed following viral infection of the construct and quantified as previously described (Koehler et al., 2017).

3.3.4 Autophagy Assays

Assessment of autophagosome formation by susceptibility to proteinase K was performed essentially as described (Velikkakath et al., 2012) with minor modifications (Stanga et al., 2019). For assessment of autophagic flux the cells were washed with phosphate-buffered saline (PBS) and incubated with Earle's Balanced Salt Solution (EBSS; Wisent, St. Bruno, Canada) for the times indicated in the figure. In some cases, 200 nM Bafilomycin A1 (Sigma-Aldrich) was included during a 2-hour starvation. The starved cells were returned to nutrient-rich medium by washing with PBS and incubating in DMEM with 10% FBS for 20 or 40 minutes. The cells were lysed by harvesting in lysis buffer (150 mM NaCl, 50 mM Tris pH 7.2, 1 mM DTT, 1% Triton X-100, 0.5 mM EDTA, Complete protease inhibitors (Roche, Basel, Switzerland)) and analyzed by western blotting for LC3 (abcam, Cambridge, MA). The data were normalized to the tubulin (Sigma-Aldrich, St. Louis, MO) signal developed from the same membrane as the LC3 blot.

3.3.5 Antibodies

Primary antibodies used in this study were Rabbit anti-LC3 (abcam, Cambridge, MA), mouse anti-LC3 (Santa Cruz, Dallas, TX), Rabbit anti-LAMP1 (abcam, Cambridge, MA), Rabbit anti-TRAPPC11 (Sacher laboratory), mouse anti-tubulin (Sigma-Aldrich, St. Louis, MO), Rabbit anti-mannosidase II (gift from Dr. Kelly Moreman), mouse anti-TRAP-α (Santa Cruz, Dallas, TX), mouse anti-FLAG (Sigma-Aldrich, St. Louis, MO), anti-neonatal myosin heavy chain (NCL-MHCn;, Leica Biosystems, Wetzlar, Germany), anti-MHC neonatal (Novocastra/Leica Biosystems, Wetzlar, Germany) anti-MHC slow (Novocastra/Leica Biosystems, Wetzlar, Germany) anti-myotilin (Novocastra/ Leica Biosystems, Wetzlar, Germany), and anti-alpha-dystroglycan (Merck-Millipore, Burlington, MA). Secondary antibodies used in this study were anti-mouse Alexafluor488 and anti-Rabbit Alexafluor647 (Life Technologies, Carlsbad, CA). Note that for all western blots displayed, the membranes were cut in the region where the protein migrates in order to maximize the number of proteins that could be analyzed on each blot.

3.3.6 Fluorescence Microscopy

The cells were washed with PBS, fixed with 4% paraformaldehyde for 20 minutes at room temperature, quenched with 0.1 M glycine for 10 minutes and permeabilized with 0.1% Triton X-100 for 8 minutes. Blocking was performed in 5% normal goat serum in PBS for 30 minutes at room temperature. Primary antibodies were diluted in 5% normal goat serum and were added to coverslips and incubated overnight at 4°C. Cells were washed two times 10 minutes with PBS. Secondary antibodies were diluted in 5% normal goat serum in PBS and applied for 1 hour at room temperature. The coverslips were washed several times with PBS with Hoescht being added during the first wash. The coverslips were then mounted with Prolong Gold AntiFade (Life Technologies, Carlsbad, CA) and sealed with nail polish. Images were recorded on an Olympus FV10i microscope fitted with a 60X objective, NA 1.35. The images were acquired with 0.25 µm increment size, deconvolved in AutoQuant (Media Cybernetics, Rockville, MD) and quantified with

Imaris (Bitplane, Concord, MA). For colocalization of LC3 and LAMP1, a total of 10 cells were analyzed for each condition.

3.3.7 Quantitative PCR

Messenger RNA (mRNA) was harvested from cells using the Quick-RNA Miniprep kit (Zymo Research, Irvine, CA) according to the manufacturer's instructions. A total of 1 μg of mRNA was subjected to first strand synthesis using MMuLV reverse transcriptase (New England Biolabs, Ipswich, MA). Polymerase chain reactions were then set up in triplicate using iTaq™ Universal SYBR® Green Supermix (Bio-Rad Laboratories, Hercules, CA). Samples were subjected to thermal cycling and detection of the fluorescent signal in a Bio-Rad CFX96 real-time PCR detection system. Quantification was performed by the $\Delta\Delta C_T$ method.

Oligonucleotides used were:

ATF6-F 5' CAGACAGTACCAACGCTTATGCC-3';
ATF6-R 5' GCAGAACTCCAGGTGCTTGAAG-3';
XBP1-F 5'-CTGCCAGAGATCGAAAGAAGGC-3';
XBP1-R 5'-CTCCTGGTTCTCAACTACAAGGC-3';
DDIT3-F 5'-GGTATGAGGACCTGCAAGAGGT-3';
DDIT3-R 5'-CTTGTGACCTCTGCTGGTTCTG-3';
BIP-F 5'-CTGTCCAGGCTGGTGTGCTCT-3';
BIP-R 5'-CTTGGTAGGCACCACTGTGTTC-3';
DNAJC3-F 5'-GGAGAGGATTTGCCACTGCTTTT-3';
DNAJC3-R 5'-CTCTGCTCGATCTTTCAGGGCA-3';
EDEM1-F 5'-ACGAGCAGTGAAAGCCCTTTGG-3';
EDEM1-R 5'-CCACTCTGCTTTCCAACCCAGT-3';
ATF4-F 5'-TTCTCCAGCGACAAGGCTAAGG-3';
ATF4-R 5'-CTCCAACATCCAATCTGTCCCG-3';
ActB-F 5'-CACCATTGGCAATGAGCGGTTC-3';
ActB-R 5'- AGGTCTTTGCGGATGTCCACGT-3'

3.4 Results

3.4.1 Clinical Summary and Molecular Genetics

Subject S1 is a male infant born at 37 weeks of gestation. He was the first child of a healthy, young Caucasian couple. The family history was unremarkable with no similarly affected individuals, consanguinity, birth defects, or miscarriages. The pregnancy history was normal. The infant's birth weight was 2948 g, length was 48 cm, and head circumference was 31.5 cm, all within the standard range (10th–90th centiles) for male Spanish neonates. Developmental delay was noted since head control was not acquired until 4 months old. The subject presented with a febrile status at five months old. Hypotonia, spasticity, and abnormal involuntary movements, including hyperkinesia and choreiform movements, appeared during the first year of life. Ability to sit, stand, or say words was never acquired. Cerebral atrophy and reduced white matter volume were observed from the first magnetic resonance imaging study (Figure 3.1A). Serum creatine kinase (CK) levels were persistently elevated, ranging from 350 to 2817 IU/l (normal value < 190 IU/l). Muscle biopsy was performed at the age of 4 years and showed minimal myopathic changes consisting of mild variation in muscle fibre diameter, a population of fibres with weak cytochrome c activity and a few fibres of normal size positive for neonatal myosin indicating fiber regeneration (Figure 3.1B). Intracellular lipids and glycogen were within normal limits. Immunohistochemistry for sarcolemmal proteins was normal. Alpha-dystroglycan glycosylation by means of immunofluorescence (clone IIH6 and VIA4-1) and immunoblot (IIH6) was not significantly reduced compared to the normal control analysed in parallel (not shown).

On recent assessment the subject was 9 years old. His height was 121 cm (centile <1, -2.45 SD), weight was 21.3 kg (centile 6, -1.58 SD) and head circumference was 44.5 cm (centile <1,-6.5 SD). Poor eye contact, axial hypotonia, spasticity, and choreiform movements persisted. He was unable to sit independently. A remarkable cerebral atrophy remained in successive magnetic resonance studies. There was no evidence of any clinical seizure since the febrile status. Successive EEGs did not register electrical

seizures or epileptiform activity. Antiepileptic treatment with valproic acid was initiated after the first febrile status at 5 months and stopped at the age of 4 years (Table 3.2). Because of global hypotonia and elevated CK, the subject was included in the MYO-SEQ project (undiagnosed myopathies/limb girdle muscular dystrophies with elevated CK). Whole exome sequencing revealed that S1 harbours two heterozygous variants in *TRAPPC11*. The first is an extended splice site variant, c.1287+5G>A (GRCh37/hg19 chr4:184605212), that is rare in both the Genome Aggregation Database (gnomAD) and in the Exome Aggregation Consortium (ExAC) database control population (0.005% and 0.002%, respectively, with no homozygotes) and has a CADD PHRED score (Rentzsch et al., 2019) of 15.64 (Table 3.1). The variant, which results in a 58 amino acid in-frame deletion (p.Ala372_Ser429del), has been previously reported in homozygosity to be associated with myopathy, infantile hyperkinetic movements, ataxia and intellectual disability in five individuals of Hutterite descent (Bogershausen et al., 2013). The second variant results in a frameshift, c.3379_3380insT (GRCh37/hg19 chr4:184633774), that is absent in both the gnomAD and ExAC control population, with a CADD PHRED score of 35.0, and results in a protein change of p.Asp1127Valfs*47 (Table 3.1). Both variants were confirmed by Sanger sequencing and were inherited each from one of the unaffected parents (Figure 3.1C).

Table 3.1 *TRAPPC11* variants and frequency for the newly-reported alleles

subject	Variant	allele frequency	CADD v1.3
S1	NM_021942.5: c.1287+5G>A: p.Ala372_Ser429del	15/282698 (gnomAD) 3/121132 (ExAC)	15.64
S1	NM_021942.5:c.3379_3380insT: p.Asp1127Valfs*47	0 (gnomAD) 0 (ExAC)	35.0
S2	NM_021942.5:c.2938G>A; p.Gly980Arg	21/282732 (gnomAD) 5/121286 (ExAC)	34.0
S3	NM_021942.5:c.2938G>A; p.Gly980Arg		

The PHRED-like scaled C-score ranks a genetic variant relative to all possible substitutions of the human genome. A scaled C-score of 20 or greater indicates that the variant is amongst the 1% most deleterious substitutions (Rentzsch et al., 2019).

Subject S2 is the fourth of six children of healthy consanguineous Turkish parents. The girl was born at 26 weeks gestational age due to preterm premature rupture of membranes and amnion infection syndrome. Birth weight was 1000 g, length was 35 cm, and head circumference was 25 cm (10^{th}-50^{th} centiles). The perinatal period was complicated by hyperbilirubinemia, pneumonia, and respiratory distress syndrome, and the subject had to be ventilated for 28 days. Muscular hypotonia and elevated CK values prompted a muscle biopsy at age 9 months that showed myopathic alterations. Her early motor development was delayed, and she achieved walking without support at age 3 years. At age 8 years, the subject was hospitalized due to pneumonia. At that age, weight was 15 kg (centile<1, -3.2 SD), length was 122 cm (10^{th} centile), and head circumference was 46 cm (centile<1, -3.1 SD). She presented with marked muscle atrophy, had difficulties when standing up from the ground (Gowers sign), and showed a waddling gait, hyperlordosis, and scoliosis. A second muscle biopsy showed features of a congenital myopathy with type 1 fiber predominance and focal Z-band abnormalities at the ultrastructural analyses (Figure 3.2). Neuropsychological testing disclosed a learning disability (IQ 75). She had normal aspartate aminotransferase (GOT) values, but elevated alanine aminotransferase (GPT) values (maximum 118 U/l, normal range <35). Her CK was elevated with values up to 500-1500 U/l. While albumin and coagulation parameters were within the normal range, cholinesterase values were reduced (minimum 606 U/l, normal range of 4000-12000). Moreover, amylase and lipase values were slightly elevated on several occasions without any clinical signs of pancreatic dysfunction. Echocardiography showed no signs of cardiac involvement (Table 3.2).

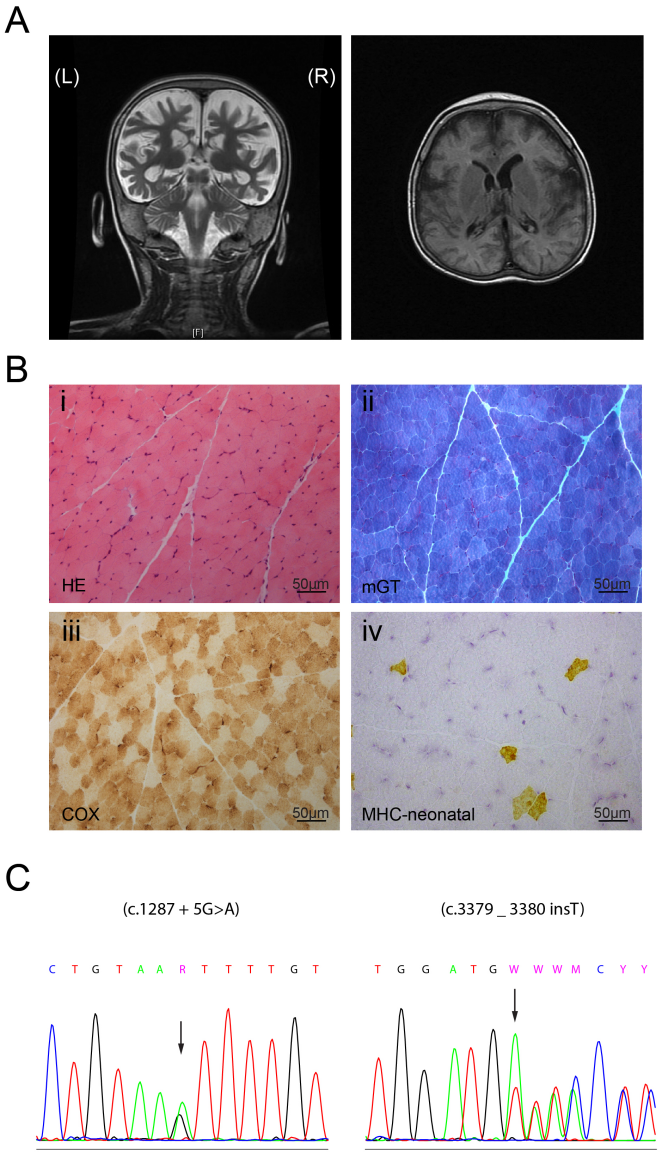

Figure 3.1 Brain and muscle abnormalities in subject S1 at age 4 years.

(A) Brain magnetic resonance imaging of the individual at the age of 3. Note cortical atrophy and reduced white matter volume in both coronal T2-weighted (left panel) and axial T1-weighted (right panel) images. (B) Muscle biopsy was performed at the age of 4 years and showed minimal myopathic changes consisting of mild variation in muscle fibre diameter (i, ii), a population of fibres with weak cytochrome c activity (iii) and a few fibres of normal size positive for neonatal myosin (iv)

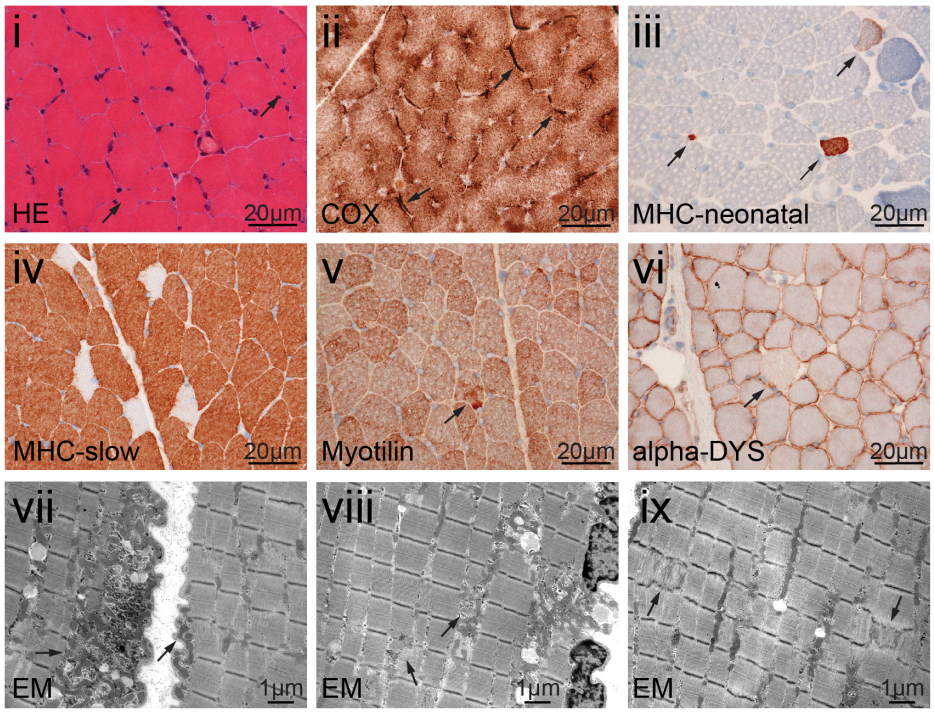

Figure 3.2 Muscle abnormalities in subject S2 at age eight years.

H&E stained sections show muscle fibers with increased variation of diameter and few fibers with internalized nuclei (arrows) (i). In the COX/SDH staining some fibers show subsarcolemmal mitochondrial aggregates (arrows) (ii). MHC-neonatal expression in few fibers indicates regenerative muscle fiber (iii). Staining with MHC slow antibodies shows type1 fiber predominance (iv). Antibodies against myotilin display a few fibers with subtle myofibrillar disintegration (arrow) (v). Sarcolemmal α-dystroglycan expression is reduced in a few fibers (arrow) (vi). Ultrastructural analysis shows that the sarcolemma is focally folded with subsarcolemmal accumulation of mitochondria (arrow) (vii) and intermyofibrillar accumulation of mitochondria (arrows) (viii), and focal Z-band abnormalities (arrows).

The subject lost ambulation at age 10 years. Progression of scoliosis necessitated spinal fusion at age 11 years, and recurrent pneumonias and declining lung function resulted in tracheostomy and invasive ventilation at age 14 years. Since then, the patient's clinical status has been stable. At last follow-up, at age 23 years, she was ventilated 20 hours per day, fed by a gastric tube, but was able to raise her arms against gravity. A diagnosis of TRAPPC11-related limb girdle muscular dystrophy 2S (LGMD2S) was made by whole exome sequencing (MYO-SEQ project) that revealed a homozygous variant c.2938G>A;

p.Gly980Arg. This variant is rare in both gnomAD and ExAC (0.007% and 0.004%, respectively, with no homozygotes) with a CADD PHRED score of 34.0 (Table 3.1).

Subject S3 is the eldest of three children of consanguineous Syrian parents. She was born at term without complications. Birth weight was 3200 g, length was 50 cm, and head circumference was 35 cm (all values 25th – 50th centile). Her early motor development was delayed, and she achieved free walking at age 2.5 years. She developed a proximal muscle weakness with difficulties when rising from the floor after age 5 years. At age 10 years, her walking distance was reduced to about 100 m, and since age 25 years, she is only able to walk a few steps. At last follow-up, at age 32 years, her condition was stable. She had normal GOT values, but moderately increased GPT values (maximum 186 U/l). Her CK was elevated up to 600-1800 U/l. In addition, amylase and lipase values were slightly elevated on several occasions without any clinical signs of pancreatic dysfunction. Her cholinesterase values were normal. Echocardiography performed several times during the course of disease was always normal, whereas her vital capacity (VC) was reduced to approximately 50%, but she has not required ventilation. An ophthalmological examination revealed a bilateral cataract (Figure 3.3A) (Table 3.2). A psychological examination at age 18 years yielded an IQ of 85, and cranial MRI at age 32 years showed a mild cortical atrophy. A muscle biopsy taken at age 27 years showed muscle fibers with features of an unspecific myopathy (Figure 3.3B) and an MRI displayed fatty muscle degeneration (Figure 3.3C). Diagnosis of TRAPPC11-related LGMD2S was established by whole exome sequencing that revealed the homozygous variant c.2938G>A; p.Gly980Arg (Bogershausen et al., 2013).

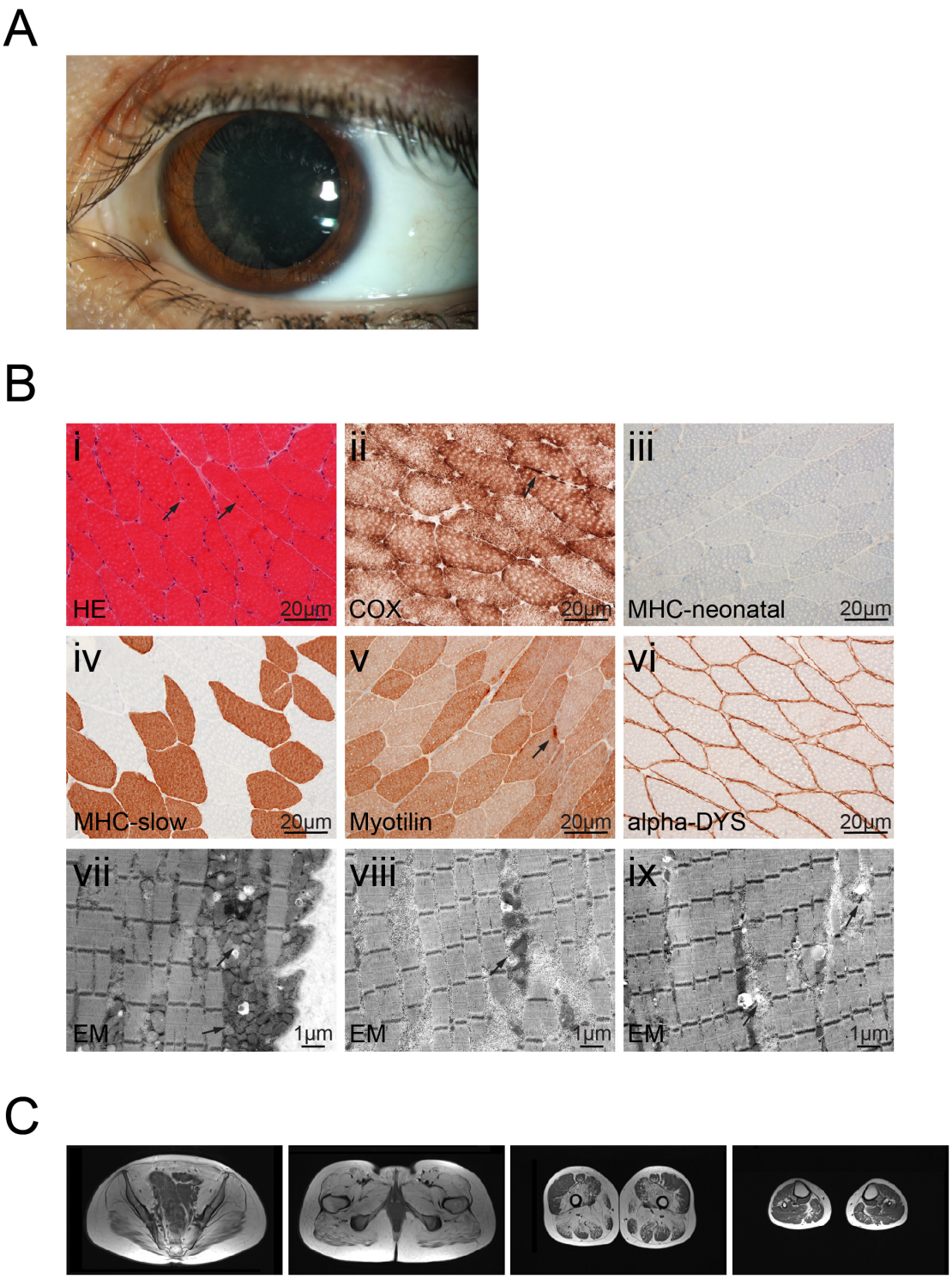

Figure 3.3 Eye and muscle abnormalities in subject S3 at age 27 years.

(A) Eye examination displays non-progressive cataracta coerulea. (B) H&E stained sections show muscle fibers with minor variation in diameter and few internal nuclei (arrows) (i). COX/SDH staining depicts some fibers with little subsarcolemnal

mitochondrial aggregates (arrow) (ii). No upregulation is seen when using antibodies against MHC neonatal in the muscle fibers (iii). Staining with antibodies against MHC slow shows normal distribution of type 1 or 2 fibers (iv). A few muscle fibers show myofibrillar disintegration with antibodies against myotilin (arrow) (v). Sarcolemmal α-dystroglycan expression is normal (vi). Ultrastructural analysis shows that the sarcolemma is focally folded with moderate subsarcolemmal accumulation of mitochondria (arrow) (vii). The myofibrillar architecture shows focal mild alterations with mitochondrial aggregates and extralysosomal glycogen (arrow) (viii) and focal unspecific loss of z-bands (arrows). (C) T1-weighted muscle MR images of S3 at age 30 years showing marked replacement of all pelvic muscles (gluteus maximus, iliacus, obturator internus, pectineus, and psoas muscles) by fat and connective tissue. At the upper thigh level, the vastus intermedius, the abductor magnus and brevis muscles were also severely affected whereas the vastus lateralis muscle was relatively spared. Similarly, the lower lower thigh muscles appeared well preserved.

Table 3.2 Clinical features of subjects in this study with *TRAPPC11* variants

	S1	S2	S3	S4
variant(s)	c.1287+5G>A/ c.3379_3380insT	c.2938G>A/ p.Gly980Arg	c.2938G>A/ p.Gly980Arg	c.1287+5G>A
age of onset	first year of life	first year of life	3-4 years	not reported, family history of early onset
muscle symptoms	axial hypotonia	axial hypotonia	axial hypotonia	None
motor ability	unable to sit or stand	unable to sit or stand	walks with support	walks without support
muscle biopsy	minimal myopathic changes	Myopathic	Myopathic	not performed
CK (IU/l)	350-2817	600-1800	400-1500	700-1000
hyperkinesia	Yes	No	No	No
spasticity	Yes	No	No	No
choreiform movements	Yes	No	No	Generalized
other neurological symptoms	No	No	No	ataxia, primary generalized seizures
intellectual disability	Yes	Yes	Yes	Moderate
microcephaly	Yes	No	No	No
neuroimaging	cerebral atrophy and reduced white matter volume	not done	mild cortical atrophy	mild cerebral atrophy
ocular involvement	No	No	Cataract	No
hepatic involvement	No	No	reduced cholinesterase levels	No

3.4.2 Fibroblasts from Subjects S1, S2 and S3 Have Membrane Trafficking Defects

TRAPPC11 was first identified as a protein that associates with the TRAPP III membrane trafficking complex (Scrivens et al., 2011). Depletion of the protein in HeLa cells resulted in Golgi fragmentation. Previous studies have suggested that some variants result in reduced levels of the protein (Bogershausen et al., 2013; Koehler et al., 2017; Liang et al., 2015), possibly leading to morphological changes in the Golgi. We found reduced levels of TRAPPC11 in S1 (Figure 3.4A), consistent with the unstable protein generated by the c.1287+5G>A allele as previously reported (subject S3.1, Figure 3.4A) (Bogershausen et al., 2013). In contrast, S2 and S3 had levels of the protein comparable to that of control (Figure 3.4A), as would be expected for a missense variant. Consistent with reduced TRAPPC11 levels, fibroblasts from S1 displayed severe Golgi morphological alterations resulting in highly fragmented Golgi membranes (Figure 3.4B, C). The Golgi alterations could be rescued by transfection of the cells with wild-type TRAPPC11 fused at either the amino- or carboxy-terminus to the biotin ligase BirA (Figure 3.4B, C), confirming that the Golgi morphological alterations were TRAPPC11-dependent. The BirA served as a steric impediment for the function of these ends of the protein as recently shown (Stanga et al., 2019). Thus, neither the carboxy- nor amino-terminus of TRAPPC11 is critical for its function in maintaining normal Golgi morphology.

We then examined the fibroblasts for membrane trafficking defects using the RUSH assay (Boncompain et al., 2012). In this assay, a fluorescent cargo protein is retained in the ER until the cells are exposed to biotin. The cargo (ST-eGFP and ManII-mCherry) is then monitored as it exits the ER and arrives in the Golgi. As shown in Figure 3.5A and B, fibroblasts from all three subjects of this study as well as subject S4 displayed a delay in arrival of both cargo proteins at the Golgi compared to control. We then examined the trafficking of a marker protein (VSVG-GFP ts045) that traverses the biosynthetic pathway, allowing for assessment of cargo arrival and release from the Golgi (Scales et al., 1997). In this assay, VSVG-GFP ts045 is retained in the ER at restrictive temperature

(40°C) and released upon downshift to permissive temperature (32°C). In fibroblasts from all three subjects as well as S4, we noted a delay in arrival of the protein at the Golgi, consistent with the results of the RUSH assay, as well as a defect in release of the protein from the Golgi (Figure 3.5C). Based on these two assays we conclude that fibroblasts from all three subjects display membrane trafficking defects along the biosynthetic pathway.

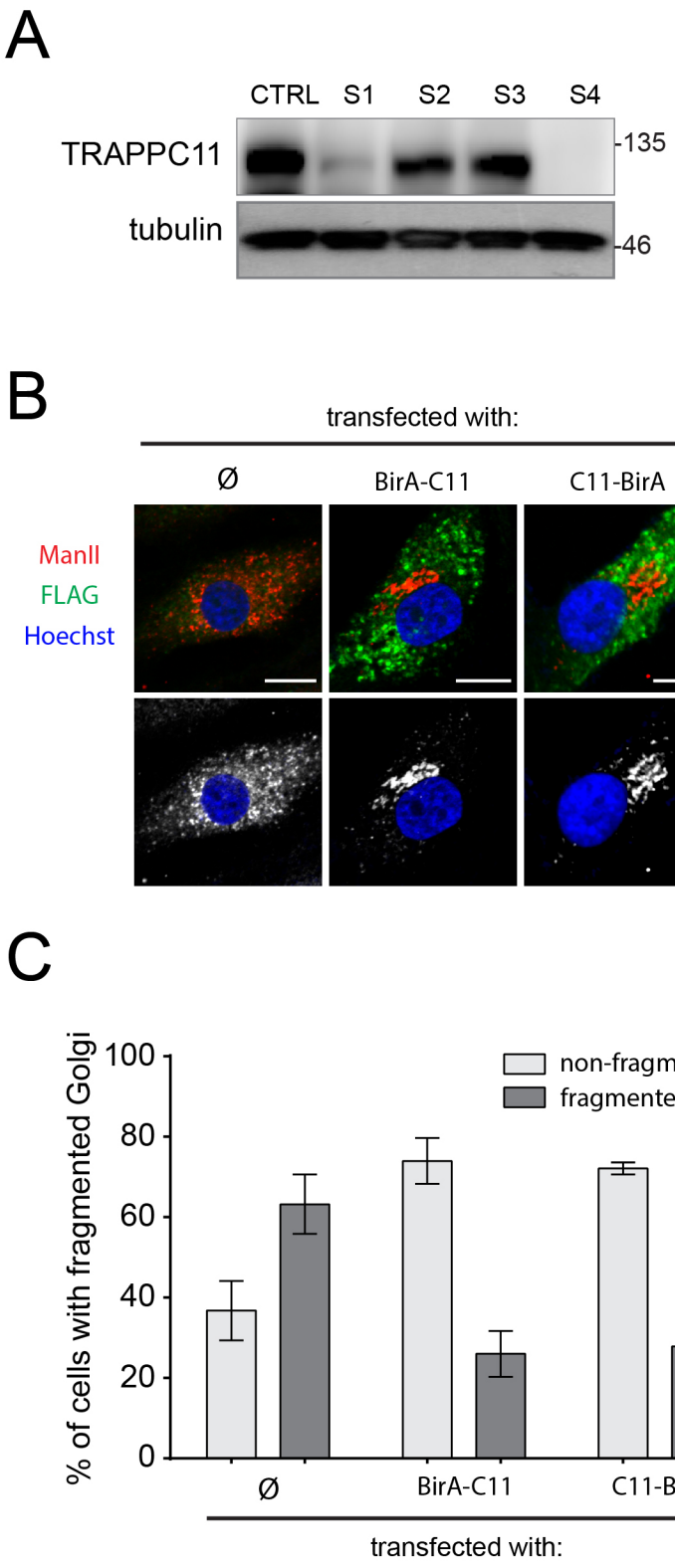

Figure 3.4 Golgi morphology is altered in fibroblasts from individual S1.

(A) Lysates were prepared from control, S1, S2 and S3 fibroblasts and probed for TRAPPC11 and tubulin (as a loading control). Molecular size standards are indicated to the right of the blots. Note that the tubulin and TRAPPC11 blots are from the same gel. (B) Fibroblasts from S1 were untransfected (ø), fixed and stained with antibodies recognizing the Golgi marker mannosidase II or transfected with a TRAPPC11 construct fused at the amino terminus or the carboxy terminus to the protein BirA (green) (BirA-C11 and C11-BirA, respectively). The BirA fusions contained a FLAG epitope tag to allow for identification of transfected cells. Note the altered morphology of the Golgi in fibroblasts from the affected individual that is rescued by either TRAPPC11 construct. The non-merged image is shown in the lower panel with the Golgi in white. (C) Quantification of the images from panel (B) was performed using criteria previously established (Milev et al., 2017; Scrivens et al., 2009). N values ranged from 25 to 38 in a single rescue experiment. Error bars indicate SEM.

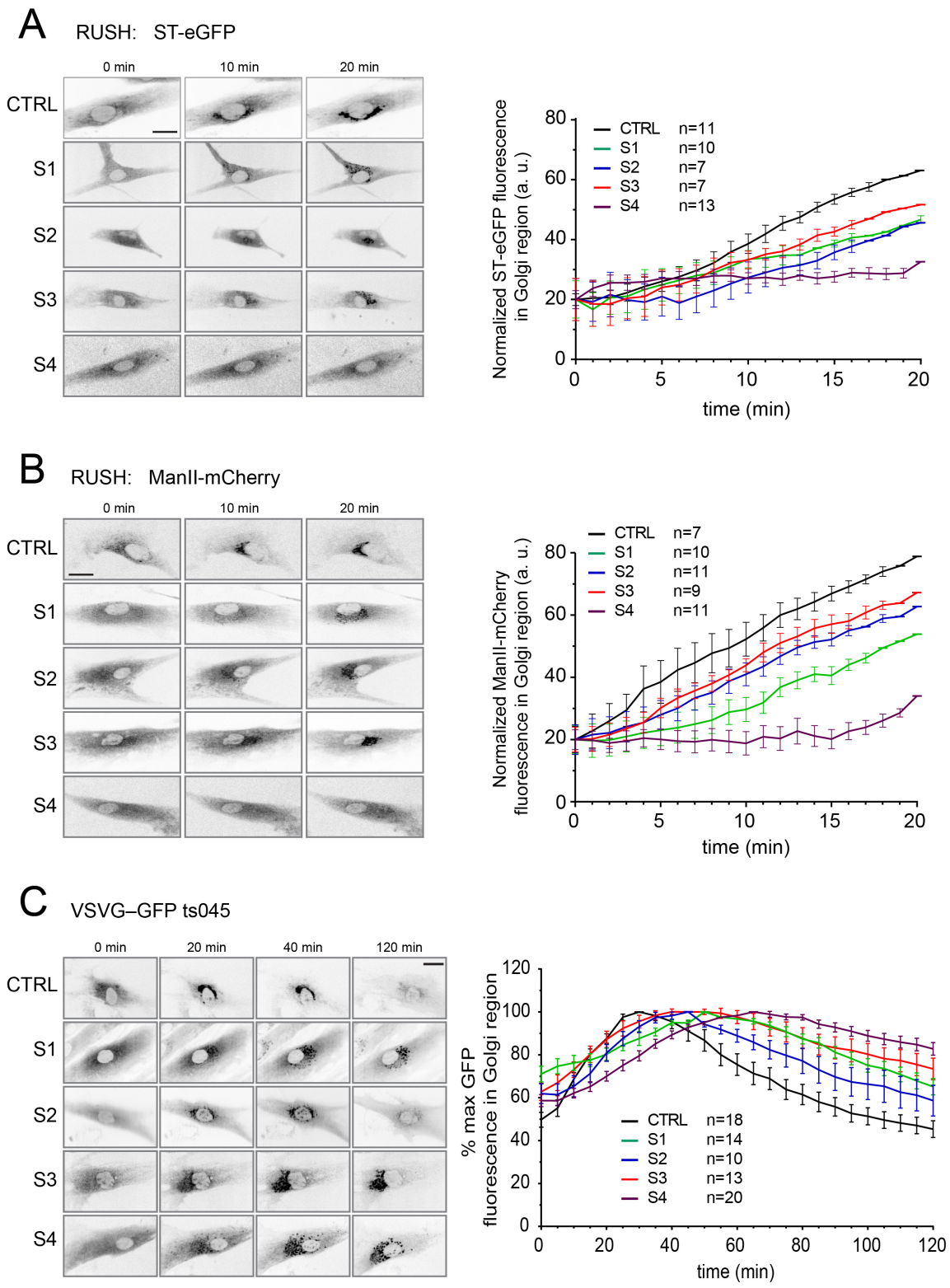

Figure 3.5 Trafficking from the ER to the Golgi and exit from the Golgi is delayed in fibroblasts from individuals S1, S2 and S3.

The RUSH assay was performed on fibroblasts from control, S1, S2 and S3 using ST-eGFP (A) and mannosidase II (ManII)-mCherry (B). The cells were imaged every minute over a period of 20 minutes after the addition of biotin to induce release of the cargo molecule from the endoplasmic reticulum. Fluorescence in the Golgi region was quantified as described in Koehler et al (2017) (Koehler et al., 2017) and is displayed to the right of the representative images. (C) Fibroblasts from control, subjects S1, S2 and S3 were infected with virus expressing VSV-G-GFP ts045. After 1 hour, the cells were shifted to the restrictive temperature of 40°C overnight. Prior to imaging the cells, cycloheximide was added. The cells were then imaged every minute over a 2-hour period at 32°C. Fluorescence in the Golgi region was quantified for the N values indicated over at least two independent experiments as described above and is displayed to the right of the representative images. The scale bars represent 25 μm and the error bars represent SEM.

3.4.3 Fibroblasts from Subjects S1, S2 and S3 Display a Defect in Protein Glycosylation

A previous study using mainly zebrafish as a model system suggested that TRAPPC11, to the exclusion of other TRAPP-associated proteins, plays an undetermined role in protein *N*-glycosylation (DeRossi et al., 2016). When examined in HeLa cells, depletion of TRAPPC11 resulted in defective glycosylation of TRAP- α, a resident ER protein whose glycosylation is independent of membrane trafficking. We therefore examined the fibroblasts from S1, S2, S3 and S4 for the glycosylation state of TRAP-α. The inclusion of S4 in this and subsequent analyses allows us to assess whether the c.3379-3380InsT allele in subject S1 is sufficient for normal TRAPPC11 function. As shown in Figure 3.6A, fibroblasts from all four subjects showed a form of TRAP-α that migrated between the fully and the unglycosylated forms of the protein in addition to a form that co-migrated with the fully glycosylated protein. The partially glycosylated form was not seen in fibroblasts from an individual with bi-allelic variants in TRAPPC12 (Milev et al., 2017), supporting our previous work in HeLa cells that indicates this is specific to defects in TRAPPC11 (DeRossi et al., 2016). These results demonstrate that, similar to a partial depletion of TRAPPC11 in HeLa cells, the TRAPPC11 variants reported herein also affect protein glycosylation.

Glycosylation defects can result in a build-up of proteins in the ER leading to ER stress, which can manifest by up regulation of a set of genes including *ATF6*, *XBP1*, *DDIT3*,

BIP, *DNAJC3*, *EDEM1* and *ATF4* responsible for a particular class of the unfolded protein response (Vacaru et al., 2014). ER stress is also associated with proteolytic processing of the ATF6 transcription factor to a faster-migrating species (Haze et al., 1999). We therefore examined fibroblasts from S1, S2, S3 and S4 for signs of ER stress by both qPCR and ATF6 processing. Except for *XBP1* expression, which showed a modest increase in subject S1 of 2.70 ± 0.49 fold compared to control, no other genes examined showed any increase (not shown). Furthermore, ATF6 processing did not reveal any significant differences when compared to control (not shown). Therefore, unlike the zebrafish *trappc11* mutant model system (DeRossi et al., 2016), we conclude that the bi-allelic *TRAPPC11* variants reported herein result in a glycosylation defect in fibroblasts but do not result in an increase in expression levels of genes that are reported to lead to ER stress.

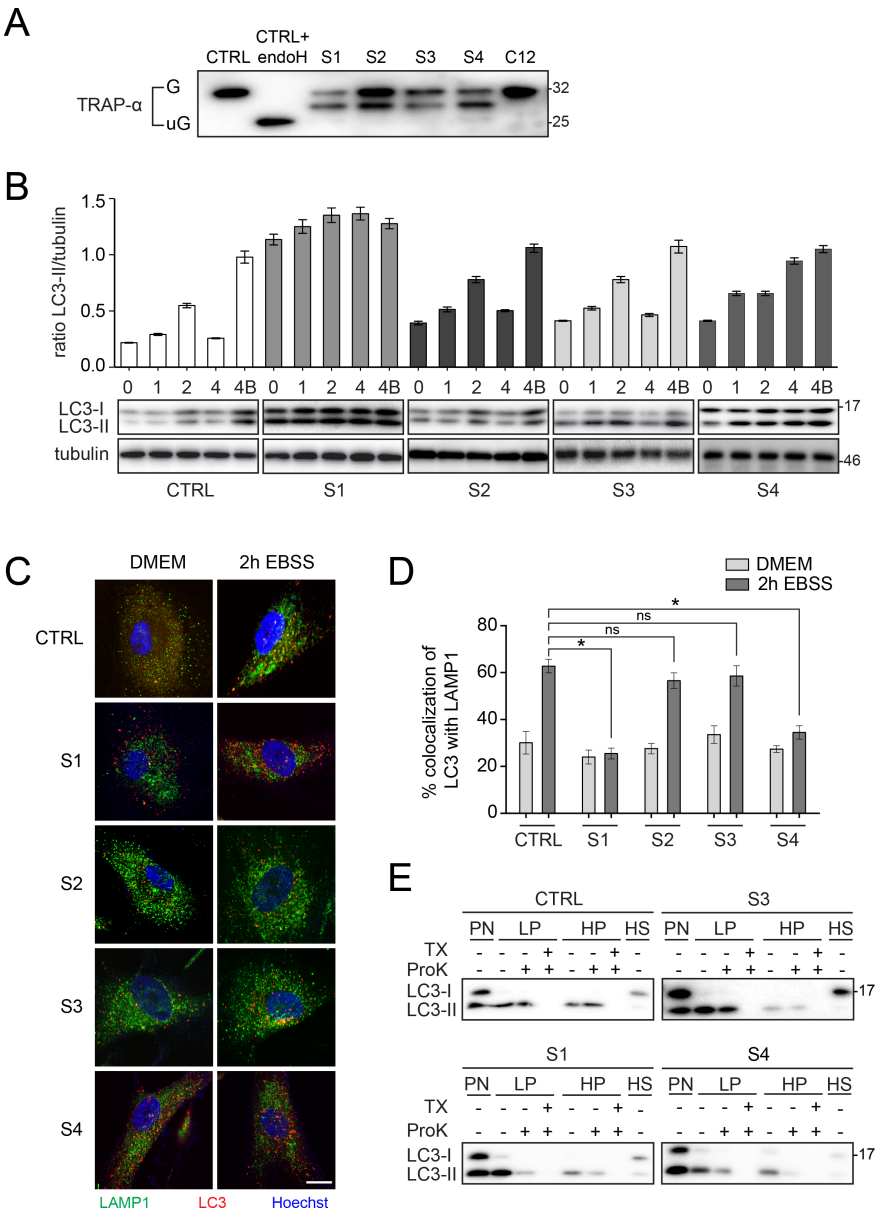

Figure 3.6 Assessment of glycosylation and autophagic flux defects in fibroblasts from individuals S1, S2, S3 and S4.

(A) Lysates were prepared from fibroblasts from control, subjects S1, S2, S3 and S4 (an individual with a homozygous c.1287+5G>A variant (Bogershausen et al., 2013)) as well as an individual with a homozygous c.145delG variant in TRAPPC12 (Milev et al., 2017) (C12). The lysates were fractionated by SDS-PAGE, transferred to PVDF membrane and probed for the ER-resident glycoprotein TRAP-α. A portion of the lysate from control cells was treated with endoglycosidase H to convert the glycosylated (G) form of the protein to the unglycosylated form (uG). (B) Fibroblasts from control, subjects S1, S2, S3 and S4 were left in nutrient rich medium (0) or starved for 1, 2 or 4 hours. One sample was starved for 4 hours in the presence of Bafilomycin A1 (4B). Lysates were prepared and probed for LC3 and tubulin as a loading control. The graph shows the ratio of the

autophagy-specific (LC3-II) form of the protein normalized to tubulin. In all cases, the tubulin blots are from the same gel as the LC3B blots. Note that samples from control and S2 were fractionated on the same gel, while S1, S3 and S4 were from different gels. Error bars indicate SEM. A representative blot from a minimum of three replicates is shown below the graph. (C) Fibroblasts from control, subjects S1, S2, S3 and S4 were left either in nutrient-rich medium or starved for 2 hours. The cells were then fixed and immunostained for LC3 and LAMP1. (D) Co-localization between LC3 and LAMP1 from the cells in panel (c) was quantified using Imaris. Statistical significance was assesed using a one-way ANOVA with posthoc Tukey HSD analysis. The asterisk (*) indicates $p<0.0001$. (E) Fibroblasts from control, subjects S1, S3 and S4 were starved for 2 hours in the presence of Bafilomycin A1, lysates were prepared and fractionated into low speed (LP), high speed (HP) pellets and a high speed supernatant (HS) fraction as described in the methods section. The fractions were subjected to proteinase K (ProK) with or without pre-treatment with the detergent Triton X-100 and then probed for LC3. Each sample was fractionated on a separate gel. Molecular size standards are indicated to the right of the blots in panels (A), (B) and (E).

3.4.4 Fibroblasts from Subject S1 Display a Defect in Autophagic Flux

We have recently shown that TRAPPC11 functions in an early stage of autophagy, after the formation of nascent isolation membranes (Stanga et al., 2019). Therefore, we examined the fibroblasts from all three subjects for defects in autophagic flux as measured by the starvation-induced accumulation and then disappearance of the autophagic marker LC3-II. As shown in Figure 6B, the fibroblasts from S1 and S4, but not S2 nor S3, displayed a defect in autophagic flux since LC3-II could not be cleared from the cells over the time course of starvation examined. The fibroblasts from S1 also displayed a high level of LC3-II even prior to starvation-induced autophagy. Although the accumulation of LC3-II prior to starvation was not as dramatic in S2, S3 and S4 as compared to S1, the levels were nevertheless elevated in the fibroblasts derived from these three subjects.

In order to confirm the autophagic flux defect, we examined the fibroblasts for co-localization between the autophagosome marker LC3 and the lysosome marker LAMP1. Co-localization would suggest that the formation of autolysosomes, organelles resulting from the fusion of autophagosomes with lysosomes, has taken place. Control fibroblasts showed a relatively high level of starvation-dependent co-localization between the marker proteins, as did fibroblasts from S2 and S3 (Figure 3.6C and D). Consistent with

the autophagic flux defect in S1, fibroblasts from this individual showed poor starvation-dependent co-localization. The same was noted for subject S4.

Using a protease protection assay (Velikkakath et al., 2012), we recently demonstrated that the starvation-dependent accumulation of LC3 punctae in S1 were in fact unsealed isolation membranes (Stanga et al., 2019). This assay works by separating lysates into two different membrane fractions (LP and HP) and a cytosolic fraction (HS). The fractions are treated with protease K either with or without detergent. If the autophagosomal marker LC3-II is susceptible to digestion in the absence of detergent, then the autophagosome membranes are not considered to be sealed. Employing this assay, we showed that, consistent with the autophagic flux and co-localization data above, fibroblasts from S3 are not defective in producing sealed autophagosomes since membrane-associated LC3 was only susceptible to protease digestion in the presence of detergent, similar to what was seen in control (Figure 3.6E). In contrast, and similar to fibroblasts derived from S1, fibroblasts from S4 in which full-length TRAPPC11 is absent also failed to seal isolation membranes into autophagosomes since LC3-II was susceptible to proteinase K treatment in the absence of detergent. Collectively, our data suggest that the extreme carboxy-terminus of TRAPPC11, but not residue Gly980, is critical for starvation-induced autophagy.

3.5 Discussion

It is becoming increasingly clear that proteins described as TRAPP subunits and thought to be stable components of a mammalian TRAPP complex, may not in fact be stably associated with the complex. This is in contrast to the yeast TRAPP proteins that seem to be stably associated with either TRAPP II or TRAPP III (Kim et al., 2006; Sacher et al., 2001; Sacher and Ferro-Novick, 2001; Sacher et al., 1998), and only break down into the likely artifactual TRAPP I upon incubation in high salt (Brunet et al., 2012). The implication of this idea is that these TRAPP-associated proteins are capable of functioning independently of the complex. This is supported by the non-identical, but partially overlapping clinical phenotypes associated with TRAPP protein variants

(reviewed in (Sacher et al., 2019)). Further support comes from the fact that several proteins including TRAPPC2, TRAPPC9, TRAPPC11 and TRAPPC12 have been uniquely implicated in collagen export, NF-κB signaling, *N*-linked protein glycosylation and chromosome congression, respectively, in addition to a role in membrane trafficking (DeRossi et al., 2016; Hu et al., 2005; Milev et al., 2015; Venditti et al., 2012). Even within TRAPP III, the complex-specific proteins TRAPPC8, TRAPPC11 and TRAPPC12 appear to have differing functions (Stanga et al., 2019). Thus, in order to better understand how these proteins can function in multiple and shared cellular processes it is necessary to identify regions of the proteins that are critical for their participation in a specific process.

We have described an individual with novel compound heterozygous *TRAPPC11* variants as well as two individuals with identical homozygous p.Gly980Arg variants that allow us to speculate on important regions of the protein that mediate different cellular processes (Figure 3.7A). The severity of the muscle weakness and the course of the disease differed distinctly between the two subjects harboring the same homozygous mutation. Therefore, it appeared meaningful to analyse the pathophysiological effects of the genetic defect in both of them. Using fibroblasts derived from these individuals, we have implicated Gly980 as part of a region critical for both membrane trafficking and *N*-linked glycosylation, but not in the maintenance of normal Golgi morphology. The Gly980 residue also does not appear to be crucial for autophagy. A multisequence alignment revealed that this region of the protein is highly conserved and that this residue in particular is invariant (Bogershausen et al., 2013). Expansion of the alignment to include more phylogenetically distant organisms confirms that this residue is indeed invariant (not shown). Although this variant was reported to likely affect protein structure, this may be very localized as it does not affect autophagy, a process that is believed to be linked to the extreme carboxy terminus (see below).

Subject S1 differs clinically from S2 and S3 mainly because of the presence of spasticity, hyperkinesia and choreiform movements. However, these clinical signs have been previously reported separately or in combination in other individuals with TRAPPC11

variants (including the c.1287+5 G>A variant) and in individuals with variants in other TRAPP proteins (TRAPPC9 and TRAPPC12) as recently reviewed (Sacher et al., 2019). Thus, some of these clinical features may be related to the function of TRAPPC11 proteins in their corresponding TRAPP complexes and to the expression of these proteins in the central nervous system. Furthermore, the impairment of autophagy observed only in S1 and associated with the c.3379_3380insT mutation may also contribute to the spasticity and choreiform movements since these clinical signs are characteristic of other human diseases in which autophagy plays a significant role (e.g. hereditary spastic paraparesis due to mutations in TECPR2 and SPASTIZIN (Jiang and Mizushima, 2014), and Huntington´s disease (Soares et al., 2019)).

With respect to the compound heterozygous case, the variant c.1287+5G>A (p.Ala372_Ser429del) was previously described in homozygous form (Bogershausen et al., 2013; Popp et al., 2017). The resulting protein appeared to be unstable as it was not detected by western analysis. One study demonstrated that this variant affects membrane trafficking (Bogershausen et al., 2013). Here we also demonstrated that this variant affects formation of autophagosomes and results in an *N*-linked glycosylation defect. These results are not unexpected considering that the protein levels of this variant are undetectable. The compound heterozygous individual also displays defects in all three processes (membrane trafficking, autophagy and *N*-linked glycosylation) as well as in maintenance of normal Golgi morphology, implicating the extreme carboxy terminus of the protein in its functions. This is based on the fact that full-length TRAPPC11 is still detectable in this individual, likely reflecting the p.Asp1127Valfs*47 protein. Further support for the importance of the extreme carboxy terminus comes from the absence of this allele in both gnomAD and ExAC. A multisequence alignment limited to humans, rodents, canine and bovine reveals that the carboxy terminus, like the rest of TRAPPC11, is well conserved (Figure 3.7B). When more phylogenetically distant organisms are included, the conservation of this region of the protein begins to drop (Figure 3.7C). Thus, we speculate that higher eukaryotes may have evolved a unique autophagy-related function in the carboxy terminus of the protein. It remains to be seen if mutations at the extreme carboxy terminus of the TRAPPC11 protein in these phylogenetically distant

organisms will affect autophagy. Recent work from our laboratory suggests that this region of the protein is important for recruiting the ATG2B-WIPI4 complex (Stanga et al., 2019), a factor that is required for the sealing of isolation membranes into enclosed autophagosomes (Velikkakath et al., 2012).

TRAPPC11 dysfunction has been implicated in protein *N*-glycosylation. The first report came from a study using a zebrafish *trappc11* mutant which displayed reduced levels of lipid-linked oligosaccharides and upregulation of genes necessary for terpenoid biosynthesis, a precursor for the carbohydrate carrier dolichol (DeRossi et al., 2016). This same study was also the first to implicate human TRAPPC11 in protein *N*-glycosylation. Two recent reports have suggested that naturally-occurring *TRAPPC11* variants are associated with defective glycosylation of the muscle protein alpha-dystroglycan (Larson et al., 2018) and altered glycosylation of both serum transferrin and apoCIII (Matalonga et al., 2017). Here, we have extended the glycosylation defect to three more *TRAPPC11* variants (subjects S1, S2/S3 and S4), suggesting that this may be a hallmark of TRAPPC11 dysfunction. While one variant in this study (subject S4) has reduced levels of the protein (Bogershausen et al., 2013), subject S1 does not show the same. Instead, this subject has a variant near the carboxy terminus of TRAPPC11. The affected region of the protein is similar to a previously published TRAPPC11 variant (p.Thr1104Ala) that was reported to have glycosylation defects (Matalonga et al., 2017), though TRAPPC11 protein levels were not reported. It is noteworthy that the latter variant also displayed a modest (2-2.5 fold) increase in the expression levels of four genes involved in the unfolded protein response (UPR), including *XBP1* which was also modestly elevated in our study. Thus, activation of UPR may be correlated to the extent of the glycosylation defect, an idea that requires further study. In the three subjects reported herein, the glycosylation defect seen in the fibroblasts might be mild since a substantial amount of fully glycosylated protein is also detected in all three subjects.

We considered the possibility that the carboxy-terminal extension of 46 residues might create an unexpected motif that could alter the function of the resulting protein. To this end we first scanned these residues in the Eukaryotic Linear Motif (ELM) database. As

expected, we identified a number of potential phosphorylation sites, kinase- and phosphatase-interacting motifs, and an *N*-linked glycosylation motif. Such motifs are not unexpected and none of them could help explain the membrane trafficking or autophagic flux defects that we reported. It should be stressed that we recently showed that only an amino-terminal tag on TRAPPC11, and not a carboxy-terminal tag, could rescue a TRAPPC11-dependent autophagy defect (Stanga et al., 2019), further highlighting the importance of the unblocked C-terminal end of TRAPPC11.

With the identification of several new individuals harboring variants in TRAPPC11, the present study strengthens the relationship between dysfunction of this gene and pathophysiology, and implicates various regions as critical for the normal function of the protein. There are now five reported variants within the foie gras domain (Bogershausen et al., 2013; Larson et al., 2018; Liang et al., 2015; Matalonga et al., 2017; Popp et al., 2017; Wang et al., 2018), suggesting that this domain is important for the function of the protein. Identification of subject S2 makes a total of three published individuals with a G980 variant (Bogershausen et al., 2013; Liang et al., 2015), and here we show that this residue is important for membrane trafficking and protein glycosylation but not for autophagy. Finally, the variants in subject S1 suggest an important role for the extreme carboxy terminus of the protein. Considering that there are two other reports of individuals having variants close to the carboxy terminus at residues Thr1104 (Matalonga et al., 2017) or Pro1005 (Wang et al., 2018), the importance of this region of the 1133 amino acid-long protein may be extended to the final ~130 amino acids, overlapping with the gryzun domain. While a function for the carboxy terminus of the protein in autophagy has recently been elucidated (Stanga et al., 2019), how this region affects membrane trafficking and protein glycosylation remains to be determined in future studies. It is notable that these latter variants are in close proximity to the gryzun domain (Figure 3.7A), a region of the protein whose function remains unknown.

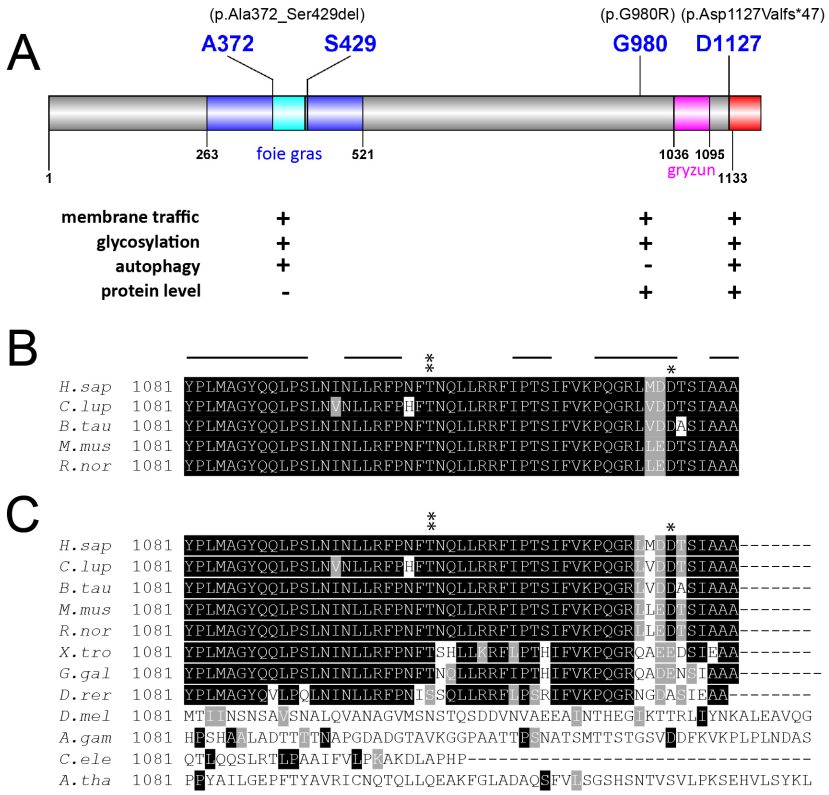

Figure 3.7 Functions associated with variants in subjects S1, S2 and S3, and the conservation of the carboxy terminus of the protein.

(A) Domain topology of TRAPPC11 showing the location and the variants described in this study. The foie gras domain (amino acids 263-521) is shaded in blue and the deletion resulting from the c.1287+5G>A variant is shaded in cyan. The first altered residue resulting from the c.3379_3380insT variant is indicated in blue and the resulting extension of the carboxy terminus is indicated in red. The gryzun domain is shaded in pink. A summary of the assay results and protein levels is indicated below the cartoon. For the assays, "+" indicates the assay was affected by the variant and "-" indicates it was not. For the protein levels, + indicates the presence of the protein and – indicates its absence. (B,C) A multiple sequence alignment of the carboxy terminus of TRAPPC11 (starting from amino acid 1081) using *H.sapiens*, *R.norvegicus*, *M.musculus*, *B.taurus* and *C.lupus* B) or the former species as well as *X.tropicalis*, *G.galus, D.rerio*, *D.melanogaster*, *A.gambiae*, C.*elegans* and *A.thaliana* (C). Black shading represents identities in at least 4 species in (B) and 9 species in (C) and gray represents similarities in at least 6 species in (C). The asterisks indicate the position of two TRAPPC11 variants that have been described in this region from the present report and in Matalonga et al (Matalonga et al., 2017). The lines above the sequences in panel (B) inidicate predicted α-helices in the human sequence using JPred4.

Chapter 4: Discussion

4.1 Overview

Although evolutionarily conserved, the mammalian TRAPP III complex appears to be significantly different from its yeast counterpart in both structure and function. Structurally, it features four peripheral subunits attached to the core of the complex rather than one. Functionally, the mammalian complex localizes to ERES and recycling endosomes in addition to just the Golgi, and it participates in COP II recruitment to the ER in addition to common roles in autophagy and ER to Golgi transport (Lamb et al., 2016; Scrivens et al., 2011; Zhao et al., 2017).

Here, I defined the role of mammalian TRAPP III in autophagy. Interestingly, at least three of the four peripheral subunits act at different steps of the pathway: TRAPPC8 participates in the formation of isolation membranes, TRAPPC11 is required to elongate isolation membranes, and TRAPPC12 acts downstream of TRAPPC11 after autophagosome formation. Based on studies in fibroblasts derived from individuals with mutations in TRAPPC11, I observed that the absence of, or alteration to, the carboxy-terminus of TRAPPC11 affected the formation of autophagosomes, a phenotype consistent with a defect in isolation membrane elongation. I also found a delay in trafficking from ER to Golgi and exit from the Golgi related to TRAPPC11 variants. These results raise an important question concerning the mechanism of TRAPP III in the secretory pathway and autophagy: whether TRAPP III indeed affects both of these processes directly, or whether its action upon one of the processes is causing a secondary effect upon the other. Since there is crosstalk between membrane trafficking and autophagy, delays in trafficking can affect the localization and availability of important cues for autophagy, just as defects in autophagy can conversely influence membrane trafficking.

4.1.1 TRAPPC11 Specifically Interacts with ATG2 and Functions in the Elongation of the Isolation Membrane

Since there could be multiple explanations for the failure to recruit ATG2 to the isolation membrane in either the absence of TRAPPC11 or when its carboxy terminus is altered, I aimed to distinguish between direct protein-protein interactions and indirect effects such as a defect in vesicular trafficking which might prevent the arrival of ATG2 at the isolation membrane. The studies in Chapter 3 helped to tease apart the causality of these effects influenced by alterations in the *TRAPPC11* gene. Subject 1 has a compound heterozygous variant causing one allele to express an unstable protein, while the other allele includes a frame-shift mutation at the carboxy-terminus. Subjects 2 and 3 both harbour a homozygous missense variant causing a point mutation in a highly-conserved region. Subject 4 harbours a homozygous variant which leads to the absence of protein. Fibroblasts from these four individuals were also compared to those from subject C12, who has a homozygous mutation in *TRAPPC12*, leading to a severely truncated protein (Chapter 2).

Consistent with previous studies showing that depletion of TRAPPC11 in HeLa resulted in Golgi fragmentation (Scrivens et al., 2011), both subject 4 (Bogershausen et al., 2013) and subject 1, with their reduced levels of protein, displayed severe Golgi fragmentation. Using the cargoes ST-eGFP and ManII-mCherry in the RUSH assay, all four subjects showed a delay in ER to Golgi traffic. Moreover, using VSVG-GFP ts045, cells from these subjects were delayed in the entire biosynthetic pathway. Even though all subjects displayed trafficking defects, subjects 1 and 4 had a blockage of autophagic flux due to unsealed isolation membranes while subjects 2 and 3 had an increased number of autophagosomes that were consumed when autophagy was induced. Similarly, cells with the TRAPPC12 variant also displayed defects in Golgi morphology and delays in the entire biosynthetic pathway (Milev et al., 2017). Nevertheless, subject C12 showed a blockage in autophagic flux with accumulation of autophagosomes. When the recruitment of ATG2 to isolation membranes was assessed, subjects 1 and 4 showed a

defect, unlike subjects 2, 3 and C12 which did not. This suggests that the delay in membrane trafficking and the defect in ATG2 recruitment are not mutually-dependent.

Since disruption of vesicular trafficking can affect the recruitment of ATG2 to isolation membranes, one might expect that other factors in the autophagy pathway would also be influenced. I next examined ATG12, a member of the ATG12-ATG5 complex, which functions as a ubiquitin-like molecule to induce the lipidation of LC3 (Walczak and Martens, 2013) and therefore acts upstream of ATG2. By analyzing isolation membranes derived from the subjects, no difference in ATG12 levels was observed. This further supports the conclusion that TRAPPC11 affects autophagy directly.

Another point of interplay between membrane trafficking and autophagy is at the level of COPII vesicles. In mammals, TRAPPC12 modulates the recruitment of Sec13/31 to the outer layer of COPII vesicles (Zhao et al., 2017). Additionally, COPII vesicles seem to be important in autophagosome biogenesis, specifically when it comes to LC3 lipidation (Ge et al., 2014). Since LC3 is already lipidated in the subject fibroblasts, COPII vesicles do not seem to have any effect on the recruitment of ATG2.

Rab proteins represent yet another link between the secretory and autophagy pathways. For example, Rab1a was found to be important for omegasome formation (Huang et al., 2011; Zoppino et al., 2010). Since current models assume that TRAPP III is a GEF for Rab1 (Li et al., 2017; Yamasaki et al., 2009), it is feasible that any change to the TRAPP complex could affect Rab1 activation. To validate the specific role of TRAPPC11, I examined whether a dominant-negative form of Rab1 could phenocopy TRAPPC11 depletion, and whether a constitutively-active form of Rab1 could suppress that same phenotype. Neither was observed, suggesting that the phenotypes seen upon depletion of TRAPPC11 are not due to a change in Rab1 activity. Collectively, my results support the model of TRAPPC11 directly and specifically recruiting ATG2 to isolation membranes, independent of its role in membrane trafficking.

4.1.2 TRAPPC11 Recruits ATG2 and WIPI4

ATG2 and WIPI4 form a complex that is found on the growing isolation membrane. Since the depletion of TRAPPC11 phenocopies depletion of either ATG2 or WIPI4, and since I suspect that TRAPPC11 directly interacts with ATG2, the order of recruitment was then probed. First, immunoblots against TRAPP proteins in cells depleted of ATG2 or WIPI4 were performed, and then these were compared to immunoblots against either ATG2 or WIPI4 in cells depleted of TRAPPC8, TRAPPC11 or TRAPPC12. I observed that when either ATG2 or WIPI4 were depleted, TRAPP proteins were recruited onto membranes upon induction of autophagy. However, when TRAPPC11 was depleted, neither ATG2 nor WIPI4 were detected on membranes, despite the fact that the recruitment of ATG12-ATG5 was not affected. Consistent with its role in the initiation of the isolation membrane, cells depleted of TRAPPC8 did not display any sign of ATG2, ATG12, WIPI4, TRAPPC11 nor TRAPPC12 on membranes, likely due to the absence of the isolation membrane. Interestingly, TRAPPC12 depleted cells showed normal recruitment of ATG2, WIPI4 and ATG12-ATG5. Overall, immunoblotting results are consistent with TRAPP III being required for the recruitment of ATG2 and WIPI4.

4.1.3 The Mechanisms of ATG2 Recruitment Differ between Mammals and Lower Eukaryotes

If TRAPPC11 is solely responsible for the recruitment of ATG2 and WIPI4 in mammalian cells, this would differ from the proposed mechanism of autophagosome biogenesis in yeast, where the complex Atg2-Atg18 can associate with the PAS independently of TRAPP complexes and is held at the membrane by Atg9 (Gomez-Sanchez et al., 2018). Additionally, Atg9 was found to recruit vesicle-tethering proteins Trs85 and Ypt1 to the PAS (Kakuta et al., 2012).

While the mechanism of autophagosome biogenesis is highly conserved between yeast and mammals, the function of Atg9 seems to have diverged. In yeast, Atg9 was found to recruit vesicle-tethering proteins Trs85 and Ypt1 to the PAS (Kakuta et al., 2012). Atg2, a key protein in autophagosome biogenesis, has two membrane-binding regions with a

role in membrane tethering during elongation of the isolation membrane, and it also possesses an amphipathic helix that targets the Atg2-Atg18 complex to the PAS and facilitates binding between Atg18 and PI(3)P (Kotani et al., 2018). Although Atg2 and Atg9 can interact, it was recently proposed that Atg2 can associate with autophagosomal membranes through lipid binding, without the assistance of Atg9. Instead, the function of Atg9 is to retain the Atg2-Atg18 complex on the PAS once it has already arrived (Gomez-Sanchez et al., 2018).

A similar but more evolved mechanism exists in mammals. Contrary to yeast cells that have a single PAS, mammalian cells have multiple omegasomes, which serve as autophagosome nucleation sites. As such, there is a potential benefit to rapid cycling of autophagy factors. Mediated by TRAPPC8, the mammalian TRAPP III complex interacts with TBC1D14 upon initiation of autophagy, allowing ATG9 vesicles to cycle from one omegasome through the endomembrane system to the Golgi, and from there to another omegasome (Lamb et al., 2016). Analogously to yeast, there is an interaction between ATG2 and the human Atg18 homologue WIPI4 at the nucleation site (Maeda et al., 2019), and it is thought that ATG2 transfers lipids between membranes, mediating *de novo* autophagosome biogenesis (Ktistakis, 2019; Osawa et al., 2019b; Osawa and Noda, 2019; Valverde et al., 2019). However, ATG9 is not involved in this process. Human ATG9 does not interact with ATG2B, nor with WIPI4 (Chapter 2), and a review of the literature did not uncover any known interactions between ATG9 and either isoform of ATG2, nor with WIPI4.

Why might mammalian cells need to employ a different mechanism of ATG2 recruitment to isolation membranes than that of lower eukaryotes? Yeast Atg9 recruits TRAPP III, Ypt1 and Atg2-Atg18 to promote the elongation of the isolation membrane, whereas mammalian ATG9 seems to have a transient role in the recruitment of TRAPP III and Rab1 through interaction with TBC1D14. ATG2-WIPI4 recruitment is still required, but it is mediated by TRAPPC11 and not ATG9. To contextualise this difference, I offer two speculative ideas. First, since there are multiple sites for autophagosome nucleation in mammalian cells, cycling ATG9 between the Golgi and these sites in a processive

fashion could be the most efficient way to provide important cues for autophagosome biogenesis simultaneously at multiple sites. Second, considering that mammalian TRAPP III is bulkier than the yeast complex, it is possible that the presence of TRAPP III on the mammalian isolation membrane somehow hinders ATG9 and renders it ineffective as an ATG2 interactor, thereby necessitating the involvement of TRAPPC11 as a specialized intermediary.

4.1.4 TRAPPC11 Also Functions Independently of the TRAPP III Complex in the N-glycosylation Pathway

Both in the autophagy pathway, where it interacts with ATG2, as well as in the secretory pathway, the functions ascribed to TRAPPC11 are dependent upon its membership in the TRAPP III complex. However, TRAPPC11 was also found to function independently of the complex and regulate N-glycosylation through the formation of lipid-linked oligosaccharides (DeRossi et al., 2016). I examined N-glycosylation in HeLa cells by observing the mobility of the ER-localized signal sequence receptor TRAPα (Wu et al., 2007). TRAPα has two glycosylation sites whose glycans are not processed in the Golgi, making it an ideal marker to identify site occupancy defects. Aberrant glycosylation of TRAPα was seen only after depletion of TRAPPC11, while depletion of either TRAPPC2, TRAPPC8 or TRAPPC12 did not affect the glycosylation process (DeRossi et al., 2016). This suggests that TRAPPC11 is the only TRAPP protein involved in N-glycosylation.

To confirm the involvement of TRAPPC11 is complex-glycosylation, I then assessed the level of glycosylation of TRAPα in fibroblasts from the aforementioned individuals with variants in TRAPPC11 (subjects 1-4) and compared them to subject C12. I observed defects in glycosylation of TRAPα in subjects 1, 2, 3 and 4, but not in subject C12. In order to further validate the specificity of TRAPPC11 in glycosylation, I also analyzed TRAPα in fibroblasts harbouring a variant in TRAPPC4. This variant results in vastly reduced TRAPPC4 levels, resulting unstable TRAPP complexes in these cells (Van Bergen et al., 2019). I found no difference compared to the control cells, which supports

the previous finding that TRAPPC11 acts in N-glycosylation independent of the TRAPP III complex (DeRossi et al., 2016).

Taken together, I propose that TRAPPC11 has an unidentified moonlighting function in protein glycosylation (DeRossi et al., 2016). This is not the first TRAPP subunit proposed to have a moonlighting function, as TRAPPC12 dissociates from the complex upon phosphorylation to regulate kinetochore stability and CENP-E recruitment (Milev et al., 2015). Further research should focus on the role of TRAPPC11 in this process from a mechanistic standpoint.

4.2 Conclusions

TRAPPC11 functions in at least three intracellular pathways: glycosylation, vesicular trafficking, and autophagy. Its role in N-glycosylation is distinct from other TRAPP proteins, and without its function in lipid-linked oligosaccharide synthesis, hypoglycosylated proteins accumulate. However, TRAPPC11 is unable to act in ER to Golgi traffic alone, rather it is incorporated into the TRAPP III complex where it is a critical factor. Apart from its function in membrane traffic, TRAPPC11 also affects autophagy as a TRAPP III subunit, through direct interaction with the ATG2-WIPI4 complex. Individuals having variants in different TRAPP subunits harbour a wide range of different phenotypes, although overlap is observed. In the case of TRAPPC11, there are an increased number of reports of individuals with neuromuscular disorders and intellectual disabilities (Bogershausen et al., 2013; Fee et al., 2017; Koehler et al., 2017; Larson et al., 2018; Liang et al., 2015; Matalonga et al., 2017).

The crosstalk between membrane trafficking and glycosylation is well documented. Following synthesis in the ER, glycosylated proteins are transported through the Golgi en route to their final destination, subject to covalent attachment and modification of glycans along the way. The glycosylation process relies heavily upon the compartmentalization of glycosylation enzymes. Any disturbance of the finely regulated balance between anterograde and retrograde trafficking could potentially lead to abnormal glycans that

cause premature degradation, mislocalization, improper retention, loss of Golgi stability and/or global trafficking delays. As such, TRAPPC11 is not the only protein involved in both membrane traffic and glycosylation. It is well documented that the COG complex is essential in intra-Golgi trafficking due to its ability to coordinate Rab GTPases, golgins, coat proteins and SNAREs during vesicle tethering (Climer et al., 2015; Sohda et al., 2010). Studies performed on individuals with congenital disorders of glycosylation revealed the importance of the COG complex in Golgi-based glycosylation, due to its role in recycling vesicles that contain glycosyl-transferases (Reynders et al., 2011; Shestakova et al., 2006). The pathologies observed in these individuals showcase the inherent link between trafficking deficiencies and an altered glycosylation pattern (Foulquier et al., 2007; Foulquier et al., 2006; Morava et al., 2007; Zeevaert et al., 2008).

Just as membrane trafficking and glycosylation are interdependent, changes to either of them can also influence autophagy. The organelles most notably affected are lysosomes, which are responsible for degrading extracellular and intracellular material delivered by either endocytosis or autophagy, respectively (Saftig and Klumperman, 2009). The components designated for degradation pass across a thick lysosomal membrane to reach an acidic compartment containing more than fifty hydrolases. To create a barrier between the acidic luminal milieu and the cytosol, membrane proteins in the lysosome are heavily glycosylated (Fukuda, 1991). The most abundant lysosomal associated membrane proteins, LAMP-1 and LAMP-2, have more than ten glycosylation sites. As one might expect, defects in the glycosylation of these proteins can trigger their retention in the ER and subsequent degradation by ERAD, which results in a deficiency of membrane proteins in lysosomes. This deficiency affects not just the lysosomal pH but also the entire physiology of the lysosome, as some hydrolases are inactive at less-acidic pH levels. To date, more than twelve different disorders have been linked to a lack of lysosomal membrane proteins. For example, Danon disease, caused by the absence of LAMP-2, is characterized by severe skeletal and cardiac myopathies and an increased number of autophagosomes in myocytes (Nishino et al., 2000). These same symptoms are also observed in individuals who have variants in TRAPPC11 (Bogershausen et al., 2013; Fee et al., 2017; Liang et al., 2015).

NPC1 is an example of a disease in which trafficking is affected by mutations to genes encoding the Niemann-Pick type C protein, leading to a subsequent defect in autophagy. The variant proteins impair amphisome formation and autophagosome maturation (Sarkar et al., 2013). This produces hepatic dysfunction, ataxia, spasticity and dementia. Some of the individuals with variants in TRAPPC11 also have disorders including liver fibrosis and fatty liver (Fee et al., 2017; Liang et al., 2015). However, some of the individuals with variant TRAPPC11 proteins also display neurodevelopmental phenotypes, which are not associated with neither Danon nor with NPC1. There is a potential link between neuronal disorders and autophagy if reduced autophagic degradation and/or dysregulated autophagy causes abnormal protein aggregates (Nah et al., 2015).

In summary, membrane trafficking is critically important to autophagy and glycosylation, among other pathways. In order to define a precise role of human TRAPP proteins in cellular physiology, one must begin by accounting for the interplay between these processes. The mechanisms underpinning the plethora of phenotypes observed across individuals with TRAPPC11 variants are key to understanding not only the functional roles of this protein, but also to developing new insights into the causes of other neuromuscular diseases. TRAPPC11 serves in trafficking as part of TRAPP III, promotes elongation of the isolation membrane by direct recruitment of ATG2, and moonlights in the synthesis of lipid-linked oligosaccharides. The burgeoning field of glycomics can further elucidate the mechanism of the N-glycosylation role, which will perhaps explain how crosstalk leads to clinical symptoms.

References

Antonescu, C.N., T.E. McGraw, and A. Klip. 2014. Reciprocal regulation of endocytosis and metabolism. *Cold Spring Harbor perspectives in biology*. 6:a016964.

Axe, E.L., S.A. Walker, M. Manifava, P. Chandra, H.L. Roderick, A. Habermann, G. Griffiths, and N.T. Ktistakis. 2008. Autophagosome formation from membrane compartments enriched in phosphatidylinositol 3-phosphate and dynamically connected to the endoplasmic reticulum. *J Cell Biol*. 182:685-701.

Bakula, D., A.J. Muller, T. Zuleger, Z. Takacs, M. Franz-Wachtel, A.K. Thost, D. Brigger, M.P. Tschan, T. Frickey, H. Robenek, B. Macek, and T. Proikas-Cezanne. 2017. WIPI3 and WIPI4 beta-propellers are scaffolds for LKB1-AMPK-TSC signalling circuits in the control of autophagy. *Nat Commun*. 8:15637.

Barlowe, C., L. Orci, T. Yeung, M. Hosobuchi, S. Hamamoto, N. Salama, M.F. Rexach, M. Ravazzola, M. Amherdt, and R. Schekman. 1994. COPII: a membrane coat formed by Sec proteins that drive vesicle budding from the endoplasmic reticulum. *Cell*. 77:895-907.

Baskaran, S., M.J. Ragusa, E. Boura, and J.H. Hurley. 2012. Two-site recognition of phosphatidylinositol 3-phosphate by PROPPINs in autophagy. *Molecular cell*. 47:339-348.

Bassik, M.C., M. Kampmann, R.J. Lebbink, S. Wang, M.Y. Hein, I. Poser, J. Weibezahn, M.A. Horlbeck, S. Chen, M. Mann, A.A. Hyman, E.M. Leproust, M.T. McManus, and J.S. Weissman. 2013. A systematic mammalian genetic interaction map reveals pathways underlying ricin susceptibility. *Cell*. 152:909-922.

Beck, R., F. Adolf, C. Weimer, B. Bruegger, and F.T. Wieland. 2009. ArfGAP1 activity and COPI vesicle biogenesis. *Traffic*. 10:307-315.

Behrends, C., M.E. Sowa, S.P. Gygi, and J.W. Harper. 2010. Network organization of the human autophagy system. *Nature*. 466:68-76.

Bogershausen, N., N. Shahrzad, J.X. Chong, J.C. von Kleist-Retzow, D. Stanga, Y. Li, F.P. Bernier, C.M. Loucks, R. Wirth, E.G. Puffenberger, R.A. Hegele, J. Schreml, G. Lapointe, K. Keupp, C.L. Brett, R. Anderson, A. Hahn, A.M. Innes, O. Suchowersky, M.B. Mets, G. Nurnberg, D.R. McLeod, H. Thiele, D. Waggoner, J. Altmuller, K.M. Boycott, B. Schoser, P. Nurnberg, C. Ober, R. Heller, J.S. Parboosingh, B. Wollnik, M. Sacher, and R.E. Lamont. 2013. Recessive TRAPPC11 mutations cause a disease spectrum of limb girdle muscular dystrophy and myopathy with movement disorder and intellectual disability. *American journal of human genetics*. 93:181-190.

Boncompain, G., S. Divoux, N. Gareil, H. de Forges, A. Lescure, L. Latreche, V. Mercanti, F. Jollivet, G. Raposo, and F. Perez. 2012. Synchronization of secretory protein traffic in populations of cells. *Nat Methods*. 9:493-498.

Bonifacino, J.S., and B.S. Glick. 2004. The mechanisms of vesicle budding and fusion. *Cell*. 116:153-166.

Bonifacino, J.S., and J. Lippincott-Schwartz. 2003. Coat proteins: shaping membrane transport. *Nature reviews. Molecular cell biology*. 4:409-414.

Boya, P., F. Reggiori, and P. Codogno. 2013. Emerging regulation and functions of autophagy. *Nat Cell Biol*. 15:713-720.

Brocker, C., S. Engelbrecht-Vandre, and C. Ungermann. 2010. Multisubunit tethering complexes and their role in membrane fusion. *Curr. Biol.* 20:R943-952.

Brunet, S., B. Noueihed, N. Shahrzad, D. Saint-Dic, B. Hasaj, T.L. Guan, A. Moores, C. Barlowe, and M. Sacher. 2012. The SMS domain of Trs23p is responsible for the in vitro appearance of the TRAPP I complex in Saccharomyces cerevisiae. *Cell Logist*. 2:28-42.

Brunet, S., and M. Sacher. 2014. In sickness and in health: the role of TRAPP and associated proteins in disease. *Traffic*. 15:803-818.

Brunet, S., D. Saint-Dic, M.P. Milev, T. Nilsson, and M. Sacher. 2016. The TRAPP Subunit Trs130p Interacts with the GAP Gyp6p to Mediate Ypt6p Dynamics at the Late Golgi. *Front Cell Dev Biol*. 4:48.

Brunet, S., N. Shahrzad, D. Saint-Dic, H. Dutczak, and M. Sacher. 2013. A trs20 mutation that mimics an SEDT-causing mutation blocks selective and non-selective autophagy: a model for TRAPP III organization. *Traffic*. 14:1091-1104.

Cai, Y., H.F. Chin, D. Lazarova, S. Menon, C. Fu, H. Cai, A. Sclafani, D.W. Rodgers, E.M. De La Cruz, S. Ferro-Novick, and K.M. Reinisch. 2008. The structural basis for activation of the Rab Ypt1p by the TRAPP membrane-tethering complexes. *Cell*. 133:1202-1213.

Chan, E.Y., A. Longatti, N.C. McKnight, and S.A. Tooze. 2009. Kinase-inactivated ULK proteins inhibit autophagy via their conserved C-terminal domains using an Atg13-independent mechanism. *Mol Cell Biol*. 29:157-171.

Chen, D., W. Fan, Y. Lu, X. Ding, S. Chen, and Q. Zhong. 2012. A mammalian autophagosome maturation mechanism mediated by TECPR1 and the Atg12-Atg5 conjugate. *Molecular cell*. 45:629-641.

Chen, Y.A., and R.H. Scheller. 2001. SNARE-mediated membrane fusion. *Nature reviews. Molecular cell biology*. 2:98-106.

Chowdhury, S., C. Otomo, A. Leitner, K. Ohashi, R. Aebersold, G.C. Lander, and T. Otomo. 2018. Insights into autophagosome biogenesis from structural and biochemical analyses of the ATG2A-WIPI4 complex. *Proc. Natl. Acad. Sci. U. S. A.* 115:E9792-E9801.

Christ, L., C. Raiborg, E.M. Wenzel, C. Campsteijn, and H. Stenmark. 2017. Cellular Functions and Molecular Mechanisms of the ESCRT Membrane-Scission Machinery. *Trends Biochem Sci*. 42:42-56.

Cinaroglu, A., C. Gao, D. Imrie, and K.C. Sadler. 2011. Activating transcription factor 6 plays protective and pathological roles in steatosis due to endoplasmic reticulum stress in zebrafish. *Hepatology*. 54:495-508.

Climer, L.K., M. Dobretsov, and V. Lupashin. 2015. Defects in the COG complex and COG-related trafficking regulators affect neuronal Golgi function. *Front Neurosci*. 9:405.

Corcelle-Termeau, E., S.D. Vindelov, S. Hamalisto, B. Mograbi, A. Keldsbo, J.H. Brasen, E. Favaro, D. Adam, P. Szyniarowski, P. Hofman, S. Krautwald, T. Farkas, N.H. Petersen, M. Rohde, A. Linkermann, and M. Jaattela. 2016. Excess

sphingomyelin disturbs ATG9A trafficking and autophagosome closure. *Autophagy*. 12:833-849.

Davis, S., J. Wang, and S. Ferro-Novick. 2017. Crosstalk between the Secretory and Autophagy Pathways Regulates Autophagosome Formation. *Developmental cell*. 41:23-32.

Davis, S., J. Wang, M. Zhu, K. Stahmer, R. Lakshminarayan, M. Ghassemian, Y. Jiang, E.A. Miller, and S. Ferro-Novick. 2016. Sec24 phosphorylation regulates autophagosome abundance during nutrient deprivation. *Elife*. 5.

Deneka, M., M. Neeft, and P. van der Sluijs. 2003. Regulation of membrane transport by rab GTPases. *Crit Rev Biochem Mol Biol*. 38:121-142.

DeRossi, C., A. Vacaru, R. Rafiq, A. Cinaroglu, D. Imrie, S. Nayar, A. Baryshnikova, M.P. Milev, D. Stanga, D. Kadakia, N. Gao, J. Chu, H.H. Freeze, M.A. Lehrman, M. Sacher, and K.C. Sadler. 2016. trappc11 is required for protein glycosylation in zebrafish and humans. *Molecular biology of the cell*. 27:1220-1234.

Dubnau, J., A.S. Chiang, L. Grady, J. Barditch, S. Gossweiler, J. McNeil, P. Smith, F. Buldoc, R. Scott, U. Certa, C. Broger, and T. Tully. 2003. The staufen/pumilio pathway is involved in Drosophila long-term memory. *Curr. Biol.* 13:286-296.

Dubowitz, V., C.A. Sewry, and A. Oldfors. 2014. Muscle biopsy: A practical approach. 4th edition. *London. Saunders Elsevier*.

Dubuke, M.L., S. Maniatis, S.A. Shaffer, and M. Munson. 2015. The Exocyst Subunit Sec6 Interacts with Assembled Exocytic SNARE Complexes. *J Biol Chem*. 290:28245-28256.

Eskelinen, E.L. 2005. Maturation of autophagic vacuoles in Mammalian cells. *Autophagy*. 1:1-10.

Fai Tse, W.K., J.W. Li, A.C. Kwan Tse, T.F. Chan, J.C. Hin Ho, R.S. Sun Wu, C.K. Chu Wong, and K.P. Lai. 2016. Fatty liver disease induced by perfluorooctane sulfonate: Novel insight from transcriptome analysis. *Chemosphere*. 159:166-177.

Fan, W., A. Nassiri, and Q. Zhong. 2011. Autophagosome targeting and membrane curvature sensing by Barkor/Atg14(L). *Proc. Natl. Acad. Sci. U. S. A.* 108:7769-7774.

Fass, E., E. Shvets, I. Degani, K. Hirschberg, and Z. Elazar. 2006. Microtubules support production of starvation-induced autophagosomes but not their targeting and fusion with lysosomes. *J Biol Chem*. 281:36303-36316.

Fee, D.B., M. Harmelink, P. Monrad, and E. Pyzik. 2017. Siblings With Mutations in TRAPPC11 Presenting With Limb-Girdle Muscular Dystrophy 2S. *J Clin Neuromuscul Dis*. 19:27-30.

Foulquier, F., D. Ungar, E. Reynders, R. Zeevaert, P. Mills, M.T. Garcia-Silva, P. Briones, B. Winchester, W. Morelle, M. Krieger, W. Annaert, and G. Matthijs. 2007. A new inborn error of glycosylation due to a Cog8 deficiency reveals a critical role for the Cog1-Cog8 interaction in COG complex formation. *Hum Mol Genet*. 16:717-730.

Foulquier, F., E. Vasile, E. Schollen, N. Callewaert, T. Raemaekers, D. Quelhas, J. Jaeken, P. Mills, B. Winchester, M. Krieger, W. Annaert, and G. Matthijs. 2006. Conserved oligomeric Golgi complex subunit 1 deficiency reveals a previously uncharacterized congenital disorder of glycosylation type II. *Proc. Natl. Acad. Sci. U. S. A.* 103:3764-3769.

Fujita, N., M. Hayashi-Nishino, H. Fukumoto, H. Omori, A. Yamamoto, T. Noda, and T. Yoshimori. 2008. An Atg4B mutant hampers the lipidation of LC3 paralogues and causes defects in autophagosome closure. *Molecular biology of the cell*. 19:4651-4659.

Fukuda, M. 1991. Lysosomal membrane glycoproteins. Structure, biosynthesis, and intracellular trafficking. *J Biol Chem*. 266:21327-21330.

Gaugel, A., D. Bakula, A. Hoffmann, and T. Proikas-Cezanne. 2012. Defining regulatory and phosphoinositide-binding sites in the human WIPI-1 beta-propeller responsible for autophagosomal membrane localization downstream of mTORC1 inhibition. *J Mol Signal*. 7:16.

Ge, L., M. Zhang, and R. Schekman. 2014. Phosphatidylinositol 3-kinase and COPII generate LC3 lipidation vesicles from the ER-Golgi intermediate compartment. *Elife*. 3:e04135.

Gedeon, A.K., A. Colley, R. Jamieson, E.M. Thompson, J. Rogers, D. Sillence, G.E. Tiller, J.C. Mulley, and J. Gecz. 1999. Identification of the gene (SEDL) causing X-linked spondyloepiphyseal dysplasia tarda. *Nat Genet*. 22:400-404.

Goh, L.K., and A. Sorkin. 2013. Endocytosis of receptor tyrosine kinases. *Cold Spring Harbor perspectives in biology*. 5:a017459.

Gomez-Navarro, N., and E.A. Miller. 2016. COP-coated vesicles. *Curr. Biol.* 26:R54-R57.

Gomez-Sanchez, R., J. Rose, R. Guimaraes, M. Mari, D. Papinski, E. Rieter, W.J. Geerts, R. Hardenberg, C. Kraft, C. Ungermann, and F. Reggiori. 2018. Atg9 establishes Atg2-dependent contact sites between the endoplasmic reticulum and phagophores. *J Cell Biol*. 217:2743-2763.

Grewal, P.K., J.M. McLaughlan, C.J. Moore, C.A. Browning, and J.E. Hewitt. 2005. Characterization of the LARGE family of putative glycosyltransferases associated with dystroglycanopathies. *Glycobiology*. 15:912-923.

Grimmel, M., C. Backhaus, and T. Proikas-Cezanne. 2015. WIPI-Mediated Autophagy and Longevity. *Cells*. 4:202-217.

Guo, B., Q. Liang, L. Li, Z. Hu, F. Wu, P. Zhang, Y. Ma, B. Zhao, A.L. Kovacs, Z. Zhang, D. Feng, S. Chen, and H. Zhang. 2014. O-GlcNAc-modification of SNAP-29 regulates autophagosome maturation. *Nat Cell Biol*. 16:1215-1226.

Haack, T.B., P. Hogarth, M.C. Kruer, A. Gregory, T. Wieland, T. Schwarzmayr, E. Graf, L. Sanford, E. Meyer, E. Kara, S.M. Cuno, S.I. Harik, V.H. Dandu, N. Nardocci, G. Zorzi, T. Dunaway, M. Tarnopolsky, S. Skinner, S. Frucht, E. Hanspal, C. Schrander-Stumpel, D. Heron, C. Mignot, B. Garavaglia, K. Bhatia, J. Hardy, T.M. Strom, N. Boddaert, H.H. Houlden, M.A. Kurian, T. Meitinger, H. Prokisch, and S.J. Hayflick. 2012. Exome sequencing reveals de novo WDR45 mutations causing a phenotypically distinct, X-linked dominant form of NBIA. *American journal of human genetics*. 91:1144-1149.

Hailey, D.W., A.S. Rambold, P. Satpute-Krishnan, K. Mitra, R. Sougrat, P.K. Kim, and J. Lippincott-Schwartz. 2010. Mitochondria supply membranes for autophagosome biogenesis during starvation. *Cell*. 141:656-667.

Hamasaki, M., N. Furuta, A. Matsuda, A. Nezu, A. Yamamoto, N. Fujita, H. Oomori, T. Noda, T. Haraguchi, Y. Hiraoka, A. Amano, and T. Yoshimori. 2013a. Autophagosomes form at ER-mitochondria contact sites. *Nature*. 495:389-393.

Hamasaki, M., S.T. Shibutani, and T. Yoshimori. 2013b. Up-to-date membrane biogenesis in the autophagosome formation. *Curr Opin Cell Biol*. 25:455-460.

Hanewinkel, H., J. Glossl, and H. Kresse. 1987. Biosynthesis of cathepsin B in cultured normal and I-cell fibroblasts. *J Biol Chem*. 262:12351-12355.

Hara, T., A. Takamura, C. Kishi, S. Iemura, T. Natsume, J.L. Guan, and N. Mizushima. 2008. FIP200, a ULK-interacting protein, is required for autophagosome formation in mammalian cells. *J Cell Biol*. 181:497-510.

Hayashi-Nishino, M., N. Fujita, T. Noda, A. Yamaguchi, T. Yoshimori, and A. Yamamoto. 2009. A subdomain of the endoplasmic reticulum forms a cradle for autophagosome formation. *Nat Cell Biol*. 11:1433-1437.

Haze, K., H. Yoshida, H. Yanagi, T. Yura, and K. Mori. 1999. Mammalian transcription factor ATF6 is synthesized as a transmembrane protein and activated by proteolysis in response to endoplasmic reticulum stress. *Mol Biol Cell*. 10:3787-3799.

Heuser, J. 1989. Changes in lysosome shape and distribution correlated with changes in cytoplasmic pH. *J Cell Biol*. 108:855-864.

Hosokawa, N., T. Sasaki, S. Iemura, T. Natsume, T. Hara, and N. Mizushima. 2009. Atg101, a novel mammalian autophagy protein interacting with Atg13. *Autophagy*. 5:973-979.

Hu, W.H., J.S. Pendergast, X.M. Mo, R. Brambilla, V. Bracchi-Ricard, F. Li, W.M. Walters, B. Blits, L. He, S.M. Schaal, and J.R. Bethea. 2005. NIBP, a novel NIK and IKK(beta)-binding protein that enhances NF-(kappa)B activation. *J Biol Chem*. 280:29233-29241.

Huang, J., C.L. Birmingham, S. Shahnazari, J. Shiu, Y.T. Zheng, A.C. Smith, K.G. Campellone, W.D. Heo, S. Gruenheid, T. Meyer, M.D. Welch, N.T. Ktistakis, P.K. Kim, D.J. Klionsky, and J.H. Brumell. 2011. Antibacterial autophagy occurs at PI(3)P-enriched domains of the endoplasmic reticulum and requires Rab1 GTPase. *Autophagy*. 7:17-26.

Hutagalung, A.H., and P.J. Novick. 2011. Role of Rab GTPases in membrane traffic and cell physiology. *Physiol Rev*. 91:119-149.

Ichimura, Y., T. Kirisako, T. Takao, Y. Satomi, Y. Shimonishi, N. Ishihara, N. Mizushima, I. Tanida, E. Kominami, M. Ohsumi, T. Noda, and Y. Ohsumi. 2000. A ubiquitin-like system mediates protein lipidation. *Nature*. 408:488-492.

Imai, K., F. Hao, N. Fujita, Y. Tsuji, Y. Oe, Y. Araki, M. Hamasaki, T. Noda, and T. Yoshimori. 2016. Atg9A trafficking through the recycling endosomes is required for autophagosome formation. *Journal of cell science*. 129:3781-3791.

Irannejad, R., and M. von Zastrow. 2014. GPCR signaling along the endocytic pathway. *Curr Opin Cell Biol*. 27:109-116.

Itakura, E., and N. Mizushima. 2010. Characterization of autophagosome formation site by a hierarchical analysis of mammalian Atg proteins. *Autophagy*. 6:764-776.

Jahreiss, L., F.M. Menzies, and D.C. Rubinsztein. 2008. The itinerary of autophagosomes: from peripheral formation to kiss-and-run fusion with lysosomes. *Traffic*. 9:574-587.

Jiang, P., and N. Mizushima. 2014. Autophagy and human diseases. *Cell Res*. 24:69-79.

Jiang, P., T. Nishimura, Y. Sakamaki, E. Itakura, T. Hatta, T. Natsume, and N. Mizushima. 2014. The HOPS complex mediates autophagosome-lysosome fusion through interaction with syntaxin 17. *Molecular biology of the cell*. 25:1327-1337.

Johansen, T., and T. Lamark. 2019. Selective Autophagy: ATG8 Family Proteins, LIR Motifs and Cargo Receptors. *J Mol Biol*.

Johnson, K., A. Topf, M. Bertoli, L. Phillips, K.G. Claeys, V.R. Stojanovic, S. Peric, A. Hahn, P. Maddison, E. Akay, A.E. Bastian, A. Lusakowska, A. Kostera-Pruszczyk, M. Lek, L. Xu, D.G. MacArthur, and V. Straub. 2017. Identification of GAA variants through whole exome sequencing targeted to a cohort of 606 patients with unexplained limb-girdle muscle weakness. *Orphanet J Rare Dis*. 12:173.

Jones, S., C. Newman, F. Liu, and N. Segev. 2000. The TRAPP complex is a nucleotide exchanger for Ypt1 and Ypt31/32. *Molecular biology of the cell*. 11:4403-4411.

Kabeya, Y., N. Mizushima, T. Ueno, A. Yamamoto, T. Kirisako, T. Noda, E. Kominami, Y. Ohsumi, and T. Yoshimori. 2000. LC3, a mammalian homologue of yeast Apg8p, is localized in autophagosome membranes after processing. *The EMBO journal*. 19:5720-5728.

Kabeya, Y., N. Mizushima, A. Yamamoto, S. Oshitani-Okamoto, Y. Ohsumi, and T. Yoshimori. 2004. LC3, GABARAP and GATE16 localize to autophagosomal membrane depending on form-II formation. *Journal of cell science*. 117:2805-2812.

Kakuta, S., H. Yamamoto, L. Negishi, C. Kondo-Kakuta, N. Hayashi, and Y. Ohsumi. 2012. Atg9 vesicles recruit vesicle-tethering proteins Trs85 and Ypt1 to the autophagosome formation site. *J Biol Chem*. 287:44261-44269.

Karanasios, E., E. Stapleton, M. Manifava, T. Kaizuka, N. Mizushima, S.A. Walker, and N.T. Ktistakis. 2013. Dynamic association of the ULK1 complex with omegasomes during autophagy induction. *Journal of cell science*. 126:5224-5238.

Keramaris-Vrantsis, E., P.J. Lu, T. Doran, A. Zillmer, J. Ashar, C.T. Esapa, M.A. Benson, D.J. Blake, J. Rosenfeld, and Q.L. Lu. 2007. Fukutin-related protein localizes to the Golgi apparatus and mutations lead to mislocalization in muscle in vivo. *Muscle Nerve*. 36:455-465.

Kim, J., M. Kundu, B. Viollet, and K.L. Guan. 2011. AMPK and mTOR regulate autophagy through direct phosphorylation of Ulk1. *Nat Cell Biol*. 13:132-141.

Kim, J.J., Z. Lipatova, and N. Segev. 2016. TRAPP Complexes in Secretion and Autophagy. *Front Cell Dev Biol*. 4:20.

Kim, Y.G., S. Raunser, C. Munger, J. Wagner, Y.L. Song, M. Cygler, T. Walz, B.H. Oh, and M. Sacher. 2006. The architecture of the multisubunit TRAPP I complex suggests a model for vesicle tethering. *Cell*. 127:817-830.

Kimura, S., T. Noda, and T. Yoshimori. 2007. Dissection of the autophagosome maturation process by a novel reporter protein, tandem fluorescent-tagged LC3. *Autophagy*. 3:452-460.

Kirchhausen, T. 2000. Three ways to make a vesicle. *Nature reviews. Molecular cell biology*. 1:187-198.

Kishi-Itakura, C., I. Koyama-Honda, E. Itakura, and N. Mizushima. 2014. Ultrastructural analysis of autophagosome organization using mammalian autophagy-deficient cells. *Journal of cell science*. 127:4089-4102.

Klann, M., H. Koeppl, and M. Reuss. 2012. Spatial modeling of vesicle transport and the cytoskeleton: the challenge of hitting the right road. *PLoS One*. 7:e29645.

Klionsky, D.J., K. Abdelmohsen, A. Abe, M.J. Abedin, H. Abeliovich, A. Acevedo Arozena, H. Adachi, C.M. Adams, P.D. Adams, K. Adeli, P.J. Adhihetty, S.G. Adler, G. Agam, R. Agarwal, M.K. Aghi, M. Agnello, P. Agostinis, P.V. Aguilar, J. Aguirre-Ghiso, E.M. Airoldi, S. Ait-Si-Ali, T. Akematsu, E.T. Akporiaye, M. Al-Rubeai, G.M. Albaiceta, C. Albanese, D. Albani, M.L. Albert, J. Aldudo, H. Algul, M. Alirezaei, I. Alloza, A. Almasan, M. Almonte-Beceril, E.S. Alnemri, C. Alonso, N. Altan-Bonnet, D.C. Altieri, S. Alvarez, L. Alvarez-Erviti, S. Alves, G. Amadoro, A. Amano, C. Amantini, S. Ambrosio, I. Amelio, A.O. Amer, M. Amessou, A. Amon, Z. An, F.A. Anania, S.U. Andersen, U.P. Andley, C.K. Andreadi, N. Andrieu-Abadie, A. Anel, D.K. Ann, S. Anoopkumar-Dukie, M. Antonioli, H. Aoki, N. Apostolova, S. Aquila, K. Aquilano, K. Araki, E. Arama, A. Aranda, J. Araya, A. Arcaro, E. Arias, H. Arimoto, A.R. Ariosa, J.L. Armstrong, T. Arnould, I. Arsov, K. Asanuma, V. Askanas, E. Asselin, R. Atarashi, S.S. Atherton, J.D. Atkin, L.D. Attardi, P. Auberger, G. Auburger, L. Aurelian, R. Autelli, L. Avagliano, M.L. Avantaggiati, L. Avrahami, S. Awale, N. Azad, T. Bachetti, J.M. Backer, D.H. Bae, J.S. Bae, O.N. Bae, S.H. Bae, E.H. Baehrecke, S.H. Baek, S. Baghdiguian, A. Bagniewska-Zadworna, et al. 2016. Guidelines for the use and interpretation of assays for monitoring autophagy (3rd edition). *Autophagy*. 12:1-222.

Klionsky, D.J., E.H. Baehrecke, J.H. Brumell, C.T. Chu, P. Codogno, A.M. Cuervo, J. Debnath, V. Deretic, Z. Elazar, E.L. Eskelinen, S. Finkbeiner, J. Fueyo-Margareto, D. Gewirtz, M. Jaattela, G. Kroemer, B. Levine, T.J. Melia, N. Mizushima, D.C. Rubinsztein, A. Simonsen, A. Thorburn, M. Thumm, and S.A. Tooze. 2011. A comprehensive glossary of autophagy-related molecules and processes (2nd edition). *Autophagy*. 7:1273-1294.

Knorr, R.L., R. Lipowsky, and R. Dimova. 2015. Autophagosome closure requires membrane scission. *Autophagy*. 11:2134-2137.

Koehler, K., M.P. Milev, K. Prematilake, F. Reschke, S. Kutzner, R. Juhlen, D. Landgraf, E. Utine, F. Hazan, G. Diniz, M. Schuelke, A. Huebner, and M. Sacher. 2017. A novel TRAPPC11 mutation in two Turkish families associated with cerebral atrophy, global retardation, scoliosis, achalasia and alacrima. *J Med Genet*. 54:176-185.

Komatsu, M., S. Waguri, T. Ueno, J. Iwata, S. Murata, I. Tanida, J. Ezaki, N. Mizushima, Y. Ohsumi, Y. Uchiyama, E. Kominami, K. Tanaka, and T. Chiba. 2005. Impairment of starvation-induced and constitutive autophagy in Atg7-deficient mice. *J Cell Biol*. 169:425-434.

Kotani, T., H. Kirisako, M. Koizumi, Y. Ohsumi, and H. Nakatogawa. 2018. The Atg2-Atg18 complex tethers pre-autophagosomal membranes to the endoplasmic reticulum for autophagosome formation. *Proc. Natl. Acad. Sci. U. S. A.* 115:10363-10368.

Koyama-Honda, I., E. Itakura, T.K. Fujiwara, and N. Mizushima. 2013. Temporal analysis of recruitment of mammalian ATG proteins to the autophagosome formation site. *Autophagy*. 9:1491-1499.

Kraft, C., and S. Martens. 2012. Mechanisms and regulation of autophagosome formation. *Curr Opin Cell Biol*. 24:496-501.

Kreis, T.E., M. Lowe, and R. Pepperkok. 1995. COPs regulating membrane traffic. *Annu Rev Cell Dev Biol*. 11:677-706.

Kriegenburg, F., C. Ungermann, and F. Reggiori. 2018. Coordination of Autophagosome-Lysosome Fusion by Atg8 Family Members. *Curr. Biol.* 28:R512-R518.

Ktistakis, N.T. 2019. Who plays the ferryman: ATG2 channels lipids into the forming autophagosome. *J Cell Biol*. 218:1767-1768.

Kuma, A., N. Mizushima, N. Ishihara, and Y. Ohsumi. 2002. Formation of the approximately 350-kDa Apg12-Apg5.Apg16 multimeric complex, mediated by Apg16 oligomerization, is essential for autophagy in yeast. *J Biol Chem*. 277:18619-18625.

Kumar, N., M. Leonzino, W. Hancock-Cerutti, F.A. Horenkamp, P. Li, J.A. Lees, H. Wheeler, K.M. Reinisch, and P. De Camilli. 2018. VPS13A and VPS13C are lipid transport proteins differentially localized at ER contact sites. *J Cell Biol*. 217:3625-3639.

Lamb, C.A., S. Nuhlen, D. Judith, D. Frith, A.P. Snijders, C. Behrends, and S.A. Tooze. 2016. TBC1D14 regulates autophagy via the TRAPP complex and ATG9 traffic. *The EMBO journal*. 35:281-301.

Lamb, C.A., T. Yoshimori, and S.A. Tooze. 2013. The autophagosome: origins unknown, biogenesis complex. *Nature reviews. Molecular cell biology*. 14:759-774.

Larson, A.A., P.R. Baker, 2nd, M.P. Milev, C.A. Press, R.J. Sokol, M.O. Cox, J.K. Lekostaj, A.A. Stence, A.D. Bossler, J.M. Mueller, K. Prematilake, T.F. Tadjo, C.A. Williams, M. Sacher, and S.A. Moore. 2018. TRAPPC11 and GOSR2 mutations associate with hypoglycosylation of alpha-dystroglycan and muscular dystrophy. *Skelet Muscle*. 8:17.

Lee, E.J., and C. Tournier. 2011. The requirement of uncoordinated 51-like kinase 1 (ULK1) and ULK2 in the regulation of autophagy. *Autophagy*. 7:689-695.

Levine, B., and D.J. Klionsky. 2017. Autophagy wins the 2016 Nobel Prize in Physiology or Medicine: Breakthroughs in baker's yeast fuel advances in biomedical research. *Proc. Natl. Acad. Sci. U. S. A.* 114:201-205.

Li, C., X. Luo, S. Zhao, G.K. Siu, Y. Liang, H.C. Chan, A. Satoh, and S.S. Yu. 2017. COPI-TRAPPII activates Rab18 and regulates its lipid droplet association. *The EMBO journal*. 36:441-457.

Li, C., and S. Yu. 2014. A perspective from transport protein particle: vesicle tether and human diseases. *Sheng Li Xue Bao*. 66:1-6.

Liang, W.C., W. Zhu, S. Mitsuhashi, S. Noguchi, M. Sacher, M. Ogawa, H.H. Shih, Y.J. Jong, and I. Nishino. 2015. Congenital muscular dystrophy with fatty liver and infantile-onset cataract caused by TRAPPC11 mutations: broadening of the phenotype. *Skelet Muscle*. 5:29.

Lipatova, Z., N. Belogortseva, X.Q. Zhang, J. Kim, D. Taussig, and N. Segev. 2012. Regulation of selective autophagy onset by a Ypt/Rab GTPase module. *Proc. Natl. Acad. Sci. U. S. A.* 109:6981-6986.

Loerke, D., M. Mettlen, D. Yarar, K. Jaqaman, H. Jaqaman, G. Danuser, and S.L. Schmid. 2009. Cargo and dynamin regulate clathrin-coated pit maturation. *PLoS Biol*. 7:e57.

Longatti, A., C.A. Lamb, M. Razi, S. Yoshimura, F.A. Barr, and S.A. Tooze. 2012. TBC1D14 regulates autophagosome formation via Rab11- and ULK1-positive recycling endosomes. *J Cell Biol*. 197:659-675.

Lu, Q., P. Yang, X. Huang, W. Hu, B. Guo, F. Wu, L. Lin, A.L. Kovacs, L. Yu, and H. Zhang. 2011. The WD40 repeat PtdIns(3)P-binding protein EPG-6 regulates progression of omegasomes to autophagosomes. *Developmental cell*. 21:343-357.

Lynch-Day, M.A., D. Bhandari, S. Menon, J. Huang, H. Cai, C.R. Bartholomew, J.H. Brumell, S. Ferro-Novick, and D.J. Klionsky. 2010. Trs85 directs a Ypt1 GEF, TRAPPIII, to the phagophore to promote autophagy. *Proc. Natl. Acad. Sci. U. S. A.* 107:7811-7816.

Maeda, S., C. Otomo, and T. Otomo. 2019. The autophagic membrane tether ATG2A transfers lipids between membranes. *Elife*. 8.

Malkus, P., F. Jiang, and R. Schekman. 2002. Concentrative sorting of secretory cargo proteins into COPII-coated vesicles. *J Cell Biol*. 159:915-921.

Matalonga, L., M. Bravo, C. Serra-Peinado, E. Garcia-Pelegri, O. Ugarteburu, S. Vidal, M. Llambrich, E. Quintana, P. Fuster-Jorge, M.N. Gonzalez-Bravo, S. Beltran, J. Dopazo, F. Garcia-Garcia, F. Foulquier, G. Matthijs, P. Mills, A. Ribes, G. Egea, P. Briones, F. Tort, and M. Giros. 2017. Mutations in TRAPPC11 are associated with a congenital disorder of glycosylation. *Hum Mutat*. 38:148-151.

Matsumoto, H., S. Noguchi, K. Sugie, M. Ogawa, K. Murayama, Y.K. Hayashi, and I. Nishino. 2004. Subcellular localization of fukutin and fukutin-related protein in muscle cells. *J Biochem*. 135:709-712.

Mauthe, M., A. Jacob, S. Freiberger, K. Hentschel, Y.D. Stierhof, P. Codogno, and T. Proikas-Cezanne. 2011. Resveratrol-mediated autophagy requires WIPI-1-regulated LC3 lipidation in the absence of induced phagophore formation. *Autophagy*. 7:1448-1461.

Meiling-Wesse, K., U.D. Epple, R. Krick, H. Barth, A. Appelles, C. Voss, E.L. Eskelinen, and M. Thumm. 2005. Trs85 (Gsg1), a component of the TRAPP

complexes, is required for the organization of the preautophagosomal structure during selective autophagy via the Cvt pathway. *J Biol Chem*. 280:33669-33678.

Meiringer, C.T., R. Rethmeier, K. Auffarth, J. Wilson, A. Perz, C. Barlowe, H.D. Schmitt, and C. Ungermann. 2011. The Dsl1 protein tethering complex is a resident endoplasmic reticulum complex, which interacts with five soluble NSF (N-ethylmaleimide-sensitive factor) attachment protein receptors (SNAREs): implications for fusion and fusion regulation. *J Biol Chem*. 286:25039-25046.

Mellman, I., and Y. Yarden. 2013. Endocytosis and cancer. *Cold Spring Harbor perspectives in biology*. 5:a016949.

Mercer, C.A., A. Kaliappan, and P.B. Dennis. 2009. A novel, human Atg13 binding protein, Atg101, interacts with ULK1 and is essential for macroautophagy. *Autophagy*. 5:649-662.

Michele, D.E., R. Barresi, M. Kanagawa, F. Saito, R.D. Cohn, J.S. Satz, J. Dollar, I. Nishino, R.I. Kelley, H. Somer, V. Straub, K.D. Mathews, S.A. Moore, and K.P. Campbell. 2002. Post-translational disruption of dystroglycan-ligand interactions in congenital muscular dystrophies. *Nature*. 418:417-422.

Michell, R.H., V.L. Heath, M.A. Lemmon, and S.K. Dove. 2006. Phosphatidylinositol 3,5-bisphosphate: metabolism and cellular functions. *Trends Biochem Sci*. 31:52-63.

Mihaela Bozic, L.v.d.B., Beth A. Milne, Nicola Goodman, Lisa Roberston, Alan R. Prescott, Thomas J. Macartney, Nina Dawe, David G. McEwan. 2019. A conserved ATG2-GABARAP interaction is critical for phagophore closure. *bioRxiv*.

Milev, M.P., C. Graziano, D. Karall, W.F.E. Kuper, N. Al-Deri, D.M. Cordelli, T.B. Haack, K. Danhauser, A. Iuso, F. Palombo, T. Pippucci, H. Prokisch, D. Saint-Dic, M. Seri, D. Stanga, G. Cenacchi, K.L.I. van Gassen, J. Zschocke, C. Fauth, J.A. Mayr, M. Sacher, and P.M. van Hasselt. 2018. Bi-allelic mutations in TRAPPC2L result in a neurodevelopmental disorder and have an impact on RAB11 in fibroblasts. *J Med Genet*. 55:753-764.

Milev, M.P., M.E. Grout, D. Saint-Dic, Y.H. Cheng, I.A. Glass, C.J. Hale, D.S. Hanna, M.O. Dorschner, K. Prematilake, A. Shaag, O. Elpeleg, M. Sacher, D. Doherty,

and S. Edvardson. 2017. Mutations in TRAPPC12 Manifest in Progressive Childhood Encephalopathy and Golgi Dysfunction. *American journal of human genetics*. 101:291-299.

Milev, M.P., B. Hasaj, D. Saint-Dic, S. Snounou, Q. Zhao, and M. Sacher. 2015. TRAMM/TrappC12 plays a role in chromosome congression, kinetochore stability, and CENP-E recruitment. *J Cell Biol*. 209:221-234.

Milev, M.P., D. Stanga, A. Schanzer, A. Nascimento, D. Saint-Dic, C. Ortez, D.N. Benito, D.G. Barrios, J. Colomer, C. Badosa, C. Jou, P. Gallano, L. Gonzalez-Quereda, A. Topf, K. Johnson, V. Straub, A. Hahn, M. Sacher, and C. Jimenez-Mallebrera. 2019. Characterization of three TRAPPC11 variants suggests a critical role for the extreme carboxy terminus of the protein. *Sci Rep*. 9:14036.

Mizushima, N., A. Yamamoto, M. Hatano, Y. Kobayashi, Y. Kabeya, K. Suzuki, T. Tokuhisa, Y. Ohsumi, and T. Yoshimori. 2001. Dissection of autophagosome formation using Apg5-deficient mouse embryonic stem cells. *J Cell Biol*. 152:657-668.

Mizushima, N., T. Yoshimori, and Y. Ohsumi. 2011. The role of Atg proteins in autophagosome formation. *Annu Rev Cell Dev Biol*. 27:107-132.

Mohamoud, H.S., S. Ahmed, M. Jelani, N. Alrayes, K. Childs, N. Vadgama, M.M. Almramhi, J.Y. Al-Aama, S. Goodbourn, and J. Nasir. 2018. A missense mutation in TRAPPC6A leads to build-up of the protein, in patients with a neurodevelopmental syndrome and dysmorphic features. *Sci Rep*. 8:2053.

Mora, R., I. Dokic, T. Kees, C.M. Huber, D. Keitel, R. Geibig, B. Brugge, H. Zentgraf, N.R. Brady, and A. Regnier-Vigouroux. 2010. Sphingolipid rheostat alterations related to transformation can be exploited for specific induction of lysosomal cell death in murine and human glioma. *Glia*. 58:1364-1383.

Morava, E., R. Zeevaert, E. Korsch, K. Huijben, S. Wopereis, G. Matthijs, K. Keymolen, D.J. Lefeber, L. De Meirleir, and R.A. Wevers. 2007. A common mutation in the COG7 gene with a consistent phenotype including microcephaly, adducted thumbs, growth retardation, VSD and episodes of hyperthermia. *Eur J Hum Genet*. 15:638-645.

Moreau, K., B. Ravikumar, M. Renna, C. Puri, and D.C. Rubinsztein. 2011. Autophagosome precursor maturation requires homotypic fusion. *Cell*. 146:303-317.

Nah, J., J. Yuan, and Y.K. Jung. 2015. Autophagy in neurodegenerative diseases: from mechanism to therapeutic approach. *Mol Cells*. 38:381-389.

Nair, U., A. Jotwani, J. Geng, N. Gammoh, D. Richerson, W.L. Yen, J. Griffith, S. Nag, K. Wang, T. Moss, M. Baba, J.A. McNew, X. Jiang, F. Reggiori, T.J. Melia, and D.J. Klionsky. 2011. SNARE proteins are required for macroautophagy. *Cell*. 146:290-302.

Nakatogawa, H., Y. Ichimura, and Y. Ohsumi. 2007. Atg8, a ubiquitin-like protein required for autophagosome formation, mediates membrane tethering and hemifusion. *Cell*. 130:165-178.

Nakatogawa, H., K. Suzuki, Y. Kamada, and Y. Ohsumi. 2009. Dynamics and diversity in autophagy mechanisms: lessons from yeast. *Nature reviews. Molecular cell biology*. 10:458-467.

Neufeld, T.P. 2010. TOR-dependent control of autophagy: biting the hand that feeds. *Curr Opin Cell Biol*. 22:157-168.

Nichols, B.J., C. Ungermann, H.R. Pelham, W.T. Wickner, and A. Haas. 1997. Homotypic vacuolar fusion mediated by t- and v-SNAREs. *Nature*. 387:199-202.

Nishino, I., J. Fu, K. Tanji, T. Yamada, S. Shimojo, T. Koori, M. Mora, J.E. Riggs, S.J. Oh, Y. Koga, C.M. Sue, A. Yamamoto, N. Murakami, S. Shanske, E. Byrne, E. Bonilla, I. Nonaka, S. DiMauro, and M. Hirano. 2000. Primary LAMP-2 deficiency causes X-linked vacuolar cardiomyopathy and myopathy (Danon disease). *Nature*. 406:906-910.

Ogawa, M., Y. Yoshikawa, T. Kobayashi, H. Mimuro, M. Fukumatsu, K. Kiga, Z. Piao, H. Ashida, M. Yoshida, S. Kakuta, T. Koyama, Y. Goto, T. Nagatake, S. Nagai, H. Kiyono, M. Kawalec, J.M. Reichhart, and C. Sasakawa. 2011. A Tecpr1-dependent selective autophagy pathway targets bacterial pathogens. *Cell Host Microbe*. 9:376-389.

Ohya, T., M. Miaczynska, U. Coskun, B. Lommer, A. Runge, D. Drechsel, Y. Kalaidzidis, and M. Zerial. 2009. Reconstitution of Rab- and SNARE-dependent membrane fusion by synthetic endosomes. *Nature*. 459:1091-1097.

Orsi, A., M. Razi, H.C. Dooley, D. Robinson, A.E. Weston, L.M. Collinson, and S.A. Tooze. 2012. Dynamic and transient interactions of Atg9 with autophagosomes, but not membrane integration, are required for autophagy. *Molecular biology of the cell*. 23:1860-1873.

Osawa, T., J.M. Alam, and N.N. Noda. 2019a. Membrane-binding domains in autophagy. *Chem Phys Lipids*. 218:1-9.

Osawa, T., T. Kotani, T. Kawaoka, E. Hirata, K. Suzuki, H. Nakatogawa, Y. Ohsumi, and N.N. Noda. 2019b. Atg2 mediates direct lipid transfer between membranes for autophagosome formation. *Nat Struct Mol Biol*. 26:281-288.

Osawa, T., and N.N. Noda. 2019. Atg2: A novel phospholipid transfer protein that mediates de novo autophagosome biogenesis. *Protein Sci*. 28:1005-1012.

Otomo, C., Z. Metlagel, G. Takaesu, and T. Otomo. 2013. Structure of the human ATG12~ATG5 conjugate required for LC3 lipidation in autophagy. *Nat Struct Mol Biol*. 20:59-66.

Otomo, T., S. Chowdhury, and G.C. Lander. 2018. The rod-shaped ATG2A-WIPI4 complex tethers membranes in vitro. *Contact (Thousand Oaks)*. 1.

Panda, P.K., A. Fahrner, S. Vats, E. Seranova, V. Sharma, M. Chipara, P. Desai, J. Torresi, T. Rosenstock, D. Kumar, and S. Sarkar. 2019. Chemical Screening Approaches Enabling Drug Discovery of Autophagy Modulators for Biomedical Applications in Human Diseases. *Front Cell Dev Biol*. 7:38.

Pereira-Leal, J.B., and M.C. Seabra. 2000. The mammalian Rab family of small GTPases: definition of family and subfamily sequence motifs suggests a mechanism for functional specificity in the Ras superfamily. *J Mol Biol*. 301:1077-1087.

Pfisterer, S.G., M. Mauthe, P. Codogno, and T. Proikas-Cezanne. 2011. Ca2+/calmodulin-dependent kinase (CaMK) signaling via CaMKI and AMP-activated protein kinase contributes to the regulation of WIPI-1 at the onset of autophagy. *Mol Pharmacol*. 80:1066-1075.

Popovic, D., and I. Dikic. 2014. TBC1D5 and the AP2 complex regulate ATG9 trafficking and initiation of autophagy. *EMBO Rep*. 15:392-401.

Popp, B., A.B. Ekici, C.T. Thiel, J. Hoyer, A. Wiesener, C. Kraus, A. Reis, and C. Zweier. 2017. Exome Pool-Seq in neurodevelopmental disorders. *Eur J Hum Genet*. 25:1364-1376.

Proikas-Cezanne, T., Z. Takacs, P. Donnes, and O. Kohlbacher. 2015. WIPI proteins: essential PtdIns3P effectors at the nascent autophagosome. *Journal of cell science*. 128:207-217.

Proikas-Cezanne, T., S. Waddell, A. Gaugel, T. Frickey, A. Lupas, and A. Nordheim. 2004. WIPI-1alpha (WIPI49), a member of the novel 7-bladed WIPI protein family, is aberrantly expressed in human cancer and is linked to starvation-induced autophagy. *Oncogene*. 23:9314-9325.

Punnonen, E.L., K. Pihakaski, K. Mattila, K. Lounatmaa, and P. Hirsimaki. 1989. Intramembrane particles and filipin labelling on the membranes of autophagic vacuoles and lysosomes in mouse liver. *Cell Tissue Res*. 258:269-276.

Puri, C., M. Renna, C.F. Bento, K. Moreau, and D.C. Rubinsztein. 2013. Diverse autophagosome membrane sources coalesce in recycling endosomes. *Cell*. 154:1285-1299.

Ramirez-Peinado, S., T.I. Ignashkova, B.J. van Raam, J. Baumann, E.L. Sennott, M. Gendarme, R.K. Lindemann, M.N. Starnbach, and J.H. Reiling. 2017. TRAPPC13 modulates autophagy and the response to Golgi stress. *J Cell Sci*. 130:2251-2265.

Ravikumar, B., K. Moreau, L. Jahreiss, C. Puri, and D.C. Rubinsztein. 2010a. Plasma membrane contributes to the formation of pre-autophagosomal structures. *Nat Cell Biol*. 12:747-757.

Ravikumar, B., K. Moreau, and D.C. Rubinsztein. 2010b. Plasma membrane helps autophagosomes grow. *Autophagy*. 6:1184-1186.

Reinhard, C., M. Schweikert, F.T. Wieland, and W. Nickel. 2003. Functional reconstitution of COPI coat assembly and disassembly using chemically defined components. *Proc. Natl. Acad. Sci. U. S. A.* 100:8253-8257.

Rentzsch, P., D. Witten, G.M. Cooper, J. Shendure, and M. Kircher. 2019. CADD: predicting the deleteriousness of variants throughout the human genome. *Nucleic Acids Res*. 47:D886-D894.

Reynders, E., F. Foulquier, W. Annaert, and G. Matthijs. 2011. How Golgi glycosylation meets and needs trafficking: the case of the COG complex. *Glycobiology*. 21:853-863.

Riedel, F., A. Galindo, N. Muschalik, and S. Munro. 2018. The two TRAPP complexes of metazoans have distinct roles and act on different Rab GTPases. *J Cell Biol*. 217:601-617.

Rieter, E., F. Vinke, D. Bakula, E. Cebollero, C. Ungermann, T. Proikas-Cezanne, and F. Reggiori. 2013. Atg18 function in autophagy is regulated by specific sites within its beta-propeller. *Journal of cell science*. 126:593-604.

Ross, E.M., and T.M. Wilkie. 2000. GTPase-activating proteins for heterotrimeric G proteins: regulators of G protein signaling (RGS) and RGS-like proteins. *Annu Rev Biochem*. 69:795-827.

Rossi, G., K. Kolstad, S. Stone, F. Palluault, and S. Ferro-Novick. 1995. BET3 encodes a novel hydrophilic protein that acts in conjunction with yeast SNAREs. *Molecular biology of the cell*. 6:1769-1780.

Roux, K.J., D.I. Kim, M. Raida, and B. Burke. 2012. A promiscuous biotin ligase fusion protein identifies proximal and interacting proteins in mammalian cells. *J Cell Biol*. 196:801-810.

Russell, R.C., Y. Tian, H. Yuan, H.W. Park, Y.Y. Chang, J. Kim, H. Kim, T.P. Neufeld, A. Dillin, and K.L. Guan. 2013. ULK1 induces autophagy by phosphorylating Beclin-1 and activating VPS34 lipid kinase. *Nat Cell Biol*. 15:741-750.

Sacher, M., J. Barrowman, D. Schieltz, J.R. Yates, 3rd, and S. Ferro-Novick. 2000. Identification and characterization of five new subunits of TRAPP. *Eur J Cell Biol*. 79:71-80.

Sacher, M., J. Barrowman, W. Wang, J. Horecka, Y. Zhang, M. Pypaert, and S. Ferro-Novick. 2001. TRAPP I implicated in the specificity of tethering in ER-to-Golgi transport. *Mol Cell*. 7:433-442.

Sacher, M., and S. Ferro-Novick. 2001. Purification of TRAPP from Saccharomyces cerevisiae and identification of its mammalian counterpart. *Methods Enzymol*. 329:234-241.

Sacher, M., Y. Jiang, J. Barrowman, A. Scarpa, J. Burston, L. Zhang, D. Schieltz, J.R. Yates, 3rd, H. Abeliovich, and S. Ferro-Novick. 1998. TRAPP, a highly conserved novel complex on the cis-Golgi that mediates vesicle docking and fusion. *EMBO J*. 17:2494-2503.

Sacher, M., N. Shahrzad, H. Kamel, and M.P. Milev. 2019. TRAPPopathies: An emerging set of disorders linked to variations in the genes encoding transport protein particle (TRAPP)-associated proteins. *Traffic*. 20:5-26.

Sadler, K.C., A. Amsterdam, C. Soroka, J. Boyer, and N. Hopkins. 2005. A genetic screen in zebrafish identifies the mutants vps18, nf2 and foie gras as models of liver disease. *Development*. 132:3561-3572.

Saftig, P., and J. Klumperman. 2009. Lysosome biogenesis and lysosomal membrane proteins: trafficking meets function. *Nature reviews. Molecular cell biology*. 10:623-635.

Saitsu, H., T. Nishimura, K. Muramatsu, H. Kodera, S. Kumada, K. Sugai, E. Kasai-Yoshida, N. Sawaura, H. Nishida, A. Hoshino, F. Ryujin, S. Yoshioka, K. Nishiyama, Y. Kondo, Y. Tsurusaki, M. Nakashima, N. Miyake, H. Arakawa, M. Kato, N. Mizushima, and N. Matsumoto. 2013. De novo mutations in the autophagy gene WDR45 cause static encephalopathy of childhood with neurodegeneration in adulthood. *Nat Genet*. 45:445-449, 449e441.

Sanderfoot, A.A., and N.V. Raikhel. 1999. The specificity of vesicle trafficking: coat proteins and SNAREs. *Plant Cell*. 11:629-642.

Sandri, M., L. Coletto, P. Grumati, and P. Bonaldo. 2013. Misregulation of autophagy and protein degradation systems in myopathies and muscular dystrophies. *Journal of cell science*. 126:5325-5333.

Sarkar, S., B. Carroll, Y. Buganim, D. Maetzel, A.H. Ng, J.P. Cassady, M.A. Cohen, S. Chakraborty, H. Wang, E. Spooner, H. Ploegh, J. Gsponer, V.I. Korolchuk, and R. Jaenisch. 2013. Impaired autophagy in the lipid-storage disorder Niemann-Pick type C1 disease. *Cell Rep*. 5:1302-1315.

Sarkar, S., V. Korolchuk, M. Renna, A. Winslow, and D.C. Rubinsztein. 2009. Methodological considerations for assessing autophagy modulators: a study with calcium phosphate precipitates. *Autophagy*. 5:307-313.

Scales, S.J., R. Pepperkok, and T.E. Kreis. 1997. Visualization of ER-to-Golgi transport in living cells reveals a sequential mode of action for COPII and COPI. *Cell*. 90:1137-1148.

Schou, K.B., S.K. Morthorst, S.T. Christensen, and L.B. Pedersen. 2014. Identification of conserved, centrosome-targeting ASH domains in TRAPPII complex subunits and TRAPPC8. *Cilia*. 3:6.

Scrivens, P.J., B. Noueihed, N. Shahrzad, S. Hul, S. Brunet, and M. Sacher. 2011. C4orf41 and TTC-15 are mammalian TRAPP components with a role at an early stage in ER-to-Golgi trafficking. *Molecular biology of the cell*. 22:2083-2093.

Scrivens, P.J., N. Shahrzad, A. Moores, A. Morin, S. Brunet, and M. Sacher. 2009. TRAPPC2L is a novel, highly conserved TRAPP-interacting protein. *Traffic*. 10:724-736.

Seranova, E., K.J. Connolly, M. Zatyka, T.R. Rosenstock, T. Barrett, R.I. Tuxworth, and S. Sarkar. 2017. Dysregulation of autophagy as a common mechanism in lysosomal storage diseases. *Essays Biochem*. 61:733-749.

Shatz, O., and Z. Elazar. 2019. ATG9 raises the BAR for PI4P in autophagy. *J Cell Biol*. 218:1432-1433.

Shestakova, A., S. Zolov, and V. Lupashin. 2006. COG complex-mediated recycling of Golgi glycosyltransferases is essential for normal protein glycosylation. *Traffic*. 7:191-204.

Shima, T., H. Kirisako, and H. Nakatogawa. 2019. COPII vesicles contribute to autophagosomal membranes. *J Cell Biol*. 218:1503-1510.

Shirahama-Noda, K., S. Kira, T. Yoshimori, and T. Noda. 2013. TRAPPIII is responsible for vesicular transport from early endosomes to Golgi, facilitating Atg9 cycling in autophagy. *Journal of cell science*. 126:4963-4973.

Soares, T.R., S.D. Reis, B.R. Pinho, M.R. Duchen, and J.M.A. Oliveira. 2019. Targeting the proteostasis network in Huntington's disease. *Ageing Res Rev*. 49:92-103.

Sohda, M., Y. Misumi, A. Yamamoto, N. Nakamura, S. Ogata, S. Sakisaka, S. Hirose, Y. Ikehara, and K. Oda. 2010. Interaction of Golgin-84 with the COG complex mediates the intra-Golgi retrograde transport. *Traffic*. 11:1552-1566.

Soreng, K., T.P. Neufeld, and A. Simonsen. 2018. Membrane Trafficking in Autophagy. *Int Rev Cell Mol Biol*. 336:1-92.

Sou, Y.S., S. Waguri, J. Iwata, T. Ueno, T. Fujimura, T. Hara, N. Sawada, A. Yamada, N. Mizushima, Y. Uchiyama, E. Kominami, K. Tanaka, and M. Komatsu. 2008. The Atg8 conjugation system is indispensable for proper development of autophagic isolation membranes in mice. *Molecular biology of the cell*. 19:4762-4775.

Staiano, L., and F. Zappa. 2019. Hijacking intracellular membranes to feed autophagosomal growth. *FEBS Lett*. 593:3120-3134.

Stanga, D., Q. Zhao, M.P. Milev, D. Saint-Dic, C. Jimenez-Mallebrera, and M. Sacher. 2019. TRAPPC11 functions in autophagy by recruiting ATG2B-WIPI4/WDR45 to preautophagosomal membranes. *Traffic*. 20:325-345.

Starai, V.J., C.M. Hickey, and W. Wickner. 2008. HOPS proofreads the trans-SNARE complex for yeast vacuole fusion. *Molecular biology of the cell*. 19:2500-2508.

Sutton, R.B., D. Fasshauer, R. Jahn, and A.T. Brunger. 1998. Crystal structure of a SNARE complex involved in synaptic exocytosis at 2.4 A resolution. *Nature*. 395:347-353.

Szatmari, Z., and M. Sass. 2014. The autophagic roles of Rab small GTPases and their upstream regulators: a review. *Autophagy*. 10:1154-1166.

Takahashi, Y., D. Coppola, N. Matsushita, H.D. Cualing, M. Sun, Y. Sato, C. Liang, J.U. Jung, J.Q. Cheng, J.J. Mule, W.J. Pledger, and H.G. Wang. 2007. Bif-1 interacts with Beclin 1 through UVRAG and regulates autophagy and tumorigenesis. *Nat Cell Biol*. 9:1142-1151.

Takahashi, Y., H. He, Z. Tang, T. Hattori, Y. Liu, M.M. Young, J.M. Serfass, L. Chen, M. Gebru, C. Chen, C.A. Wills, J.M. Atkinson, H. Chen, T. Abraham, and H.G. Wang. 2018. An autophagy assay reveals the ESCRT-III component CHMP2A as a regulator of phagophore closure. *Nat Commun*. 9:2855.

Tamura, N., T. Nishimura, Y. Sakamaki, I. Koyama-Honda, H. Yamamoto, and N. Mizushima. 2017. Differential requirement for ATG2A domains for localization to autophagic membranes and lipid droplets. *FEBS Lett*. 591:3819-3830.

Tan, D., Y. Cai, J. Wang, J. Zhang, S. Menon, H.T. Chou, S. Ferro-Novick, K.M. Reinisch, and T. Walz. 2013. The EM structure of the TRAPPIII complex leads to the identification of a requirement for COPII vesicles on the macroautophagy pathway. *Proc. Natl. Acad. Sci. U. S. A.* 110:19432-19437.

Taussig, D., Z. Lipatova, and N. Segev. 2014. Trs20 is required for TRAPP III complex assembly at the PAS and its function in autophagy. *Traffic*. 15:327-337.

Thomas, L.L., and J.C. Fromme. 2016. GTPase cross talk regulates TRAPPII activation of Rab11 homologues during vesicle biogenesis. *J Cell Biol*. 215:499-513.

Thomas, L.L., A.M.N. Joiner, and J.C. Fromme. 2018. The TRAPPIII complex activates the GTPase Ypt1 (Rab1) in the secretory pathway. *J Cell Biol*. 217:283-298.

Thumm, M., R.A. Busse, A. Scacioc, M. Stephan, A. Janshoff, K. Kuhnel, and R. Krick. 2013. It takes two to tango: PROPPINs use two phosphoinositide-binding sites. *Autophagy*. 9:106-107.

Tooze, S.A. 2013. Current views on the source of the autophagosome membrane. *Essays Biochem*. 55:29-38.

Tsuboyama, K., I. Koyama-Honda, Y. Sakamaki, M. Koike, H. Morishita, and N. Mizushima. 2016. The ATG conjugation systems are important for degradation of the inner autophagosomal membrane. *Science*. 354:1036-1041.

Tsukada, M., and Y. Ohsumi. 1993. Isolation and characterization of autophagy-defective mutants of Saccharomyces cerevisiae. *FEBS Lett*. 333:169-174.

Vacaru, A.M., A.F. Di Narzo, D.L. Howarth, O. Tsedensodnom, D. Imrie, A. Cinaroglu, S. Amin, K. Hao, and K.C. Sadler. 2014. Molecularly defined unfolded protein response subclasses have distinct correlations with fatty liver disease in zebrafish. *Dis Model Mech*. 7:823-835.

Valverde, D.P., S. Yu, V. Boggavarapu, N. Kumar, J.A. Lees, T. Walz, K.M. Reinisch, and T.J. Melia. 2019. ATG2 transports lipids to promote autophagosome biogenesis. *J Cell Biol*. 218:1787-1798.

Van Bergen, N.J., Y. Guo, N. Al-Deri, Z. Lipatova, D. Stanga, S. Zhao, R. Murtazina, V. Gyurkovska, D. Pehlivan, T. Mitani, A. Gezdirici, J. Antony, F. Collins, M.J.H. Willis, Z.H. Coban Akdemir, P. Liu, J. Punetha, J.V. Hunter, S.N. Jhangiani, J.M. Fatih, J.A. Rosenfeld, J.E. Posey, R.A. Gibbs, E. Karaca, S. Massey, T.G. Ranasinghe, P. Sleiman, C. Troedson, J.R. Lupski, M. Sacher, N. Segev, H. Hakonarson, and J. Christodoulou. 2019. Deficiencies in vesicular transport mediated by TRAPPC4 are associated with severe syndromic intellectual disability. *Brain*.

Velikkakath, A.K., T. Nishimura, E. Oita, N. Ishihara, and N. Mizushima. 2012. Mammalian Atg2 proteins are essential for autophagosome formation and important for regulation of size and distribution of lipid droplets. *Mol Biol Cell*. 23:896-909.

Venditti, R., T. Scanu, M. Santoro, G. Di Tullio, A. Spaar, R. Gaibisso, G.V. Beznoussenko, A.A. Mironov, A. Mironov, Jr., L. Zelante, M.R. Piemontese, A. Notarangelo, V. Malhotra, B.M. Vertel, C. Wilson, and M.A. De Matteis. 2012. Sedlin controls the ER export of procollagen by regulating the Sar1 cycle. *Science*. 337:1668-1672.

Volinia, S., R. Dhand, B. Vanhaesebroeck, L.K. MacDougall, R. Stein, M.J. Zvelebil, J. Domin, C. Panaretou, and M.D. Waterfield. 1995. A human phosphatidylinositol 3-kinase complex related to the yeast Vps34p-Vps15p protein sorting system. *The EMBO journal*. 14:3339-3348.

Walczak, M., and S. Martens. 2013. Dissecting the role of the Atg12-Atg5-Atg16 complex during autophagosome formation. *Autophagy*. 9:424-425.

Wang, J., S. Menon, A. Yamasaki, H.T. Chou, T. Walz, Y. Jiang, and S. Ferro-Novick. 2013. Ypt1 recruits the Atg1 kinase to the preautophagosomal structure. *Proc. Natl. Acad. Sci. U. S. A.* 110:9800-9805.

Wang, W., M. Sacher, and S. Ferro-Novick. 2000. TRAPP stimulates guanine nucleotide exchange on Ypt1p. *J Cell Biol*. 151:289-296.

Wang, X., Y. Wu, Y. Cui, N. Wang, L. Folkersen, and Y. Wang. 2018. Novel TRAPPC11 Mutations in a Chinese Pedigree of Limb Girdle Muscular Dystrophy. *Case Rep Genet*. 2018:8090797.

Wei, Y., M. Liu, X. Li, J. Liu, and H. Li. 2018. Origin of the Autophagosome Membrane in Mammals. *Biomed Res Int*. 2018:1012789.

Weidberg, H., E. Shvets, T. Shpilka, F. Shimron, V. Shinder, and Z. Elazar. 2010. LC3 and GATE-16/GABARAP subfamilies are both essential yet act differently in autophagosome biogenesis. *The EMBO journal*. 29:1792-1802.

Welchman, R.L., C. Gordon, and R.J. Mayer. 2005. Ubiquitin and ubiquitin-like proteins as multifunctional signals. *Nature reviews. Molecular cell biology*. 6:599-609.

Wen, X., and D.J. Klionsky. 2016. An overview of macroautophagy in yeast. *J Mol Biol*. 428:1681-1699.

Wendler, F., A.K. Gillingham, R. Sinka, C. Rosa-Ferreira, D.E. Gordon, X. Franch-Marro, A.A. Peden, J.P. Vincent, and S. Munro. 2010. A genome-wide RNA interference screen identifies two novel components of the metazoan secretory pathway. *EMBO J*. 29:304-314.

Willett, R., T. Kudlyk, I. Pokrovskaya, R. Schonherr, D. Ungar, R. Duden, and V. Lupashin. 2013. COG complexes form spatial landmarks for distinct SNARE complexes. *Nat Commun*. 4:1553.

Witkos, T.M., and M. Lowe. 2015. The Golgin Family of Coiled-Coil Tethering Proteins. *Front Cell Dev Biol*. 3:86.

Xie, Z., U. Nair, and D.J. Klionsky. 2008. Atg8 controls phagophore expansion during autophagosome formation. *Molecular biology of the cell*. 19:3290-3298.

Yamamoto, H., S. Kakuta, T.M. Watanabe, A. Kitamura, T. Sekito, C. Kondo-Kakuta, R. Ichikawa, M. Kinjo, and Y. Ohsumi. 2012. Atg9 vesicles are an important membrane source during early steps of autophagosome formation. *J Cell Biol*. 198:219-233.

Yamasaki, A., S. Menon, S. Yu, J. Barrowman, T. Meerloo, V. Oorschot, J. Klumperman, A. Satoh, and S. Ferro-Novick. 2009. mTrs130 is a component of a mammalian TRAPPII complex, a Rab1 GEF that binds to COPI-coated vesicles. *Molecular biology of the cell*. 20:4205-4215.

Yip, C.K., J. Berscheminski, and T. Walz. 2010. Molecular architecture of the TRAPPII complex and implications for vesicle tethering. *Nat Struct Mol Biol*. 17:1298-1304.

Yoshida, A., K. Kobayashi, H. Manya, K. Taniguchi, H. Kano, M. Mizuno, T. Inazu, H. Mitsuhashi, S. Takahashi, M. Takeuchi, R. Herrmann, V. Straub, B. Talim, T. Voit, H. Topaloglu, T. Toda, and T. Endo. 2001. Muscular dystrophy and neuronal migration disorder caused by mutations in a glycosyltransferase, POMGnT1. *Developmental cell*. 1:717-724.

Young, A.R., E.Y. Chan, X.W. Hu, R. Kochl, S.G. Crawshaw, S. High, D.W. Hailey, J. Lippincott-Schwartz, and S.A. Tooze. 2006. Starvation and ULK1-dependent cycling of mammalian Atg9 between the TGN and endosomes. *Journal of cell science*. 119:3888-3900.

Yu, L., C.K. McPhee, L. Zheng, G.A. Mardones, Y. Rong, J. Peng, N. Mi, Y. Zhao, Z. Liu, F. Wan, D.W. Hailey, V. Oorschot, J. Klumperman, E.H. Baehrecke, and M.J. Lenardo. 2010. Termination of autophagy and reformation of lysosomes regulated by mTOR. *Nature*. 465:942-946.

Zeevaert, R., F. Foulquier, J. Jaeken, and G. Matthijs. 2008. Deficiencies in subunits of the Conserved Oligomeric Golgi (COG) complex define a novel group of Congenital Disorders of Glycosylation. *Mol Genet Metab*. 93:15-21.

Zeytuni, N., and R. Zarivach. 2012. Structural and functional discussion of the tetra-trico-peptide repeat, a protein interaction module. *Structure*. 20:397-405.

Zhao, S., C.M. Li, X.M. Luo, G.K. Siu, W.J. Gan, L. Zhang, W.K. Wu, H.C. Chan, and S. Yu. 2017. Mammalian TRAPPIII Complex positively modulates the recruitment of Sec13/31 onto COPII vesicles. *Sci Rep*. 7:43207.

Zheng, J.X., Y. Li, Y.H. Ding, J.J. Liu, M.J. Zhang, M.Q. Dong, H.W. Wang, and L. Yu. 2017. Architecture of the ATG2B-WDR45 complex and an aromatic Y/HF motif crucial for complex formation. *Autophagy*. 13:1870-1883.

Zhou, F., S. Zou, Y. Chen, Z. Lipatova, D. Sun, X. Zhu, R. Li, Z. Wu, W. You, X. Cong, Y. Zhou, Z. Xie, V. Gyurkovska, Y. Liu, Q. Li, W. Li, J. Cheng, Y. Liang, and N. Segev. 2017. A Rab5 GTPase module is important for autophagosome closure. *PLoS Genet*. 13:e1007020.

Zong, M., X.G. Wu, C.W. Chan, M.Y. Choi, H.C. Chan, J.A. Tanner, and S. Yu. 2011. The adaptor function of TRAPPC2 in mammalian TRAPPs explains TRAPPC2-

associated SEDT and TRAPPC9-associated congenital intellectual disability. *PLoS One*. 6:e23350.

Zoppino, F.C., R.D. Militello, I. Slavin, C. Alvarez, and M.I. Colombo. 2010. Autophagosome formation depends on the small GTPase Rab1 and functional ER exit sites. *Traffic*. 11:1246-1261.

Zou, S., Y. Chen, Y. Liu, N. Segev, S. Yu, Y. Liu, G. Min, M. Ye, Y. Zeng, X. Zhu, B. Hong, L.O. Bjorn, Y. Liang, S. Li, and Z. Xie. 2013. Trs130 participates in autophagy through GTPases Ypt31/32 in Saccharomyces cerevisiae. *Traffic*. 14:233-246.